1. INTRODUCTION

1.1 Background

The disposal of fine-grained mining and industrial waste by formation of hydraulic-fill tailings dams is becoming a design and construction activity of increasing scale. In light of the increasing pressure on the mining industry to sustain stringent safety and environmental standards it is becoming more important to gain technical knowledge of the waste problem. Currently only a small amount of technical information is available on the safe disposal of mine waste. This area has become a priority research subject for Geotechnical engineers.

The upper layers of the tailings residue dams is in the unsaturated state that is caused by high evaporative fluxes due to South Africa's dry climate. An important contribution to the shear strength of the unsaturated soil is the matric suction component. The ability to incorporate the matric suction component in shear strength calculations will allow for safer designs. This is as a result of the increased safety factor in stability and bearing capacity calculations due to the additional incorporation of the matric suction.

1.2 Objectives

- Investigate the use of the mid-plane suction probe and perform calibration.
- Develop an appropriate test method to obtain a complete soil-water characteristic curve for Mispah gold tailings.
- Develop a test method to simulate the daywall of Mispah tailings dam.
- Investigate the increase in suction induced shear strength of drying tailings with depth.

1.3 Scope

- Tests were conducted on gold tailings from Vaal Operation's Mispah tailings dam.

- Measurements of suction pressures were made with the use of a mid-plane suction probe with a capacity of 350kPa.

- Field tests were carried out on the daywall of Mispah tailings dam, which comprised of vane shear measurements, suction measurements with depth, measurement of crack width and sampling of material to determine material properties.

- Two sets of laboratory tests were carried out on the material. Firstly the trough test, to determine the soil-water characteristics of the gold tailing and then the drying box test which simulated the drying and desiccation of the gold tailings in the daywall.

1.4 Methodology

- Investigate the proper use and performance of the mid-plane suction probe and perform a calibration.

- Develop a test procedure from which the soil-water characteristics of the Mispah gold tailings can be obtained.

- Perform experimental work on Mispah gold tailings to obtain soil-water characteristics using the developed test procedure.

- Develop a test procedure to simulate the drying and desiccation of Mispah gold tailings in the daywall.

- Simulate daywall of Mispah gold tailings dam to obtain soil parameters needed to calculate the suction induced shear strength with depth, using the developed test procedure.

- Develop a test procedure for conducting field tests on the daywall of Mispah gold tailings dam.

- Perform field tests on the daywall of Mispah gold tailings to obtain material parameters to compare with the laboratory results.

- Draw meaningful conclusions from the results

1.5 Organisation of the Report

The report consists of the following chapters and appendices:

- Chapter 1 serves as an introduction to the report.

- Chapter 2 contains a technical introduction to suctions, suction induced shear strength and gold mine tailings based on a literature study

- Chapter 3 discusses the development of the test methods to obtain the soil-water characteristics of the gold mine tailings and to simulate the drying and desiccation of the gold tailings in the daywall.

- Chapter 4 contains the laboratory data obtained from the experimental work on the Mispah gold tailings as well as the field test measurements obtained from the field tests conducted on the daywall of Mispah tailings dam.

- Chapter 5 serves as a discussion on the results obtained from the experimental work.

- Chapter 6 contains the conclusions and recommendations of the study.

- Chapter 7 contains the list of references.

- Appendix A, B, and C serve as an extension of Chapter 4.

2 LITERATURE REVIEW

2.1 Introduction

This chapter is intended to provide the reader with a summary of the fundamental principals associated with soil mechanics, as well as provide a literature review of recent research related to this field of study. The chapter begins with a detailed discussion of the properties of unsaturated soils such as surface tension and capillary.

Since the single primary aim of the research project is the measurement of soil suctions, a review of soil suction theory is given. Of particular interest, is the operating principal of the high air-entry disk (Fredlund et. al. 1993) and its application to the mid-plane suction probe (Van Heerden 2000) that was used to measure the suctions in the test material.

Another important principal discussed is the soil water characteristic curve, which gives the relationship between volumetric water content and negative suction pressures. Fredlund suggested a set of equations as well as a graphical method to construct the soil water characteristic curve. The work by Fredlund was used to construct the soil water characteristic curves for the gold mine tailings used in this research project. Another important relationship associated with this curve is the relationship between degree of saturation and void ratio given by Vanapalli.

Other principles such as stress state, shear strength, and critical state are also discussed in this chapter. The expression derived by Vanapalli et al. for the determination of shear strength in unsaturated soil was used extensively throughout the research. This expression was used to obtain a relationship between suctions and shear strength.

Since the test material used was obtained from the daywall of a gold mine tailings dam, the chapter concludes with a discussion on all processing, tailings transport, discharge, depositioning and disposal methods.

2.2 Unsaturated Soil Properties

2.2.1 Introduction

Until recently unsaturated soil has been described as a three-phase system, consisting of:

- water phase
- air phase
- soil particles

Research by Fredlund et al. (1977) indicates the important role of the air-water interface (contractile skin). As a result, the contractile skin was introduced as a fourth phase. When the air phase is continuous, the contractile skin interacts with the soil particles and thus influences the mechanical behaviour of the soil.

The contractile skin has a thickness in order of only a few molecules, therefore, it does not influence the mass or the volume of unsaturated soils. It is thus, considered as part of the water phase when establishing the volume-mass relationships.

2.2.2 Surface tension

The contractile skin causes surface tension, which results from the intermolecular forces acting within the contractile skin. Molecules on the interior of the water, experiences equal forces in all directions. Those within the contractile skin, however, experience an unbalanced force towards the interior of the water (Figure 2.1).

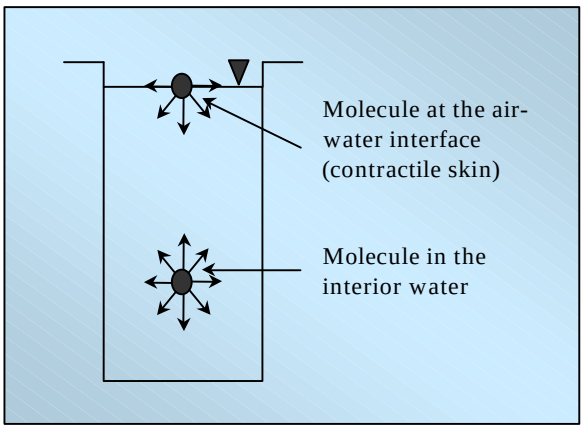

Figure 2.1: Intermolecular forces on contractile skin (Fredlund and Rahardjo, 1993)

The surface tension causes the contractile skin to behave like an elastic membrane, subjected to different pressures on each side. The membrane will thus, assume a concave curvature towards the larger pressure, and exert a tension in the membrane in order to reach equilibrium. By considering equilibrium across the membrane, it is possible to relate the pressure difference across the curved surface as a function of the radius of curvature and the surface tension, which is tangential to the contractile skin surface (Fredlund and Rahardjo 1993).

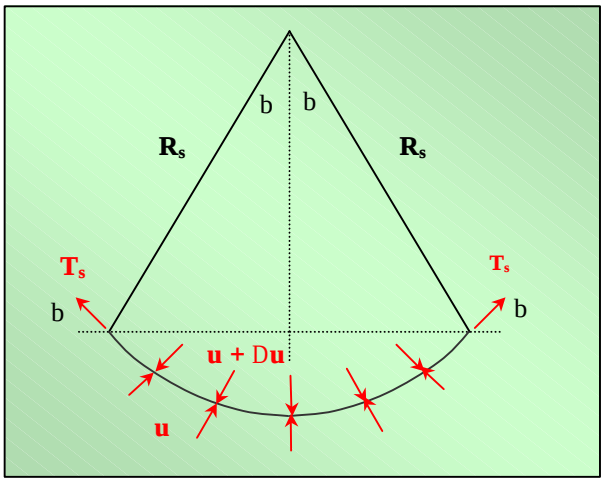

Figure 2.2: Curved two-dimension surface (Fredlund and Rahardjo, 1993)

The pressure acting on the membrane is denoted by *u* and *(u+Du)*. The membrane has a radius of curvature, R_s, and surface tension, *Ts*. Using this model it is possible to derive Kelvin's capillary equation by considering vertical equilibrium:

ΣF_y : $$2T_s \sin b = 2\Delta u R_s \sin b \qquad \textbf{[2.1]}$$

$$\therefore \Delta u = \frac{T_s}{R_s} \qquad \textbf{[2.2]}$$

with: $2R_s \sin b$ - projected length of membrane [m]

Du - change in pore pressure [kPa]

Equation [2.2] can be extended to a three-dimensional warped membrane using the Laplace equation:

$$\Delta u = T_s\left(\frac{1}{R_1} + \frac{1}{R_2}\right) \qquad \textbf{[2.3]}$$

If the radius of curvature is the same in all directions ($R_1 = R_2$):

$$\Delta u = \frac{2T_s}{R_1} \qquad \textbf{[2.4]}$$

In an unsaturated soil, the contractile skin would be subjected to the ambient environment pressure, u_a, which is larger than the water pressure, u_w. This pressure difference is referred to as matric suction. It is this pressure difference, that causes the contractile skin to curve as described in [2.4], rendering Kelvin's capillary equation:

$$(u_a - u_w) = \frac{2T_s}{R_1} \qquad \textbf{[2.5]}$$

with: $(u_a - u_w)$ - matric suction [kPa]

As the matric suction of the soil increases, the radius of curvature, of the contractile skin decreases. The curved contractile skin is often called a meniscus. When the pressure difference goes to zero, the radius of curvature, R, goes to infinity. A flat air-water interface, therefore, exists when the matric suction approaches zero.

2.2.3 Capillarity

The capillarity phenomenon is associated with the matric suction component of total suction. The height of water rise and the radius of curvature have a direct effect on the water content versus matric suction relationship in the soils.

The mechanism of capillarity can be illustrated by placing a small glass tube into water under atmospheric conditions, as shown in Figure 2.3. The rise of the water in the tube is a result of surface tension, T_s, in the contractile skin that acts around the circumference of the meniscus at an angle, a, from the vertical and the hygroscopic properties of the tube (Holtz and Kovacs, 1981).

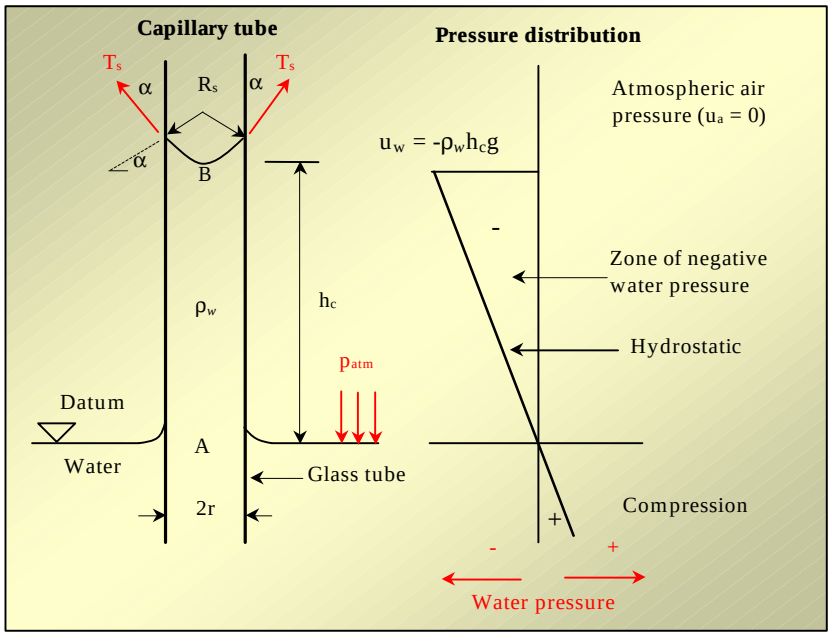

Figure 2.3: Physical model related to capillarity (Holtz and Kovacs, 1981)

When considering the vertical force equilibrium of the weight of the water column, and the vertical resultant of the surface tension (which is responsible for holding the weight of the column), it is possible to derive the equation for capillary height:

$$2prT_s \cos a = pr^2 h_c r_w g \qquad \textbf{[2.6]}$$

with:

r - radius of capillary tube [m]

T_s - surface tension of the water [N]

a - contact angle [degree]

h_c - capillary height [m]

g - gravitational acceleration [9.81m.s^{-2}]

Equation [2.6] can be re-arranged to give the maximum height of water in the capillary tube:

$$h_c = \frac{2T_s}{r_w g R_s} \qquad \textbf{[2.7]}$$

with:

R_s - radius of curvature of the meniscus [m]

Points *A* and *B* shown in Figure 2.3 are in hydrostatic equilibrium, with the elevation of point *A* considered as the datum where the pressure is atmospheric. Point *B* is located at a height of h_c from the datum. By considering hydrostatic equilibrium, it is shown that the hydraulic head at point *B* must also be equal to zero. This means that the pressure head at point *B* is equal to the negative value of the elevation at point *B*. The water pressure at point *B* can be calculated as follows:

$$u_w = -r_w g h_c \qquad \textbf{[2.8]}$$

with: u_w - water pressure [kPa]

The water pressure above point *A* in the capillary tube is negative, with the water being subjected to a tensional force. Below point *A* the water pressure is positive due to hydrostatic conditions. With the air pressure at point *B* being atmospheric and the water pressure negative, it is possible to express the matric suction as follows:

$$(u_a - u_w) = r_w g h_c \qquad \textbf{[2.9]}$$

Substituting [2.7] into [2.9] gives rise to matric suction being written in terms of surface tension:

$$(u_a - u_w) = \frac{2T_s}{R_s} \qquad \textbf{[2.10]}$$

This is the same equation for pressure difference across the contractile skin that was derived earlier with the radius of curvature, R_s, being analogue to the pore radius, *r*.

Eventhough soils are random assemblages of particles, and resulting voids are similarly random and highly irregular, the capillary tube analogy (although imperfect), helps to explain capillary phenomena observed in real soils. In principle, the capillary pressure and capillary rise will be similar in soils and in glass tubes. The radius of the tube is analogous to the pore radius in soils, with a decrease in pore radius resulting in higher capillary height (Fredlund and Rahardjo, 1993).

2.3 Soil Suction

2.3.1 Introduction

Soil suction is commonly referred to as total suction that that is comprised of two components, namely, matric suction ($u_a - u_w$) and osmotic suction, p. In equation form this can be written as:

$$y = (u_a - u_w) + p \qquad \textbf{[2.11]}$$

with: $(u_a - u_w)$ - matric suction [kPa]

u_a - pore-air pressure [kPa]

u_w - pore-water pressure [kPa]

p - osmotic suction [kPa]

2.3.2 Matric suction

The matric suction component, ($u_a - u_w$), is commonly associated with the capillary phenomenon arising from surface tension of water, where the radius of curvature is inversely proportional to the difference between the air and water pressure across the surface (Fredlund and Rahardjo, 1993).

In soils, the pores with small radii act as capillary tubes that cause the soil water to rise above the water table. The capillary water has negative pressure, with respect to the air pressure that is generally atmospheric in the field. The capillary model, however, can not justify the extremely high suction pressures often encountered in soils (Holtz and Kovacs, 1981).

2.3.3 Osmotic suction

Osmotic suction can be explained best, by considering pure water, placed in contact with a solution through a semi-permeable membrane. The membrane allows water to flow through it, while at the same time, restricting the flow of the solution. The concentration difference between solubles creates the potential for water to flow through the semi-permeable membrane to the solution. If the flow of water is restricted, a differential pressure known as osmotic suction (p) is created between the two (Fredlund and Rahardjo, 1993).

Geotechnical problems relating to soil suction are mostly caused by environmental changes. These environmental changes alter the matric suction of the soil and consequently the overall equilibrium of the soil. Research by Fredlund et al indicates that in practise osmotic suction is negligible compared to total suction. It is thus, convenient to ignore the effect of osmotic suction in the research project.

2.3.4 The direct measurement of suction

Negative pore-water pressure is mainly measured directly, with the use of high air entry ceramic disks. A high air entry disk acts as a membrane between air and water (Figure 2.4).

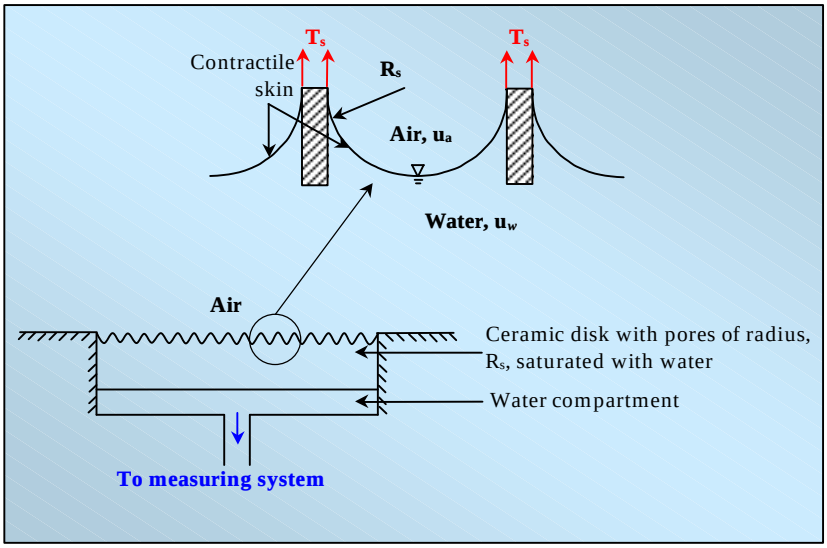

Figure 2.4: Operating principle of a high air entry disk as described by Kelvin's capillary model (Fredlund and Rahardjo, 1993)

The disk is ceramic with small pores of uniform size. Once the disk is saturated with water, air cannot pass through the disk due to the ability of the contractile skin to develop a surface tension, T_s, that resists the flow of air. The contractile skin acts like a thin membrane joining the small pores of radius, R_s, on the surface of the ceramic disk (Fredlund and Rahardjo, 1993).

The maximum matric suction maintainable across the surface of the disk is called the air entry value, AES. The air entry suction of a disk can be described by Kelvin's equation [2.5]. The air entry suction of a disk, is primarily controlled by the radius of curvature of the largest pore in the disk. The pore sizes are controlled by the preparation and sintering process used to manufacture the disk, with smaller pore sizes resulting in a larger air entry value.

The high air entry disk is used as an interface between the unsaturated soil and the measuring system, with the water in the disk acting as a link between the pore water and the water in the measuring system. The measuring system consists of a transducer plate, which is deflected due to the suction. Deflection of the transducer plate results in a change in resistance value. The change in resistance is converted to a pressure value through an amplifier and displayed on a digital display.
Once the matric suction has exceeded the air entry value of the disk, air will pass through the disk and enter the measuring system. Air is compressible as opposed to water, which is incompressible. The air that entered the system is compressed, which results in erroneous measurements of the pore-water pressure in a closed system

2.3.5 The mid-plane suction probe

By incorporating a 3 bar high air entry disk, Theron (2000) developed a mid-plane probe that can be used to measure suction pressure directly in tailings material (Figure 2.5).

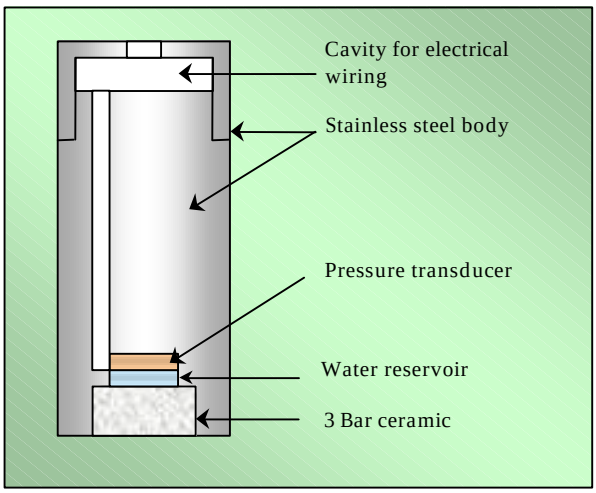

Figure 2.5: Schematic diagram of the mid-plane suction probe (Theron, 2000)

The body of the probe is machined from stainless steel, with the miniature Kyowa PS 2KA pressure transducer embedded in a cavity, leaving a gap of 0.1mm for the water reservoir between the surface of the transducer and the ceramic disk. The water reservoir has a volume of 2.8mm^3 that will inhibit cavitation, thus, increasing the maximum measurable suction to approximately 450 kPa.

To ensure saturation, the probe is placed into a triaxial cell, completely filled with de-aired water. A GDS pressure controller is used to cycle the pressure inside the cell between 50 and 350 kPa for 24, hours to ensure that any occluded air bubbles inside the probe have dissolved. Complete saturation is necessary to ensure an acceptable response time during suction measurement. To maintain the probe in a saturated state, the probe is kept in a container filled with de-aired water.

The mid-plane suction probe was used extensively by Theron (2000), Luyt (2001) and Van Heerden (2002) to measure suctions in gold tailings. Tests were developed to obtain soil-water characteristic curves for tailings samples.

2.4 The Soil-water Characteristic Curve

2.4.1 Introduction

The soil-water characteristic curve (SWCC) for a soil illustrates the relationship between water content and soil suction. The water content can be defined as the amount of water contained within the pores of the soil, and can be expressed as gravimetric water content, *w*, volumetric water content, *q*, or degree of saturation, *S*. In soil science, volumetric water content, *q*, is most commonly used (Leong and Rahardjo, 1997).

2.4.2 Volume-mass relationships for water content

Volumetric water content, *q*, can be defined as the ratio of the volume of water to the total volume of soil. Relationships can be written between the various volume-mass designations for water content. Vanapali et al. (1996) suggested that the relationship between volumetric water content and degree of saturation be written as:

$$q = \frac{Se}{(1+e)} = Sn \qquad \textbf{[2.12]}$$

with:

q - volumetric water content

S - degree of saturation

e - the void ratio

n - the porosity

Volumetric water content,*q*, can also be written in terms of gravimetric water content, *w*, in the form:

$$q = wr_d \qquad \textbf{[2.13]}$$

with:

w - gravimetric water content of soil

r_d - dry density of soil [kg / m^3]

When the soil-water characteristic curve is considered over the entire suction range, volumetric water content is referred to as zero water content. In this case, the normalised volumetric water content is equivalent to the degree of saturation, provided that the volume change of the soil structure is negligible:

$$\Theta = \frac{q}{q_s} = \frac{V_w / V_t}{V_v / V_t} = \frac{V_w}{V_v} = S \qquad \textbf{[2.15]}$$

with:

V_w - volume of water in the soil specimen [m^3]

V_v - volume of voids in the soil specimen [m^3]

V_t - total volume of soil specimen [m^3]

Equation [15] indicates that the normalised water content is identical to the degree of saturation, when referred to zero water content, and the volume change of the soil is negligible (Fredlund et al. 1994).

2.4.3 Features of a soil-water characteristic curve

The Soil Water Characteristic Curve (SWCC) is a plot of volumetric water content (y-axis) versus soil suction (x-axis). The SWCC is a semi-log graph with the soil suction plotted on a logarithmic scale.

A typical SWCC takes the form of Figure 2.6, which illustrates the relationship between volumetric water content and matric suction. The volumetric water content at zero matric suction is called the saturated volumetric water content, q_s, and corresponds to the porosity of the soil that represents the total volume of water that the soil can store (Fredlund and Xing, 1994).

The main curve shown in Figure 2.6 is a desorption curve, with the adsorption curve differing from the former as a result of hysteresis. The nonuniformity in pore size distribution in a soil, results in hysteresis in the soil-water characteristics curve. At a given matric suction, the soil water content during the wetting and drying process are different (Fredlund and Rahardjo, 1993).

The endpoint of the adsorption curve may differ from the starting point of the desorption curve, due to air entrapment in the soil (Fredlund and Xing, 1994). The ratio of water content and the change in soil matric suction, represents the storage potential. The steeper the slope over a specific range of soil suctions, the greater water storage potential (Leong and Rahardjo, 1997).

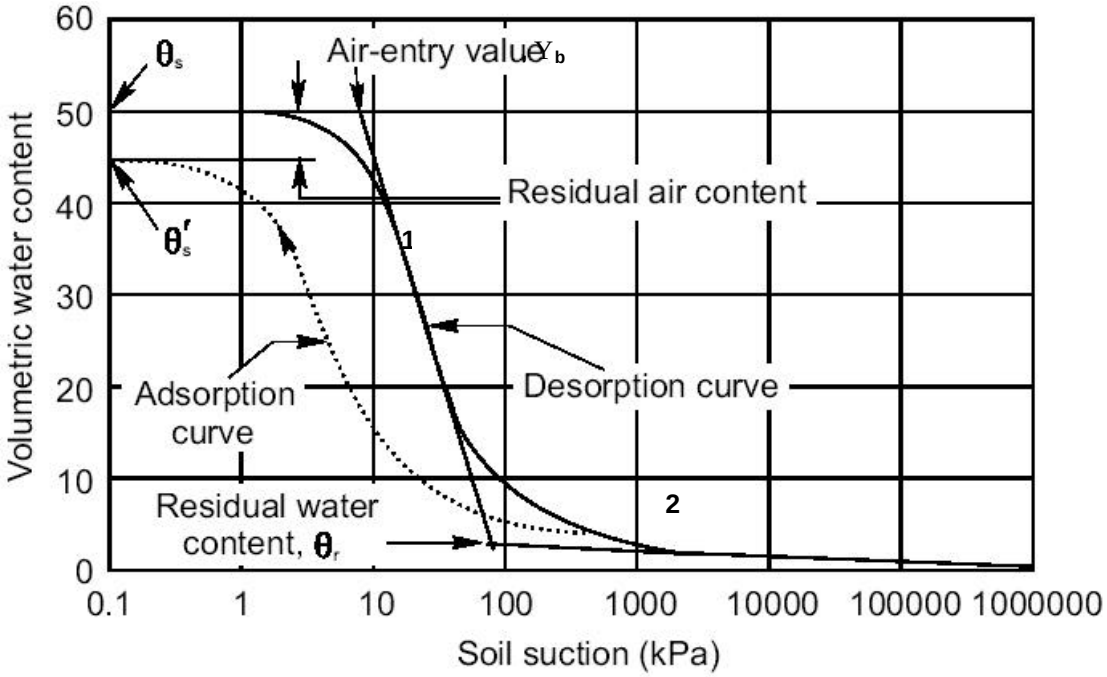

Figure 2.6: Typical desorption and adsorption curves (Fredlund et al. 1994)

The soil matric suction that corresponds to the initial draining of the soil pores, is referred to as the air entry value, Y_b. Beyond the air entry value, the specimen starts to desaturate and continues to desaturate as the suctions increase.

The water content at which the SWCC begins to flatten after the air entry value, is called the residual water content, q_r. Below the residual water content, a large increase in suction is required to remove additional water from the soil. Sillers (1997) more recently defined residual water content as: "the water content, where the soil-water goes from being held within the soil primarily by capillary action, to the soil-water being held primarily by adsorptive forces." At zero water content, the soil matric suction is approximately 1,000,000 kPa (Fredlund et al. 1994).

Due to the vagueness of the residual water content's definition, an empirical procedure for its quantification was formulated by Vanapalli et al. 1998 (Figure 2.6). The procedure involved, first drawing a tangent line through the inflection point (line 1) on the straight-line portion of the SWCC. A second line was drawn from the point at 1 000 000 kPa, tangent to the original curve (line 2). The residual volumetric water content was defined as the point where line 1 and line 2 intersected.

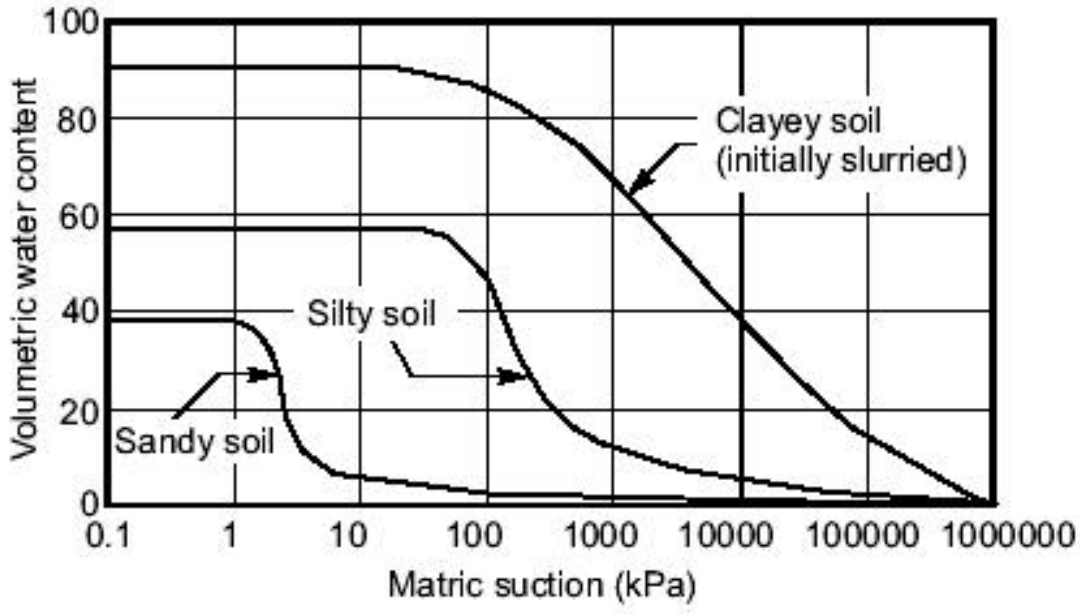

Figure 2.7: Soil-water characteristic curve for sandy, silty and clayey soil (Fredlund and Xing, 1994)

Typical soil-water characteristic curves for a sandy soil, a silty soil ,and a clayey soil were plotted using a semi-logarithmic scale are shown in Figure 2.7. The saturated water content and the air-entry value generally increase with the increase of the soil's plasticity and percentage fines. Other factors such as stress history, soil structure, and initial water content also affect the shape of the soil-water characteristics curves (Fredlund and Xing, 1994).

2.4.4 Soil-water characteristic curve equations

Most of the soil-water characteristic curve equations are empirical in nature and based on the shape of the soil-water characteristic curve. It also appears that each equation is applicable to a particular group of soils. Although it may be observed that the general shape of the soil-water characteristics curve is sigmoidal, it will be found that most of the current soil-water characteristic equations do not give a sigmoidal curve (Leong and Rahardjo, 1997).

Fredlund and Xing (1994) provided an analytical basis for mathematically defining the entire SWCC. The equation is applicable over the entire range of suctions from 0 to 1,000,000 kPa. This empirical relationship is based on pore size distribution, with the assumption that the soil consists of a set of interconnected pores, which are randomly distributed. The equation is most commonly written in terms of volumetric water content, q:

$$q = C(y)\frac{q_s}{\left\{\ln\left[e+\left(\frac{y}{a}\right)^n\right]\right\}^m} \qquad \textbf{[2.17]}$$

with:

e - natural number, 2.71828

a - approximate of the air-entry value of the soil

n - parameter controlling the slope at the inflection point in the SWCC

m - parameter that is related to the residual q_r

$C(Y)$ - a correcting function that forces the SWCC through a suction of 1 000 000 kPa and zero water content.

The correction factor is defined as:

$$C(y) = \frac{-\ln\left(1+\frac{y}{C_r}\right)}{\ln\left[1+\left(\frac{1{,}000{,}000}{C_r}\right)\right]} + 1 \qquad \textbf{[2.18]}$$

with: C_r - is the suction value corresponding to residual water content q_r

Equation [2.17] can be written in a normalised form by dividing both sides of the equation by the volumetric water content at saturation:

$$\Theta = C(\Psi)\left[\frac{1}{\ln\left[e+\left(\frac{\Psi}{a}\right)^n\right]}\right]^m = S \qquad \textbf{[2.19]}$$

A graphical estimation of the four parameters *a*, *n*, *m* and Y_r, in [2.17] can be obtained from a semi-log plot of the SWCC as shown if Figure 2.8.

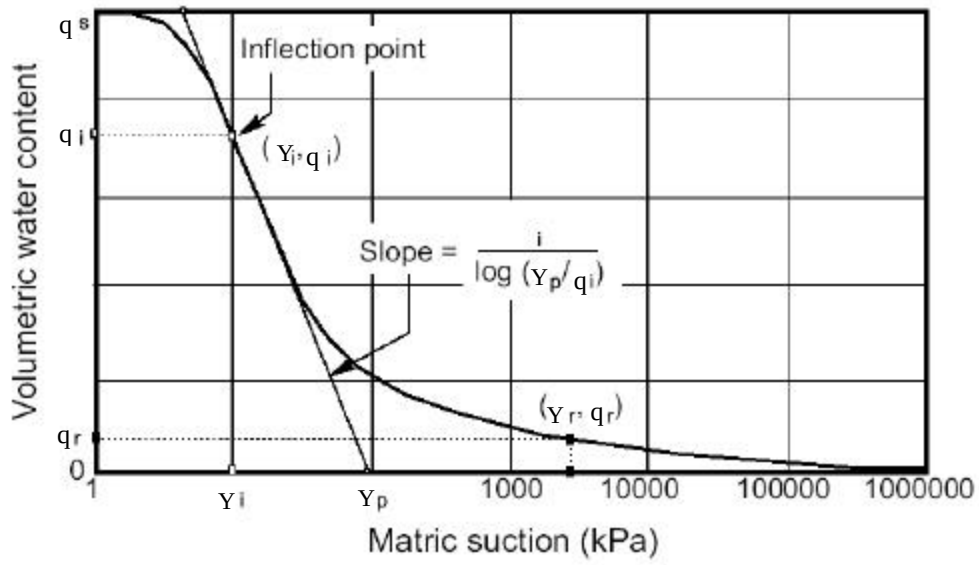

Figure 2.8: A sample plot for the graphical solution of the four parameters a, n, m and Y_r (Fredlund and Xing, 1994)

First, the suction corresponding to the residual water content, Y_r, is determined by locating a point where the curve starts to drop linearly in the high suction range. The magnitude will generally be in the range of 1000 to 3000 kPa. After the inflection point (Y_I;q_I) has been located on the semi-log plot, a tangent line is drawn through the point. With *s* denoting the slope of the tangent line on the semi-log plot. Thereafter, fitting parameters a, n, and m can be determined as follows:

$$a = \Psi_i \qquad \textbf{[2.20]}$$

$$m = 3.67 \ln\left[\frac{q_s C(\Psi_i)}{q_i}\right] \qquad \textbf{[2.21]}$$

$$n = \frac{1.31^{m+1}}{mC(\Psi_i)} 3.72 s^* \qquad \textbf{[2.22]}$$

$$s^* = \frac{s}{q_s} - \frac{\Psi_i}{1.31^m (\Psi_i + \Psi_r) \ln[1 + (1000000/\Psi_r)]} \qquad \textbf{[2.23]}$$

$$s = \frac{q_i}{\ln(\Psi_p / \Psi_r)} \qquad \textbf{[2.24]}$$

with: Ψ_p - intercept of the tangent line on the semi-log plot and the matric suction axis.

A graphical estimation only gives approximate values for the parameters. After comparison with other models, Vanapali and Fredlund (2000) found this best-fit curve method to be particularly reliable for sand and silts. A best-fit curve to the experimental data of Kid Creek tailings is shown in Figure 2.9 (Yang, 1992).

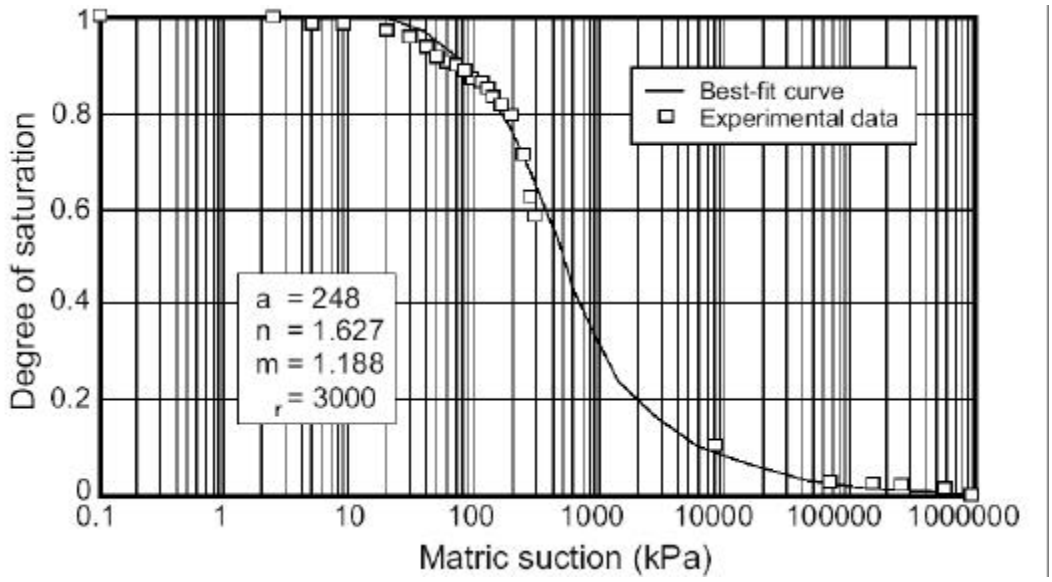

Figure 2.9: A best-fit curve to the experimental data of Kid Creek tailings (Yang, 1992)

To obtain a closer fit to experimental data the three parameters *a*, *n*, and *m*, can be determined using a least squared method.

2.4.5 Determination of soil-water characteristic curve

Various experimental methods have been formulated for the experimental determination of the SWCC.

Trough Test:

Van Heerden (2001) developed a simple and inexpensive test method to determine the SWCC for gold mine tailings using a mid-plane suction probe.

Shrinkage troughs were made from 25mm uPVC conduit, of about 200mm lengths cut in half along the length. The troughs were lined with a lubricant before each test, to ensure free movement of the sample during shrinkage. Thereafter gold tailings material, of different gradations, were placed into the trough in slurry form.

The suction pressures were measured in the tailings at different intervals by placing the probe directly onto the tailings material. Volume changes of the drying tailings material in the troughs were measured with a vernier. Due to the limiting range of suctions measurable by the mid-plane suction probe, it was only possible to determine the first section of the SWCC. Problems were also encountered with accurately determining the change in volume.

The Fredlund Soil-water Characteristics Cell:

The Fredlund Soil-water Characteristics Cell is currently the best testing equipment commercially available to obtain the complete SWCC for any soil (Figure 2.10).

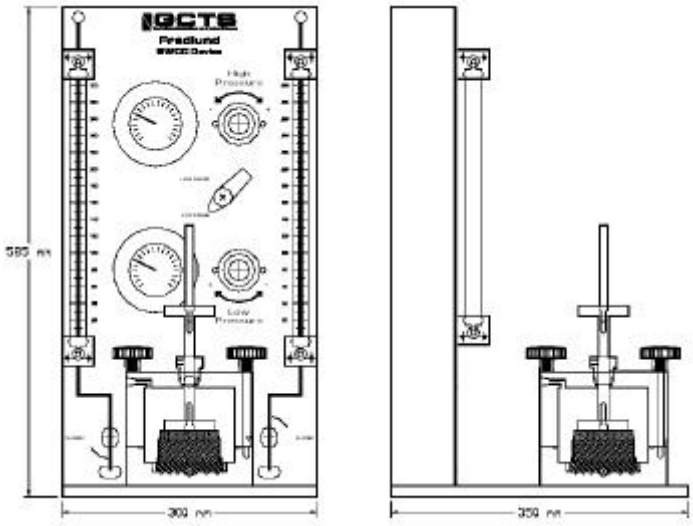

Figure 2.10: The Fredlund Soil Water Characteristic Cell

The Fredlund Soil-water Characteristic Cell allows you to control suctions up to 1,500 kPa and is capable of applying one-dimensional loading to the specimens with a diameter of up to 75mm. The cell is made of stainless steel with hand-operated knobs for fast specimen set-ups. The device includes a pressure panel with dual gauges and regulators for the precision at low-pressure ranges. Several different High Air Entry Value ceramic stones are provided and can be easily interchanged.

SWCC from grain-size distribution and volume-mass properties:

Fredlund et al. (1997) formulated an indirect method of estimating the SWCC from the grain-size distribution curve and volume-mass properties. The grain size distribution is divided into small groups of uniformly sized particles (Figure 2.11).

A packing porosity and SWCC is assumed for each group of particles and, thereafter, the incremental SWCC is summed to produce a final SWCC. Prediction of the SWCC from grain-size distribution allows for inexpensive description on the behavior of unsaturated soils.

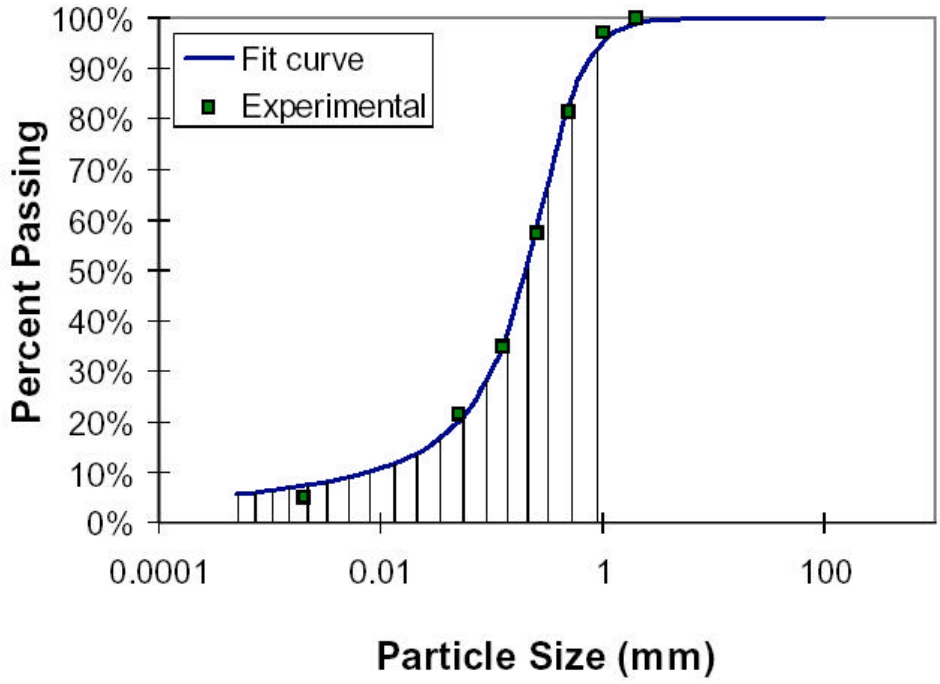

Figure 2.11: Small divisions of particle size used to build complete SWCC (Fredlund et al. 1997)

2.5 Stress State of Unsaturated Soil

2.5.1 Introduction

The Mohr-Coulomb theory (using the effective stress state), is commonly used for predicting the shear strength of saturated soils. Even though soils encountered in engineering practice are often unsaturated, slope stability analysis is usually based on saturated shear strength parameters. These approaches are conservative to varying degrees, in that the influence of the soil suction is ignored (Fredlund and Rahardjo, 1993).

2.5.2 Stress states for saturated soils

The stress state variable for saturated soil has been called effective stress and is commonly expressed as follows:

$$s' = s - u \quad \textbf{[2.25]}$$

with:
s' - effective stress
s - total stress
u - pore-water pressure

The total normal stress in a soil is a function of the density or the total weight of the soil. The magnitude and distribution of the total normal stress is also affected by the application of external loads such as buildings or the removal of soil through excavations (Terzaghi, 1936).

In the derivation, the pore pressure is assumed to act over the total area considered (A_{tot}). The effective stress is thus a fictitious, average, stress in the soil skeleton, which is consequently obtained as the sum of the forces transmitted through the points of grain contacts divided by the total area (Oberg and Sällfors, 1995). Thus, the stress in the grains at the points of contact are substantially higher than the effective stress in the soil, calculated according to [2.25].

2.5.3 Effective stress equation for unsaturated soil

Unsaturated soil behaviour is more complex than saturated soil behaviour, with unsaturated soil being viewed as a three-phase system (Fredlund and Morgenstern, 1977). Some of the first proposed effective stress equations, attempted to provide a single-valued stress state variable, with the soil properties incorporated into the description of the variable. This resulted into difficulties, since experimental results have shown that the soil properties do not yield a single-valued relationship to the imposed effective stress, and that the variable should be independent of soil properties (Fredlund and Rahardjo, 1993).

Recently, the effective stress equation has been separated into two independent stress state variables, and the need for the incorporation of soil properties in the stress state description no longer exists. The consideration of the contractile skin as a phase lends support to the theoretical justification for two independent stress state variables, for an unsaturated soil (Fredlund and Morgenstern, 1977).

Bishop et al. (1960) suggested a tentative expression for effective stress for unsaturated soil:

$$s' = (s - u_a) + c(u_a - u_w) \qquad \textbf{[2.26]}$$

with:
- u_a - pore-air pressure
- c - parameter related to the degree of saturation of the soil

The parameter c is a soil parameter with values between zero and unity. The value depends on the saturation, soil type, the moisture hysteric state, and stress conditions. The main disadvantage of this expression is the parameter, c, whose value depends on many factors and is extremely difficult to determine.

Fredlund and Morgenstern (1977) presented a theoretical stress analysis of an unsaturated soil on the basis of multiphase continuum mechanics. The soil particles were assumed to be incompressible and the soil was treated as chemically inert. These assumptions are consistent with those used in saturated soil mechanics.

Fredlund (1973) developed rigorous force equilibrium of a cubical, unsaturated soil element, assuming four independent phases: the soil particles; pore air phase; pore water phase, and air water interface. It was shown that the state of stress is fully defined by 3 stress variables, $(s - u_a)$, $(s - u_w)$ and $(u_a - u_w)$. Any two of the three possible normal stress variables can be used to describe the stress state of an unsaturated soil. Thus, there are three possible combinations that can be used as stress state variables for unsaturated soils. They are:

1) $(s - u_a)$ and $(u_a - u_w)$
2) $(s - u_w)$ and $(u_a - u_w)$
3) $(s - u_a)$ and $(s - u_w)$

The stress state variables can then be used to formulate constitutive equations, to describe the shear strength behaviour, and volume change behaviour of unsaturated soils. This eliminates the need to find a single-valued effective stress equation that is applicable to both shear strength and volume change problems. For most engineering problems the pore-air pressure is atmospheric (zero gauge pressure).

2.5.4 Unsaturated shear strength equation

The wetted area of contact between soil particles decreases with an increase in soil suction. This indicates a relationship between the rate at which shear strength changes in unsaturated conditions, to the wetted area of water contact between the soil particles. Thus, a relationship exists between the SWCC and the shear strength of unsaturated soil (Vanapalli et al. 1996).

At lower values of matric suction, the pore-water pressure acts directly to increase the effective stress by contributing to the shear strength. This condition applies until the air-entry takes place under the applied matric suction. The rate at which suction contributes towards shear strength can be related to the normalised area of water, a_w. The normalised area of water is defined as:

$$a_w = \frac{A_{dw}}{A_{tw}} \qquad \textbf{[2.27]}$$

with:

A_{dw} - the total area of water at 100% saturation [mm^2]

A_{tw} - the total area of water corresponding to any degree of saturation [mm^2]

The normalised area of water, a_w, is a dimensionless number. This number can be visualised as representing the amount of water in the soil. The value of a_w varies from unity at saturation, to a small value under residual state conditions, and zero when the soil is dry. Due to the fact that the normalised water content, Θ, varies in a similar manner, a relationship between the two parameters can be written:

$$a_w = \left(\Theta^k\right) \quad \textbf{[2.28]}$$

with: κ - fitting parameter

The shear strength contribution due to suction, τ_{us}, in terms of the normalised area of water, a_w, can be written as:

$$t_{us} = (u_a - u_w)(a_w \tan f') \quad \textbf{[2.29]}$$

Substituting [2.28] into [2.29], results in [2.30]:

$$t_{us} = (u_a - u_w)\left[\left(\Theta^k\right)(\tan f')\right] \quad \textbf{[2.30]}$$

It was proposed by Vanapalli et al. (1996) that the shear strength of an unsaturated soil (at any given value of suction), be written as the sum of the saturated shear strength and the shear strength contribution due to suction:

$$t = [c' + (s_n - u_a)\tan f'] + (u_a - u_w)\left[\left(\Theta^k\right)(\tan f')\right] \quad \textbf{[2.31]}$$

The first part of the equation is the saturated shear strength when the pore-air pressure, u_a, is equal to the pore-water pressure, u_w. This part of the equation is a function of normal stress, as the shear strength parameters *c'* and *f'* are constant for a saturated soil. The second part of the equation is the shear strength contribution due to suction, which can be predicted using the SWCC.

Extending the same concept, another equation was proposed by Vanapalli et al. (1996) for predicting the shear strength without using the parameter, *k*. The equation is:

$$t = [c' + (s_n - u_a)\tan f'] + (u_a - u_w)\left[(\tan f')\left(\frac{q - q_r}{q_s - q_r}\right)\right] \quad \textbf{[2.32]}$$

with: q_r - residual volumetric water content

Equation [2.34] can also be written in terms of degree of saturation:

$$t = [c' + (s_n - u_a)\tan f'] + (u_a - u_w)\left[(\tan f')\left(\frac{S - S_r}{100 - S_r}\right)\right] \quad \textbf{[2.33]}$$

with: S_r - residual degree of saturation

Both the residual volumetric water content, q_r, and the residual degree of saturation, S_r, can be determined from the SWCC as discussed earlier.

2.5.5 Transition to saturated case

The effective stress equation for saturated soils applies, whether or not the pore pressure is positive or negative, as long as the pores are filled with water. Thus, the shear strength equation for the saturated case can be derived from the unsaturated shear strength equation by inserting $u_a = 0$ and $S = 100$:

$$t = [c' + (s_n - u_a)\tan f'] + (u_a - u_w)\left[(\tan f')\left(\frac{S - S_r}{100 - S_r}\right)\right] = c' + (s_n - u_w)\tan f' \quad \textbf{[2.34]}$$

2.5.6 The shear strength behaviour of unsaturated soils

The function derived by Vanapalli et al. (1996) describes both the linear portion of the shear strength envelope for matric suctions up to the air-entry suction, AES, and the non-linear portion for matric suction in excess of the AES, when the soil starts to desaturate.

Oloo and Fredlund (1996) explained the non-linearity of the shear strength envelope as being the result of the diminishing contribution of matric suction to the shear strength as the water content of the soil approaches the residual water content. At some higher suction, the contribution of matric suction to shear strength diminishes until, the soil reaches the residual state. At any suction higher than the AES, and lower than the residual suction, the slope of the failure envelope would increase as the net normal stress is increased.

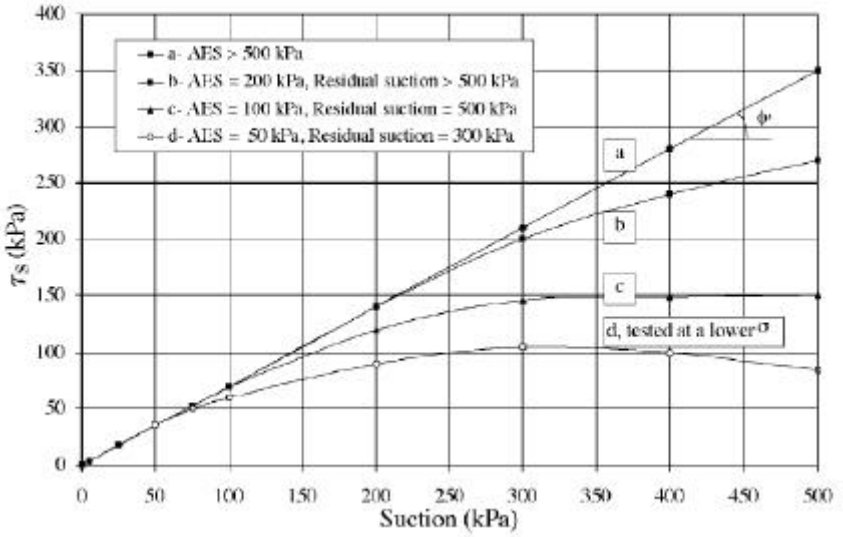

Figure 2.12: Graphical representation of the shape of the failure envelope with respect to matric suction for various soils (Rassam et al. 2002)

In unsaturated soils, the pore-water pressure acts as a tensile or hydraulic stress. If, however, the pore water pressure exceeds the mechanical stress applied (due to heating), changes in the inter-, intra-aggregate and particle bonding forces, results in an alteration of the strength properties. The maximum strength of soil samples either depends on the maximum pre-stressed, or on the most negative pore water pressure applied. It can thus be stated that soil hydraulic properties are only valid for a given mechanical, hydraulic and thermal stress situation. It can, therefore, only be used at that defined conditions (Herkal et al., 1995).

2.6 Soil Suction and The Critical State

2.6.1 Introduction

Geotechnical analyses often require an understanding of the development or change in the stress state, resulting from various stress patterns. These changes can be visualised by drawing a series of Mohr circles that follows the loading process. However, the pattern of stress state change may become confusing when the load pattern is complex. It is, therefore, better to use only one stress point on a Mohr circle to represent the stress state in the soil (Fredlund and Rahardjo 1993).

2.6.2 Stress Points

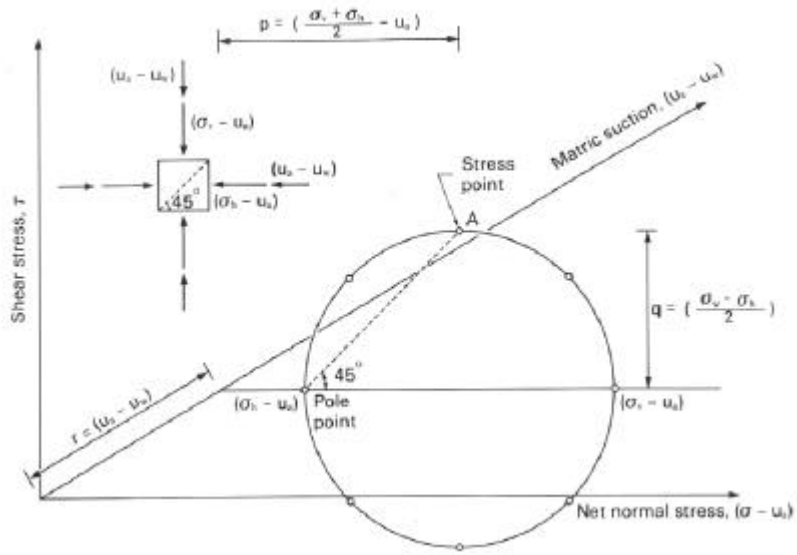

Figure 2.13: Representative stress point for an extended Mohr circle (Fredlund and Rahardjo, 1993).

Figure 2.13 shows a two-dimensional Mohr circle, with the vertical and horizontal planes being principal planes. The stress point representing the Mohr circle has the coordinates of (p, q, r), with:

$$p = \left(\frac{s_1 + s_3}{2} - u_a \right) \quad \textbf{[2.35]}$$

$$q = \left(\frac{s_1 - s_3}{2} \right) \quad \textbf{[2.36]}$$

$$r = (u_a - u_w) \quad \textbf{[2.37]}$$

with:

(s_1 - u_a) - vertical net normal stress

($s_2 - u_a$) - horizontal normal stress

($u_a - u_w$) - matric suction

The q-coordinate is one half the deviator stress (s_1 - s_3). The selected stress point represents the state of stress on a plane with an orientation of 45° from the principal planes (Figure 2.13).

The vertical net normal stress for the condition shown in Figure 2.11 is greater than the horizontal net normal stress, resulting in a positive *q*-coordinate. For hydrostatic or isotropic stress states the *q*-coordinate is equal to zero due to the absence of shear stresses (Fredlund and Rahardjo, 1993).

2.6.3 Stress paths

Stress paths are used to describe the change in the stress state of a soil. The stress path is a curve that is drawn through the stress points for successive stress states (Lambe 1967). The principle of stress paths can be explained by firstly, considering a soil element where initially the horizontal net normal stress, $(s_3 - u_a)$, is equal to the vertical net normal stress, $(s_1 - u_a)$, at a particular matric suction value.

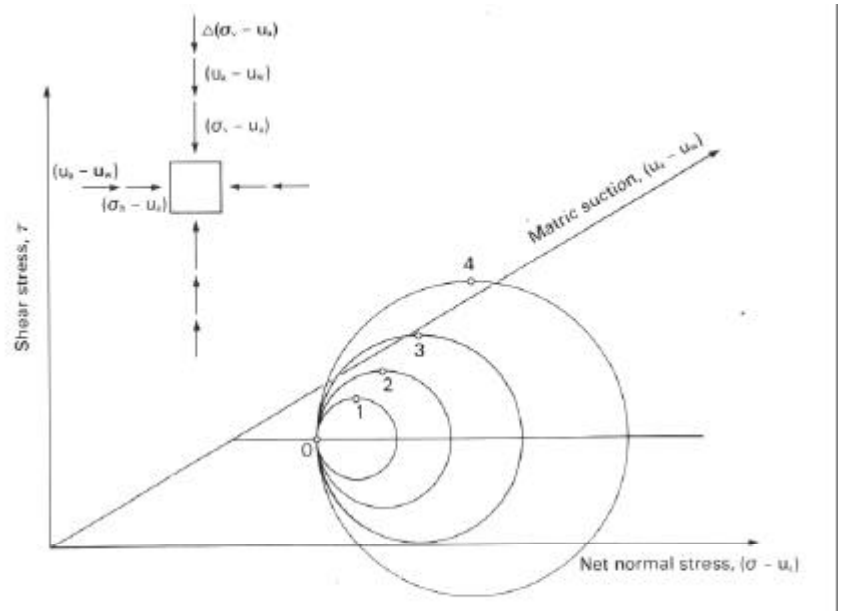

Figure 2.14: A series of Mohr circles (Fredlund and Rahardjo, 1993)

This stress state is represented by point 0 in Figure 2.14. As the vertical net normal stress is increased, the Mohr circle expands, moving from point 0 to points 1, 2, 3, 4, etc. These stress points represent a continuous series of Mohr circles or stress states. The stress path for this loading condition is shown in Figure 2.15, where the stress points are plotted on the *p-q-r* diagram.

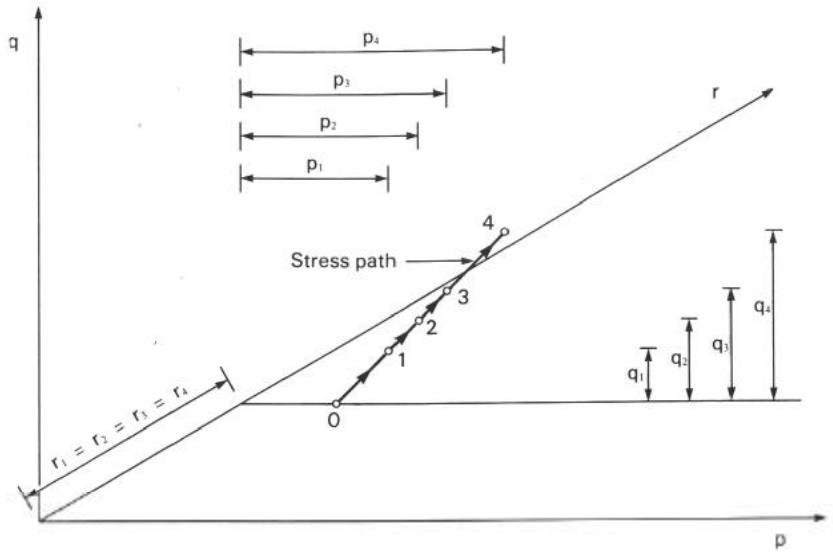

Figure 2.15: A stress path for a series of stress states (Fredlund and Rahardjo, 1993)

The *p*-, *q*- and *r*-coordinates represent the net normal stress, the shear stress, and the matric suction at each stage of loading. The stress path is established by joining the stress points that results in a linear or curved path, depending on the loading pattern. The stress path shown in Figure 2.15 illustrates a loading condition where the matric suction is maintained constant.

The r-coordinate is generally considered to be equal to the pore-water pressure, with the pore-air pressure in the field usually equal to atmospheric pressure. The matric suction can, therefore, be plotted as being equivalent in magnitude to the pore-water pressure.

2.7 Gold Mine Tailings dams

2.7.1 Introduction

Tailings can be defined as a by-product of the extraction process, with tailings consisting of finely ground and chemically treated rock flower in a slurry with process water (Vermeulen, 2000). Tailings consist of sand and silt-sized particles of milled rock, from which the mineral values have been removed. Under normal circumstances, tailings contain hardly any clay-size particles, and when sheared, behave as a frictional cohesion-less material with frictional angles in the range of 29-35°.

2.7.2 Ore processing

Fundamental to an understanding of the nature of tailings is a basic knowledge of how they are produced. Ore that has been removed from its natural bed, by means of drilling and blasting, is transported underground through ore passes via chute's, and tramways and is loaded into skips, which are hoisted to the surface (Vick, 1983).

Due to the fact that different parts of the operation of mining and milling are performed at different rates, the ore is stored on the surface in bins, tanks or stockpiles. This provides a reservoir of material between the successive processes. Storage also has the advantage of allowing blending of different ores, as to provide a consistent feed to the mill (Wills, 1985).

Ore entering the mill from the mine normally contains a small proportion of material, which is potentially harmful to the mill equipment and processes. For example, large pieces of iron and steel broken off from mine machinery can jam in the crushers, and are thus removed by either hand sorting or with the use of electron magnets. Metal detectors can also be used.

Central to most ore milling procedures are the initial steps of crushing and grinding. Crushing is usually performed in stages, with the aim of reducing rock fragments from mine-run size to a size, that can be accepted as feed to grinding equipment. Jaw and gyratory crushers are common forms of primary crushing equipment, with Gyratory crushers being used for secondary crushing.

Grinding further reduces the size of the fragments produced by crushing, by means of rod mills and ball mills. These units operate by tumbling crushed ore, together with heavy steel balls or rods, in a rotating drum. Grinding represents the final stage in the physical reduction of ore from rock to tailing size (Vick, 1983).

Thereafter, concentration of those particles that contain the highest mineral value is usually performed by one of several processes. The type of concentration varies according to ore type and three general classes in use are:

- gravity separation
- magnetic separation
- froth flotation

Separation and removal of mineral values in the concentrate leaves the remaining barren particles as tailings. Further optional processes may include leaching or heating. The final stage in the process is, recovering excess water from the tailings, in preparation for pumping the tailings slurry to the disposal impoundment. The most common means of dewatering is by means of thickeners. This consists of a tank with rotating arms, that conveys the settled tailings solids to the centre of the tank, where they are collected and pumped to the disposal area. Hydrocyclones are also used for dewatering (Vick, 1983).

2.7.3 Tailings transport, discharge and depositioning

Transport of tailings commonly commences through pipes by gravity flow, either with or without pumping as dictated by relative elevation of the mill and the tailings impoundment. Deposition of an above-water tailings beach, around the perimeter of a tailings dam is usually desirable. Beach depositioning may be accomplished by either open-ended pipes or spigotting.

Following the discharge of the tailings into the impoundment area, the coarser particles tend to settle from suspension, relatively near the point of discharge. Remaining coarse particles, finer particles, and colloidal particles are carried further to the decant pond, where they eventually sediment in the standing water.

For most types of tailings, the beach slopes downward to the decant pond on an average grade of 0.5-2.0% within the first 15m. At more distant points on exposed beaches, the beach slope may flatten to as little as 0.1%. At these locations depositional processes may come to resemble natural stream channel sedimentation.

The depositional processes used produces highly heterogeneous beach deposits. In the vertical direction, tailings beach deposits are frequently layered, with percent fines typically varying as much as 10-20% over several centimetres in thickness. If discharge points are widely spaced, variations in fines content of 50% can occur over short vertical distances. Such extreme layering produced by thin slimes layers, within otherwise sandy beaches, results from periodic encroachment of ponded water onto the beach where thin layers of fines settle from suspension.

Horizontal variability is usually also significant, with coarser particles settling from the slurry as they move over the beach. The finer suspended particles (slimes),only settle after the slurry has reached the still water of the decant pond.

Sedimentation of slimes from suspension in ponded water does not involve sorting, but is a relatively straightforward process of vertical settling. The rate of slimes sedimentation can have important effects on the size of the decant pond necessary for water clarification, and the quantity of water available for mill recycle.

Where possible, water is decanted with the use of decant towers, siphons, or pumps from the pool, and returned to the mill for re-use. Decant towers are most commonly used in Southern Africa, and consist of vertical concrete risers with intake ports that extend from the bottom of the impoundment upward through the tailings deposit. An example of a decant tower is shown in Figure 2.14. The use of decant towers, requires a concrete conduit extending beneath the tailings deposit, and through the dam to exit beyond its toe (Vick, 1987).

Figure 2.16: Decant tower at Mispah tailings dam

2.7.4 Tailings disposal methods

Surface disposal of tailings, makes use of dams and embankments of various types, to form impoundments that retain both the tailings and mill effluent. Surface impoundments are formed by either water-retention dams or raised embankments. Water-retention type dams are constructed to their full height prior to the beginning of discharge, where the raised embankments construction is staged over the life of the impoundment. Surface embankments in Southern Africa most commonly consist of raised embankments.

Raised embankments begin initially with a starter dyke, constructed usually of natural soil borrow, and sized to impound the initial two years' mill tailings output. This includes appropriate allowances for storage of flood inflows. The advantages of raised embankments are that the expenditures is distributed over the life of the impoundment, and that the total volume of fill required for the ultimate embankment, does not need to be available initially.

Raised embankments, regardless of the type of material used in their construction, fall generally into four classes:

- upstream
- downstream
- centreline
- daywall-nightpan paddock

These designations refer to the direction in which the embankment crest moves, in relation to its initial starter dike position as the embankment increases in height.

Upstream Method

Initially a started dike is constructed, and tailings are discharged from the crest to form a beach. The beach then becomes the foundation for a second perimeter dike (Figure 2.17). Central to the application of the upstream method, is that the tailings form a reasonable competent beach for supporting the perimeter dike. The major advantage of this method is the cost and simplicity, since only minimal volumes of mechanically placed fill are necessary for the construction of the perimeter dikes, and that large embankment heights can be obtained at very low costs.

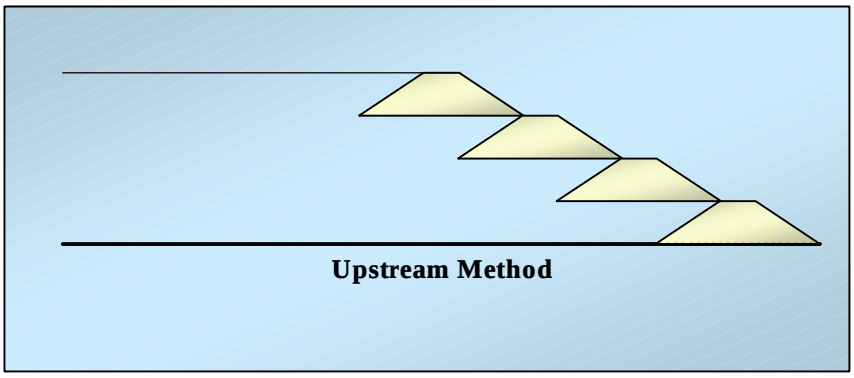

Figure 2.17: Upstream depositional method (Vick,1987)

The rates at which upstream embankments can be safely raised are determined by the rate of mill tailings production, and topographic configuration of the impoundment site. Rapid rates of height increases, can produce excess pore pressures within the deposit that can be potentially dangerous. It will, thus, be necessary to slow down the rates of height increase, rendering enough time for the dissipation of the excess pore water pressure. In Southern Africa the upstream method is most commonly used, due to the semi-arid conditions reigning in most parts of the country, and due to the limitations on land use for the purpose of tailings storage.

Downstream Method

Initially, tailings are discharged behind a starter dike. Subsequent raises are constructed by placing embankment fill on the downstream slope of the previous raise (Figure 2.18). This method is well suited to conditions where significant storage of water, along with the tailings, is necessary since the phreatic surface can be maintained at low levels within the embankment. The raising rates are essentially unrestricted because the downstream raises are structurally independent of the spigotted tailings deposit.

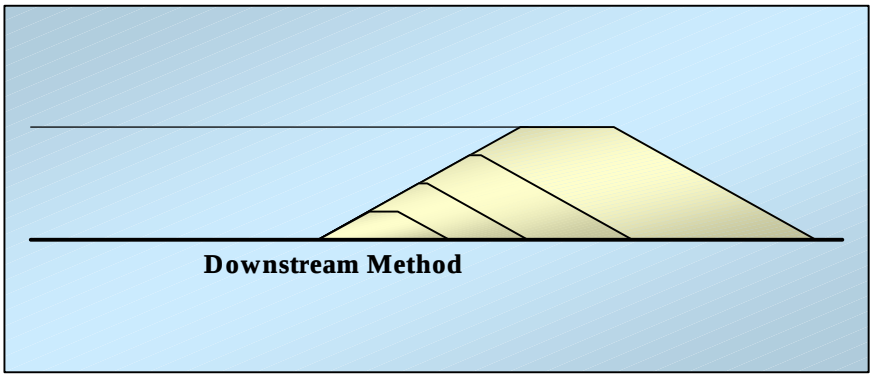

Figure 2.18: Downstream depositional method (Vick, 1987)

This method, however, requires careful, advanced planning because the toe of the dam progresses outwards as the height increases, and thus the ultimate height of the embankment is often determined by the space left for the toe. The main disadvantage of this method is that comparatively large volumes of embankment fill are required.

Centreline Method

Initially a started dike is constructed and tailings is deposited from the dike crest to form a beach. Subsequent raises are constructed by placing fill onto the beach and onto the downstream slope of the previous raise (Figure 2.19). The centrelines of the raises are coincident as the embankment progresses upward. Unlike the upstream embankments, this method cannot be used for permanent storage of large depths of water.

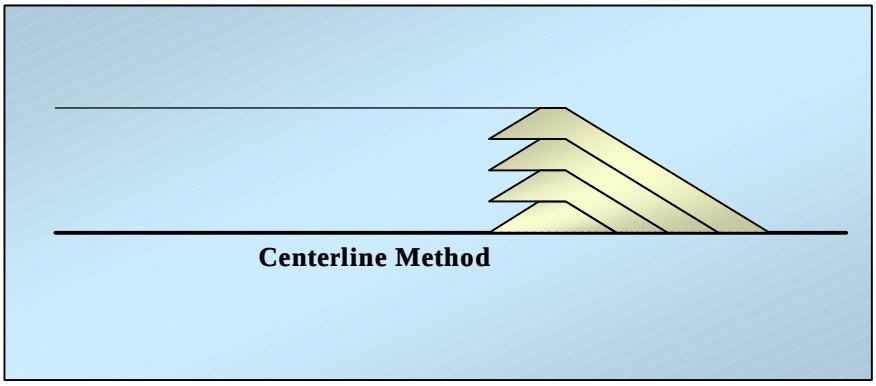

Figure 2.19: Centerline disposal method (Vick, 1987)

The overall raising rate is not generally restricted by considerations related to pore pressure dissipation, however the height of fill placed upon the beach in the upstream portion of the embankment is sometimes restricted by the undrained shear strength of the beached materials.

Daywall-Nightpan Paddock System

Tailings dams in South Africa are usually constructed using the Daywall-Nightpan Paddock system. This form of construction relies on a temperate to semi-arid climate and low water table conditions, or acceptable evaporation rates, to improve the properties of the deposited material. Upstream, downstream, and centreline configurations may be employed.

The upstream paddock system is almost used exclusively in South Africa, with its prevailing dry and hot climate in the mining areas. Compacted earth starter walls and under-drainage are initially constructed, to ensure that the rate-of-rise does not exceed 2.5 m/yr by the time the starter wall is overtopped. The tailings then take over from the starter wall as the main embankment wall. The dam is divided into two sections, the perimeter or daywall and the interior or night area, also known as the nightpan (Figure 2.20). The daywall is designed to provide sufficient freeboard, to retain the accumulated water from deposited tailings, and that from the design storm.

The daywall is generally 10-30m at an average slope of 35°, and is sectioned into paddocks around the perimeter. Each paddock is filled from its midpoint by a delivery station. Wall raising is done by tractor plough or by shovel packing. During the day, tailings slurry is delivered into these daywall paddocks to a depth of about 150-200mm. The excess water is decanted into the nightpan through temporary pipes inside the inner wall of the daywall.

During the night, tailings is discharged into the nightpan from delivery stations located just inside the daywall. The excess water is decanted off the next day, with the use of a penstock decant or barge pump.

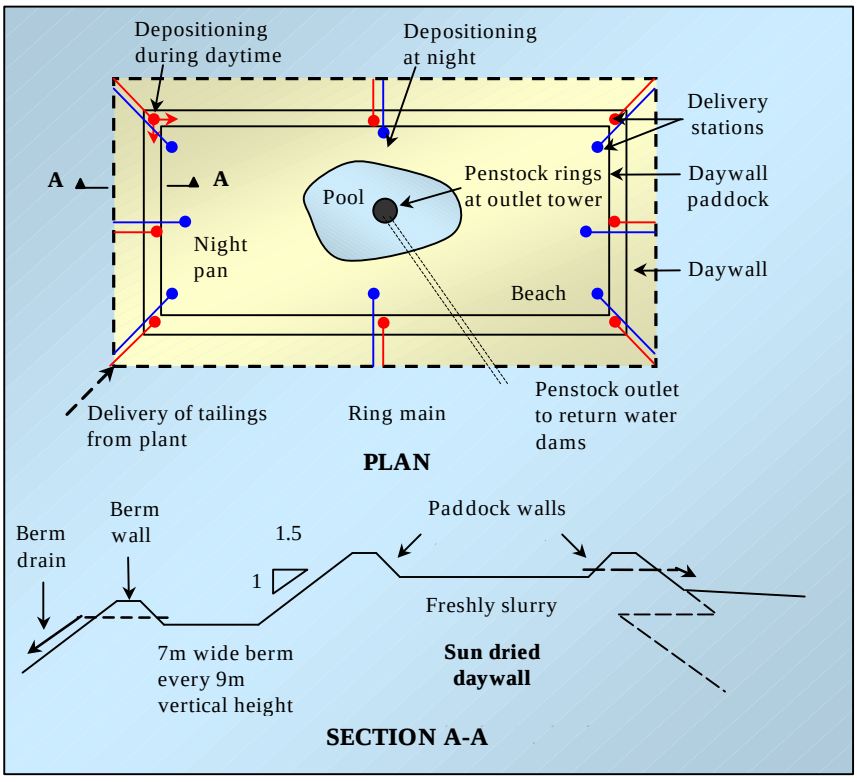

Figure 2.20: Daywall-Nightpan Paddock System (Wagener, 1997)

2.7.5 Engineering behaviour of tailings

The engineering behaviour of tailings is determined by the characteristics of the material itself and by the nature of the deposit. Tailings depositioning by spigotting, results in two distinct classes of material: sands deposited by hydraulic sorting, and finer grained slimes deposited by sedimentation.

Sand tailings generally shares the engineering behaviour of loose to medium-dense deposits of natural sand. Slimes on the other hand, are complex materials. They may exhibit properties similar to natural sands in some cases, natural clays in others, or a combination of both.

Compressibility is not so widely varying, but tailings is generally more compressible than corresponding types of natural soils due to the looser state they usually assume upon deposition. Consolidation characteristics are a function of both permeability, and compressibility, and as a result are very complex. Consolidation characteristics are important in evaluating the time rate of pore pressure dissipation, within the tailings deposit. The shear strength of tailings is often higher than that for similar natural soils. This is due to the high degree of particle angularity exhibited by most tailings.

3 EXPERIMENTAL METHOD

3.1 Introduction

The rate of rise, of tailings dams, is primarily influenced by the time it takes the tailings material in the daywall to obtain the required shear strength, through drying and desiccation. Therefore, a method was devised to determine the shear strength of drying tailings material with the use of the suction probe.

The suction readings, Y, obtained from the probe at different depths, are incorporated into Equation [2.32], with the corresponding values of volumetric water content, q, to obtain the shear strength during the experiment. Before this can be done it is, however, necessary to obtain the residual volumetric water content of the tailings from the Mispah Residue dam. This is achieved by conducting a trough test to obtain portions of the Soil Water Characteristic Curve. These portions are extended with the use of curve fitting to obtain the full SWCC. From the full SWCC the residual volumetric water content is determined. Insitu tests are conducted to validate the shear strength as a function of time calculated with the proposed methods.

3.2 Material Used

Gold tailings dam material is used as the test material during experimental work. The material is obtained from Vaal Reef Operation's Mispah residue dam. The Mispah residue dam is the latest addition to the Vaal River Operations Mine impoundment structures. The Vaal River Operations is situated next to the Vaal River, bordering on the Northwest Province and the Freestate province, between Potchefstroom and Klerksdorp. The mine operates mainly in the Vaal Reef on the Witwatersrand Complex.

Mispah dam was commissioned in November 1993. This dam receives approximately 236,228 tons of tailings per month from the No. 8 Shaft, Gold Processing Plant. The dam is situated on a thin Karoo Cover over Dolomite. The dam is at present (June 2003) 18.9m high with a planned final height of 60m.

The average rate of rise is 1.53 meters per year, or approximately 127.5 mm per month. The distance between the delivery points is approximately 250 meters, with depositioning taking place every 14 to 16 days. The slope of the walls is approximately 34°, which corresponds well to the angle of response, determined for the tailings material by Vermeulen (2001).

At Mispah residue dam, a set of insitu tests was conducted out at three locations on the daywall. Bulk samples, for laboratory testing, were also collected from the daywall interface. A sample of the Mispah gold tailings was then sent to a commercial laboratory for testing, in order to obtain the required soil parameters and grading curves. These results, however, proofed to be faulty and incomplete. It was, thus, decided to use the soil parameters, and grading curves obtained through extensive research done on the composition and state of Mispah gold tailings, by Vermeulen (2001). Table 3.1 provides a summary of the parameters:

Table 3.1: Soil parameters for Mispah whole tailings (Vermeulen 2001):

SOIL PARAMETERS					
Description	**Symbol**	**Value**	**Description**	**Symbol**	**Value**
Specific Gravity	G_s	2.74	Cohesion	c [kPa]	0
Liquid Limit	LL [%]	29	Grading (Coarse Silt)	D_{10} [µm]	2
Plastic Limit	PL [%]	22		D_{30} [µm]	10
Plasticity Index	PI	7		D_{50} [µm]	30
Angle of Response	ϕ [deg]	34.5		D_{90} [µm]	125

3.3 Equipment

3.3.1 Suction probe

The direct measurement of suction pressures is achieved with the use of a miniature suction probe (Figure 2.5), which is very similar to the mid-plane suction probe designed by Theron (2000). The only difference that exists in comparison to the original probe design, is the incorporation of a 1 MPa pressure transducer, as opposed to the 200kPa transducer. Some changes were also made to the dimensions of the probe body. The new design makes maintenance of the electrical wiring possible, and the smaller water reservoir increases the measuring range.

Section 2.3.5 discusses how the suction probe operates and how it can be used to measure the change in matric suction (directly in the drying tailings material), by placing the face of the ceramic on the material. In order to ensure that accurate readings are obtained, the ceramic and reservoir need to be completely saturated and calibrated.

Saturation

To ensure a good response time for the probe, it is completely saturated before use. The probe contains a 300kPa ceramic tip with an approximate air entry value of between 300 and 400kPa. To saturate the probe, it is placed into a triaxial cell, completely filled with de-aired water. The pressure inside the cell is controlled with a GDS pressure controller (Figure 3.1). The same procedure followed by Theron (2000) is incorporated for the saturation of the probe.

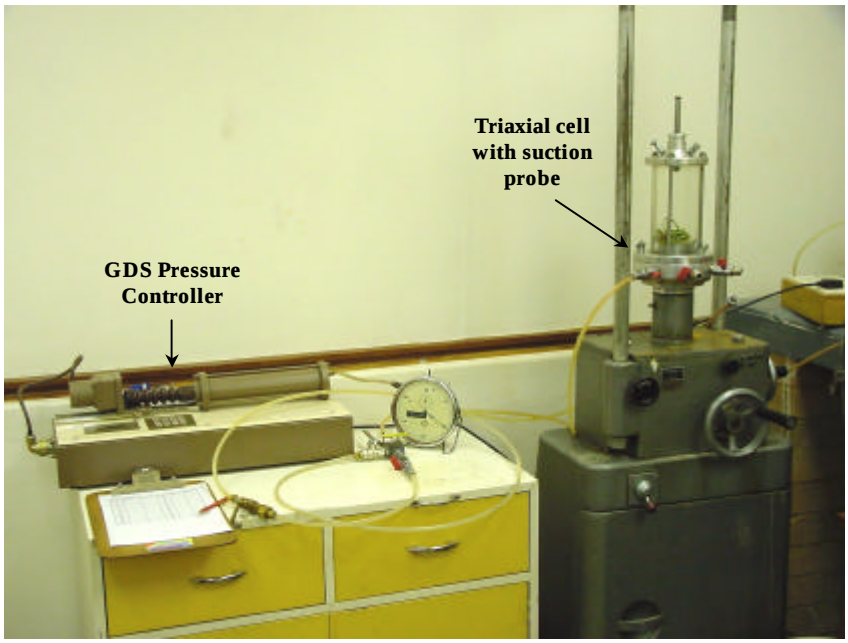

Figure 3.1: Saturation of miniature suction probe

By cycling the pressure inside the cell continuously, between 500 and 1000kPa, full saturation of the ceramic tip and reservoir is ensured. Complete saturation results in an immediate response from the probe. To maintain the probe in a saturated state, the probe has to be stored in a container filled with de-aired water.

Calibration

To ensure a 1:1 relationship between the measured and actual suctions within the sample, it is necessary to calibrate the suction probe. The suction probe is connected to the GDS pressure controller, with watertight connections, for the calibration procedure.

An available line from the GDS pressure controller is used for the dissipation of excess pressures, in order to reach a zero atmospheric pressure, in both the GDS and the suction probe. The GDS can apply positive water pressures larger than 350kPa, but can only apply negative pressures to a maximum of -60kPa (Limited by cavitation).

The calibration procedure involves raising the pressure, using the GDS, in increments of 50kPa to 350kPa and lowering the pressure to zero in increments of 50kPa, while taking measurements of the pressure from the probe at each target value. The probe is then zeroed, and the GDS pressure lowered to -60kPa in increments of 20kPa and increased again to zero. Figure 3.2 indicates a 1:1 relationship between the measured and actual suction value.

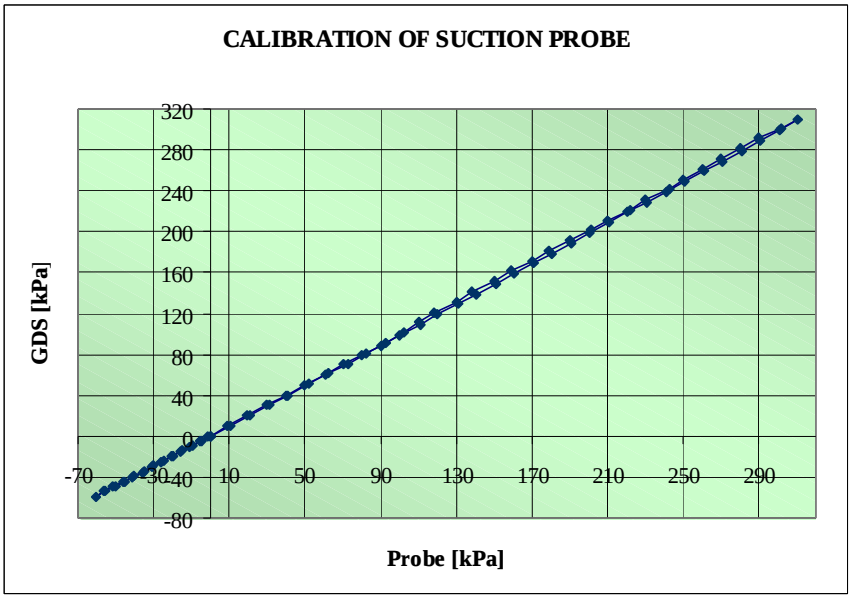

Figure 3.2: Calibration of the suction probe

Placement

After the probe is saturated and calibrated, it is ready to measure suctions. The following two requirements need to be met to ensure a fast response time:

- Complete saturation of the probe.
- A good hydraulic contact between the probe's ceramic tip and the tailings material being measured.

It is fairly easy to achieve a good bond while the material is still moist and soft, but as the material dries out, it becomes more difficult to obtain a good bond. A different approach is used for each of the different types of experiments conducted. This is to ensure that suitable hydraulic contact between the probe's ceramic tip and the tested tailings material. These different methods will be subsequently discussed, with each of the different experimental procedures.

3.3.2 Shrinkage troughs

The method used to determine the volumetric water content versus suction relationship (SWCC), for the particular tailings materials, is based on the work done by Van Heerden (2001). This method incorporates the use of so called shrinkage troughs. This method is modified in order to increase measurement accuracy for this particular application, as indicated in Figure 3.3.

Figure 3.3: Shrinkage troughs

The modified shrinkage troughs are made from 53 mm diameter uPVC conduit of about 462 mm lengths, cut in half along the length. The larger sized trough improves the accuracy of length, and depth measurements during the drying process. The volume changes are then determined using the equations derived by Van Heerden (2001) for the particular trough geometry.

3.3.3 Drying box

The main purpose of a drying box is the containment of the tailings material for measurement purposes (Figure 3.4). A drying box was designed to simulate a section of a daywall, allowing vertical seepage of the water under gravity. Since horizontal seepage plays a lesser role in the daywall, the sides of the drying box are made of non-pervious material. To observe the layering and the drying of the material, two sides of the box are constructed using glass.

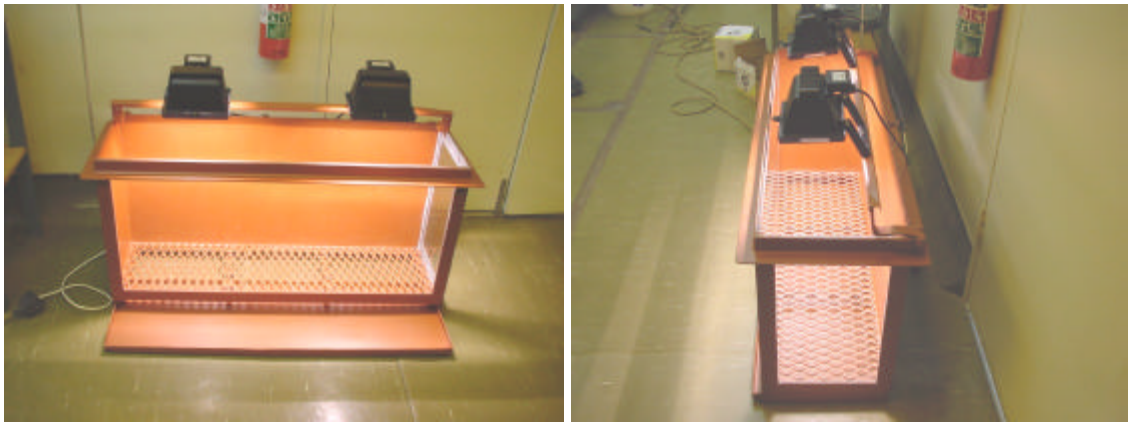

Figure 3.4: Drying Box

The base area of the box is 305 x 1013 mm and is made from expanded metal. The box depth is 450 mm, to accommodate the pouring of two 150 mm thick material layers (lifts). The expanded metal is then covered with a grade A2 Bidim Geotextile, which is fixed to the box with the use of silicon (Figure 3.5).

Figure 3.5: Bidim Geotextile cover

The Bidim was designed using the grading of the Mispah whole tailings and allowed for free drainage of the water under gravity, while preventing the movement of tailing particles. Table 3.2 provides a summary of the Bidim Grade A2 specification:

Table 3.2: Specifications of Grade A2 Bidim Geotextile

SPECIFICATIONS		
Property	**Value**	**Code**
Permeability	2.54×10^{-4}	SABS 0221-88
Porosity	$n \geq 60\%$	GTS
Trapezoidal tear	175 N	ASTM D5433-85
Penetration load	1 kN	SABS 0221-88
Puncture resistance	32 mm	CPA
Tensile strength	7 kN / m	SABS 0221-88
Pore size	$100\ \mu m < O_{95w} < 250\ \mu m$	

To increase the heat energy available in order to allow for evaporation to take place, two 250 W Halogen lights are connected to a moveable arm 300 mm above the top of the box. A catchment pan is placed underneath the expanded metal base to catch the water seeping through the Bidim. This allows for the measurement of the moisture loss due to seepage. To obtain readings of the height of water level, and settlement, a stainless steel ruler is fastened to the front of the drying box.

The geometry of the drying box allows for only two consecutive lifts to take place. Thereafter, the material is removed and both the Bidim Geotextile and the drying box are cleaned thoroughly and left to dry at room temperature. This is due to the sensitivity of the Bidim to heat exposure.

3.3.4 Tailings dispenser

To prevent damage to the Bidim Geotextile, a dispenser is constructed to evenly dispense the tailings slurry into the drying box (Figure 3.6). The dispenser consists of a 25 l container fastened to a ball valve and 20 mm PVC piping. The function of the ball valve is to regulate the flow of the slurry and to close off the system.

Figure 3.6: Tailings dispenser

The piping is shaped into an H-section and reinforced with metal strips. The dispensing of the material takes place through the bottom of the 20 mm PVC pipes forming the H-section. The pipes were drilled with a 5 mm drill at a spacing of 10 cm. The H-section is placed on top of the drying box before the dispensing of the slurry commences under gravity.

3.3.5 Load cell

In order to determine the weight loss, due to evaporation and drainage, it is necessary to weigh the drying box with the tailings material inside. A 1 kN load cell is used to weigh the system by fixing the load cell to the drying box, with the use of cables. The drying box is raised using a 2 ton overhead crane hooked to the cables. This results in the load cell carrying the load. The load cell output is amplified and displayed by a DMD 20 amplifier with a resolution of 0.1kg.

3.3.6 Tube samplers

In order to determine the saturation of the tailings material, it is critical that an undisturbed sample be obtained of a known volume and preserved moisture content. For this purpose two stainless steel tube samplers are used (Figure 3.7). The larger tube sampler is used for site sampling and is identical to the one designed and manufactured by Vermeulen (2001). The smaller tube sampler is used to obtain samples during the laboratory testing of the tailings material.

The two samplers consist mainly of two parts: the top-cap and the sampling tube. The top-cap is fitted with a Klinger valve that serves as a vent when pushing the sampler into the material. The top cap is lined with a rubber mat that provides a good seal between the top-cap and the tube when the sampler is extracted with the vent closed. In a case where it was not possible to extract the sampler without disturbing the sample, the material around the sampler needed to be removed.

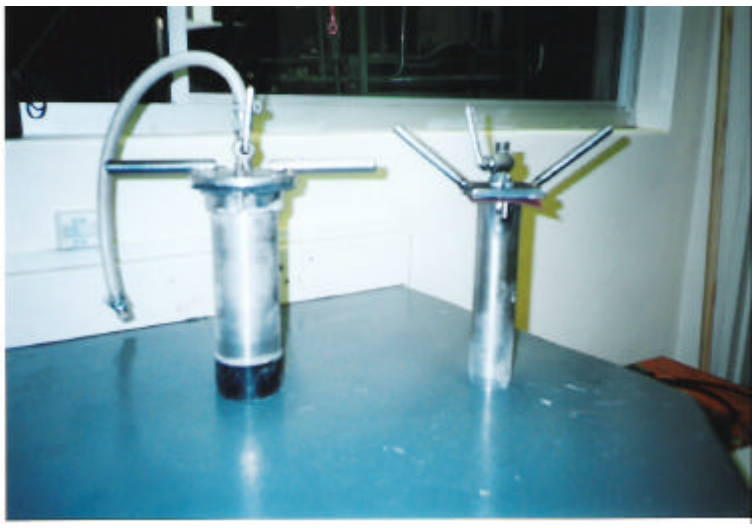

Figure 3.7: Tube samplers

The larger sampling tube is 230 mm long with an inside diameter of 75 mm and an outside diameter of 76 mm, resulting in a 1 mm wall thickness over the driving length. The whole sampler is machined from a solid stainless steel tube and is polished on the inside for smoothness. The smaller tube sampler is 232 mm long with an inside diameter of 40.4 mm and outside diameter of 43.4, resulting in a 3 mm wall thickness.

The wall thickness of the smaller tube sampler is limited by the fact that it is manufactured from seamless stainless steel tubing. Operation of the samplers are according to the guidelines of good quality undisturbed sampling, as proposed by Clayton et al. (1995).

3.3.7 Hand Vane Shear

The hand Vane Shear Test basically consisted of pushing a four-bladed vane, mounted on a solid rod, into the soil and rotating it from the surface. Vane shear tests are carried out in the field and in the laboratory. In its conventional form, the vane has four rectangular blades and a height to diameter ratio of two.

The hand vain shear instrument is used to validate the shear strength as a function of time calculated with the proposed methods (Figure 3.8), it also renders an estimated ultimate shear strength. There are limitations when using the vane shear. These include the tests only being able to be conducted in soft, saturated, cohesive soils that won't permit drainage, or that won't dilate during the test period. Due to the anisotropy of the deposited tailings material, and the presence of silt, the readings obtained can be erroneous to some degree, but since the vane shear is only used to validate the calculated shear strengths, it is assumed to be negligible.

The pointer is rotated clockwise to come to rest against the dog plate, in order to zero the instrument. The vane is then pushed slowly (with a single thrust), into the material with as little sideways movement and rotation as possible, to a depth of about 6 - 8 cm. Holding the instrument in one hand, the head is rotated clockwise, at a speed equivalent to a complete revolution per minute. After the sample is sheared, the pointer remains at the reading of the shear strength determined from the corresponding vane spindle used.

Figure 3.8: Hand vane shear

Two vane spindle sizes are used during the testing. The 32 mm spindle is used in softer material with shear strengths up to 30 kPa. At this strength, the material is still relatively soft. After the material's strength has exceeded 30 kPa, the 19 mm spindle is used for the shear strength measurements.

3.3.8 Base plate stabiliser

To ensure good hydraulic contact between the suction probe and the tailings surface in the field, a stabilizing mechanism is constructed (Figure 3.9). A triangular metal base plate, with three steel legs pinned into the surface, prevents relative movement between the tailing's surface and the probe. The probe is fastened to the base plate by a clamp, which allows free movement of the probe in any direction.

A rubber membrane between the probe and clamp surface increases the friction for further stability. Adding additional mass to the one clamp allows for the probe to be forced against the surface by gravity. The wiring between the probe and the amplifier is fastened to the second arm.

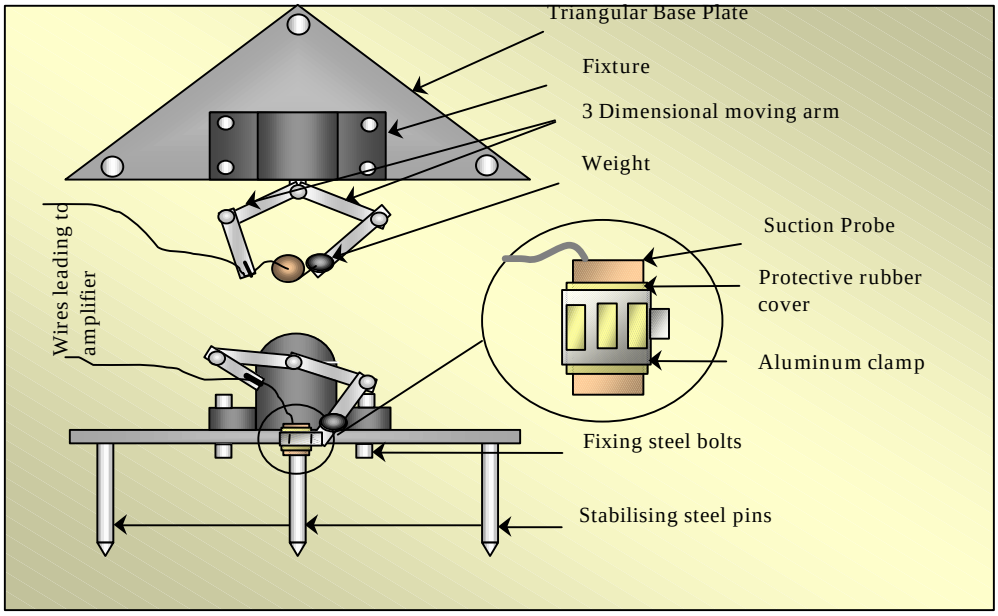

Figure 3.9: Base plate stabiliser

3.3.9 Probe holder

The purpose of the probe holder is to hold the suction probe in position while suction pressures are taken at different depths (Figure 3.10). The holder's shaft is made from threaded rod that is wound up, or downwards, through a nut with the use of the handle. The nut is fastened to a wooden support to provide stability. A clamp is fastened to the threaded rod by means of two washers and nuts, allowing the rod to rotate inside the nut without rotation of the probe. This clamp is used to hold the probe.

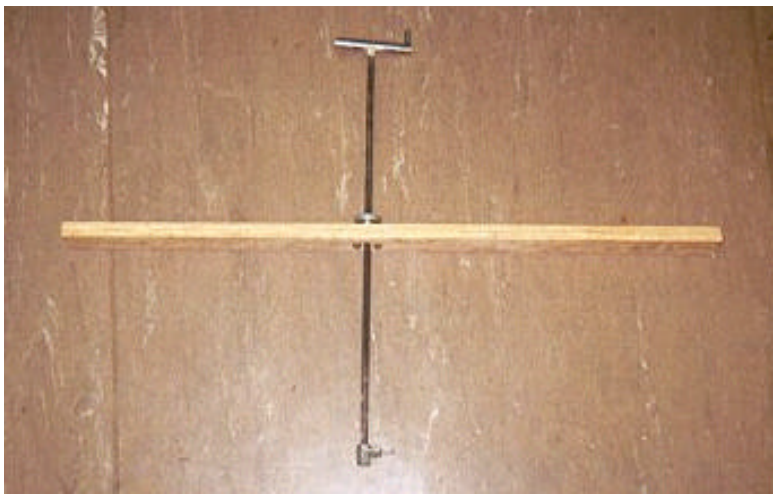

Figure 3.10: Probe holder

3.4 Trough Test

Before the commencement of the experiment the saturation and calibration of the probe was completed. All the needed equipment for the experiment had to be at hand.

3.4.1 Preparation of material and trough

The preparation procedure corresponds to the method used by Van Heerden (2002). The trough is thoroughly cleaned before it is lined with Vaseline, which allows for free movement of the shrinking material. Thereafter, the trough is weighed, M_{trough}.

A known mass of dried tailings is thoroughly mixed with distilled water until a moisture content of approximately 45% is reached. The tailings slurry is then poured into the trough until it is nearly filled. Thereafter, the remaining mixture is weighed and placed into the oven to dry. To avoid the entrapment of any air bubbles, the trough is tapped a few times.

3.4.2 Measurement of change in mass, suction and volume

After preparing of the trough and material, the trough is placed onto a stand. The stand is used to hold the probe in position, while the drying of the material commences. To ensure that the mass readings are taken at the same time as the suction readings, the stand and the trough are placed on an accurate scale (Figure 3.11). Readings of the suction, mass, and volume are taken hourly until the first suction pressures develop and, thereafter, every 30 min.

To increase the heat energy available in order to allow for evaporation to take place, a 150 W Halogen light is fastened approximately 1 m above the sample. This helps speed up the drying of the material in the modified trough, and also ensure the same ambient conditions as in the drying box.

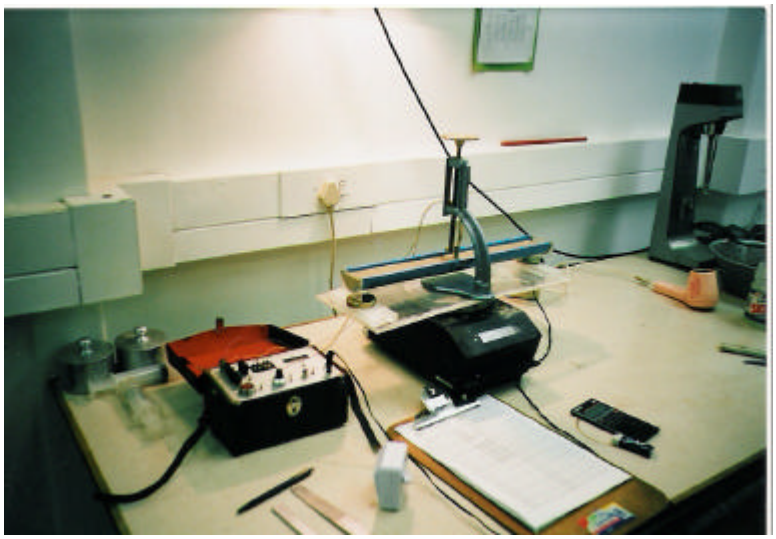

Figure 3.11: Experimental set-up for the determination of the SWCC

3.4.3 Determination of volume-mass relations

After the remaining mixture has dried out completely, it is possible to determine the mass of solids that are not poured into the trough. This renders the mass of solids inside the trough. With the mass of solids (M_s) known, it is possible to determine the initial moisture content (w_0), at the start of experiment, with the following equation:

$$w_0 = \frac{\left(M_i - M_{trough}\right)}{M_s} - 1 \qquad \textbf{[3.1]}$$

with:

M_s - mass of solids [kg]

M_i - initial mass of sample [kg]

M_{trough} - mass of trough [kg]

w_0 - initial moisture content [%]

With the mass of solids staying constant, it is possible to calculate the water content at each stage with:

$$w = \frac{\left(M_{sample} - M_{trough} - M_s\right)}{M_s} = \frac{M_w}{M_s} \qquad \textbf{[3.2]}$$

with:

M_{sample} - mass of sample taken at every stage [kg]

M_w - mass of water at every stage [kg]

Since the volume measurements are not taken at the same time as the mass and suction readings, it is necessary to make use of the 2nd order polynomial function derived by Van Heerden (2002), with the use of regression analysis. With the volume and moisture content known for the sample at a certain time, it is possible to determine the void ratio, *e*, and degree of saturation, *S*, with the following equations:

$$e = \frac{\left(V_{sample} \times G_s \times r_w\right)}{M_s} - 1 \qquad \textbf{[3.3]}$$

$$S = \frac{\left(G_s \times w\right)}{e} \qquad \textbf{[3.4]}$$

with:

V_{sample} - volume of the sample [cm^3]

G_s - specific gravity [2.74]

r_w - density of water [0.000981 kg/cm^3]

With both the void ratio and the degree of saturation known it is possible to calculate the volumetric water content, *q*, with [2.12].

3.4.4 Determination of SWCC

It is only possible to sustain full hydraulic contact between the drying material and the suction probe, to a suction pressure of approximately 200kPa. Thereafter, the ceramic comes into contact with the atmosphere and starts losing moisture at an increasing rate. This results in air entry taking place. Thus, it is only possible to obtain a SWCC to suction pressure of approximately 200 kPa. The values calculated for the volumetric water content, using the experimental data, are then plotted against the corresponding suction pressures on a semi-log scale to produce a partial SWCC.

The method described in Section 2.4.4 is modified in order to obtain a complete SWCC. The partial graph is extended to obtain the point of intersection, Y_p, of the tangent line on the matric suction axis. The point of inflection, (Y_i,q_i) is estimated from the partial curve. With the residual suction pressure of the tailings falling outside the measurable range of the suction probe, a range of values (1000 kPa to 3000 kPa), are chosen for Y_r

Al the parameters are then used to construct various complete curves. Thereafter, it is possible to obtain the corresponding residual volumetric water content, q_r, and residual suction pressure, Y_r, from the best fitting curve.

3.5 Drying Box Test

This experiment consists of pouring tailings slurry into the drying box and observing the changes in mass, settlement, suction and strength as the drying of the material commences.

To observe the effect of rewetting on the material strength and suction profile, a second tailings layer (second lift) is poured on top of the completely dry and desiccated tailings material of the previous layer (first lift). Before the commencement of the experiment, the load cell is used to obtain the mass of the drying box with the Bidim Geotextile, $M_{box.}$

The drying period on site is about 14 days (336 hours), rendering approximately 182 hours of daytime and 154 hours of nighttime. Since most of the drying takes place during the day, the tailings material is placed under the halogen lights continuously for 9 days (216 hours), allowing time for the lights to switch off and cool down periodically.

3.5.1 Drying of material

The preparation of the tailings material takes place two days before the experiment commences. The tailings material is scooped into containers and placed in an oven at 100°C for 12 hours, to ensure that the material dries out completely. Thereafter, the dried material is left to cool down overnight.

3.5.2 Mixing and pouring of tailings slurry

The information obtained for the insitu conditions of Mispah Residue dam, indicate that a single deposition of tailings slurry, results in a layer thickness of approximately 15 cm with final moisture content of 20%. In order to obtain the same height during the experiment, it is determined that 0.04 m^3 of tailings is needed for each successive lift. To obtain a feed density of 1.3 l/kg (as used at Mispah Residue dam), a total amount of 58 kg of tailings and 75.4 kg of water is used for each successive lift.

The water and the tailings are mixed in five portions, since mixing takes place by hand. This ensures that the water and tailings are thoroughly mixed and all the clusters of tailings are completely dissolved. With the tailings completely dissolved, the slurry is poured into the container of the disperser. The valve is then opened for the tailings slurry to be deposited into the drying box. This procedure is repeated five times. Figure 3.12.a and 3.12.b shows the drying box just after the first and second lift has been poured, respectively.

The halogen lights are then positioned above the tailings material and switched on. A fan is positioned behind the lights to ensure free movement of air over the surface of the material, as well as to simultaneously cool down the lights. The ambient and soil temperatures are kept at approximately 21° C.

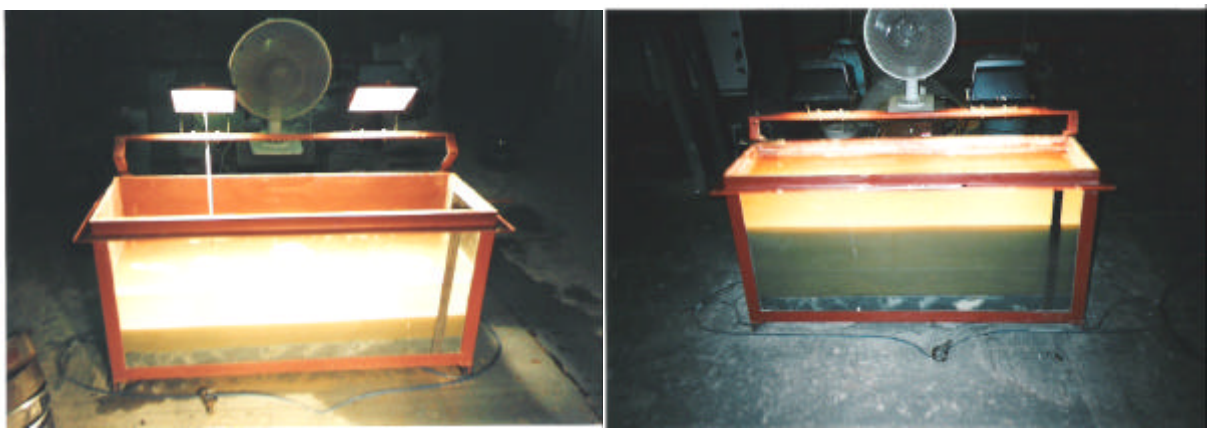

Figure 3.12: a) Completion of first lift b) Completion of second lift

3.5.3 Measurement of water level and sedimentation

After pouring the slurry, the initial height of water and settlement are taken. For both the first and second lift, the height of the water level and settlement reading are taken hourly until the two levels coincide. Thereafter, settlement readings are taken once a day until the completion of the experiment.

3.5.4 Weighing of drying box and tailings

With all the material poured, the drying box and the slurry is weighed to obtain the initial mass, M_i. Thereafter, the drying box and the tailings are weighed daily with the use of the load cell as discussed in Section 3.2.4. Figure 3.13 shows how the weighing system operated.

Figure 3.13: Weighing of drying box and tailings

3.5.5 Measurement of air and soil temperature

The air and soil temperature is recorded once a day with the use of a thermometer and a soil thermometer, respectively. These readings are then recorded to ensure that the drying material is exposed to the same ambient conditions during testing.

3.5.6 Measurement of crack propagation

For each lift, the crack distribution and widths are sketched and recorded daily. This takes place before the suction measurements and sampling, in order to avoid any disturbance of the tension cracks. The information from these readings is used to obtain the daily linear shrinkage of the contained material.

3.5.7 Suction measurement and sampling

The measurement of the suction pressures commences with the use of the suction probe, as discussed in Section 3.2.1. During the first lift the surface suction readings are taken before an undisturbed sample is extracted. Thereafter, another set of suction readings is taken at the bottom of the cavity left by the extracted sample.

The procedure for the second lift is similar to that of the first lift, except that suction readings are taken at two depths instead of one. The surface readings are taken before an undisturbed sample is extracted and the suction pressures measured at the first depth. Then another undisturbed sample is extracted below the base of the existing hole. The suction pressures are then measured at the new depth.

Surface suction measurements

The surface suctions are measured 2 days after the slurry is poured for the first lift. Before this time, the pore pressures are predominantly positive. During the second lift, the surface suctions are only measured after 3 days due to the increased volume of material.

The probe is placed on the tailings surface with the tip of the probe in hydraulic contact with the pore water. The probe is held in position with the probe holder. After approximately 12 min the suction pressures stabilise and a reading is taken (Figure 3.14). This process is repeated three times at three different locations on the tailings surface.

Figure 3.14: Suction measurements using the probe holder

Extraction of first sample

The main purpose of the sampling is to determine the degree of saturation of the material after cracking has occurred. During the first lift, the first sample is extracted to a depth of 8cm, with the small tube sampler. This takes place after 3 days, when the first cracks appear, and the material gains enough strength to render a proper sample. Thereafter a sample was taken daily to the end of the experiment. During the second lift the first sample was extracted, to a depth of 10 cm, with the small tube sampler after 4 days. This was due to the increased volume of material that needed to dry.

After the extraction of the sample, it is removed from the sampler and measurements are taken of its diameter and height at three different positions. The sample is then weighed and placed in the oven at 100°C to dry for 12 hours. Thereafter, it is removed and weighed again. Samples are taken at different positions in the drying box to allow the pore pressures to stabilise between successive samplings.

Suction measurements at first depth

After the extraction of the sample, during the first and second lift, the tip of the probe is positioned on the base of the hole to obtain the suction pressure at the required depths of either 8 cm or 10 cm. The probe is then left in position for 12 min before the reading is taken. Thereafter, the probe is moved to another position on the base of the hole, before another suction reading is taken. This procedure is repeated for three different positions.

Extraction of second sample

This only applies to the second lift. The small tube sampler is pushed another 10 cm past the base of the cavity left by the extraction of the first sample. After the extraction of the second sample, it is removed from the sampler and measurements are taken of its diameter and height at three different positions. The sample is then weighed and placed in the oven at 100°C to dry for 12 hours. Thereafter, it is removed and weighed again. Samples are then taken at different positions in the drying box to allow the pore pressures to stabilise between successive samplings.

Suction measurements at second depth

This only applies to the second lift. After the sample is extracted the tip of the probe is positioned on the base of the hole to obtain the suction pressure at a depth of 20 cm. The probe is then left in that position for 12 min before the reading is taken. Thereafter, the probe is moved to another position on the base of the hole, before suction readings are taken. This procedure is repeated for three different positions.

Replacement of material

After the suction pressures are measured at all the required depths, for both the first and second lift, the cavity is filled with tailings material at approximately the same moisture content as the bulk of the material in the drying box.

3.5.8 Vane shear measurements

Vane shear measurements are made at different depths for the different lifts. For the first lift, vane shear measurements are made at depths of 5 and 10 cm at three positions from day 3 onward. For the second lift, vane shear measurements are made at depths of 5, 10 and 20 cm at three positions from day 4 onward. The size of the spindle that is used depends on the strength of the material as discussed in Section 3.2.8.

3.5.9 Determination of volume-mass relations

The volume-mass relations are calculated from the readings obtained from the bulk material inside the drying box before cracking commences. After cracking has begun, it becomes extremely difficult to accurately determine the volume of the bulk material.

The undisturbed sample extracted from the bulk material between cracks, however, represents a material volume undisturbed by "voids" formed by cracking. This volume can easily be determined accurately, by measuring the diameter and height of the cylindrical sample.

Consequently, after the formation of cracks, the volume and mass of the cylindrical sample is used to determine mass-volume relations. This procedure, however, can not be performed before cracking has commenced, since the material is too weak to support the extraction of a sample.

Volume-mass relations from bulk material

With the initial mass of solids (M_s) and water (M_{wi}) known, it is possible to determine the moisture content from the change in the daily mass readings (M), which indicates the loss of mass due to the drainage and evaporation of the water. The moisture content is thus calculated with:

$$w = \frac{M_{wi} - (M - M_{box} - M_s)}{M_s} = \frac{M_w}{M_s} \qquad \textbf{[3.5]}$$

with:
- M_{box} - mass of drying box [kg]
- M - daily total mass measurement [kg]
- M_w - mass of water [kg]
- M_{wi} - initial mass of water [kg]
- M_s - mass of solids [kg]

The volume of the bulk material (V_{box}) is determined with the height of the material, inside the drying box, and the inside base area of the drying box. With the volume and moisture content known, it is possible to determine the void ratio, e, and degree of saturation, S, with Equations [3.3] and [3.3]. With both the void ratio and the degree of saturation known, it is possible to calculate the volumetric water content, q, with [2.12].

Volume-mass relations from sample

With the initial mass (M_i) and the mass of solids (M_s) known for each sample, it is possible to determine the moisture content of the sampled material.

$$w = \frac{(M_i - M_s)}{M_s} = \frac{M_w}{M_s} \quad \textbf{[3.6]}$$

with:

M_w - mass of water [kg]

M_s - mass of solids [kg]

M_i - initial mass of sample [kg]

The volume of each sample (V_{sample}) is determined from the measurements made after sampling has taken place. With the volume and moisture content known for the each sample, it is possible to determine the void ratio, *e*, and degree of saturation, *S*, with Equations [3.3] and [3.3]. With both the void ratio and the degree of saturation known it is possible to calculate the volumetric water content, *q*, with [2.12].

3.6 Field Testing

Before the insitu tests were conducted, a suitable location on the daywall was identified. The crack formations were studied to locate an area where the material between cracks was almost square shaped ("blocks"). The adjacent "blocks" of material had approximately the same dimensions. This ensured an accurate representation of mutual linear shrinkage between the "blocks" of material. Figure 3.15 shows two areas with the preferred geometry in "block" formation.

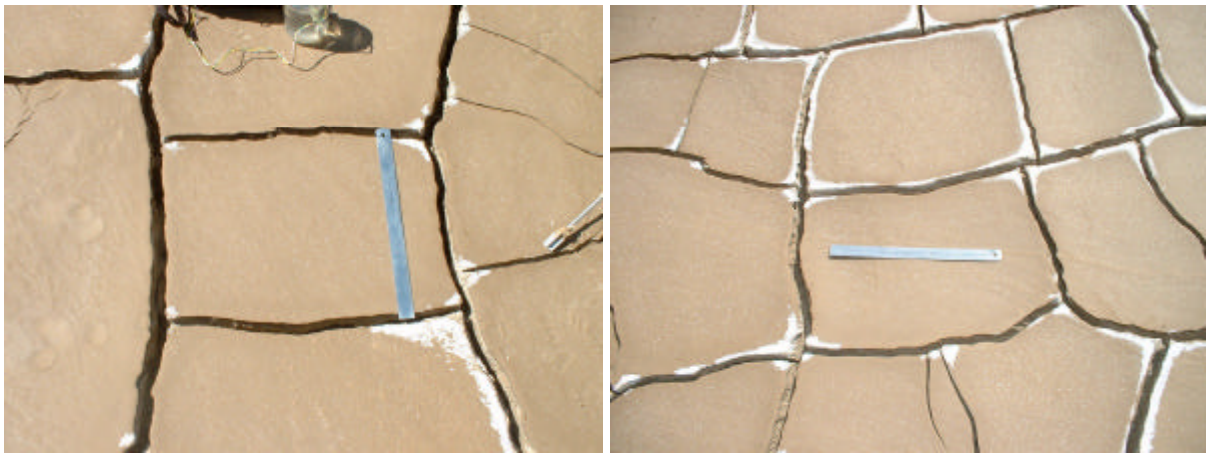

Figure 3.15: Blocks formed by crack formation

3.6.1 Measurement of crack widths and distribution

After the suitable location was found, measurements of the "block" dimensions and the surrounding crack widths were made. Starting from the one side, the first block's length and width are measured. Thereafter the crack widths were measured along the perimeter of the block, at three positions on each side. This process was repeated for all the "blocks" along the chosen section.

3.6.2 Sampling

The main purpose of the sampling is to determine the moisture content and degree of saturation of the material. The larger tube sampler is used for the extraction of undisturbed samples insitu. A full sample is extruded to a depth of 20 cm from the first two "blocks" of the series of chosen "blocks". This is done to obtain an average moisture content and degree of saturation over the full depth. Figure 3.16 shows two full sized undisturbed samples.

Figure 3.16: Full sized samples

Thereafter, samples are only taken at 5 cm depth intervals, up to 20 cm, in order to obtain the variation of the moisture content and degree of saturation with depth.

After extraction of the sample, it is removed from the tube sampler and measurements of its height and diameter are taken at three positions. Thereafter, the sample is wrapped in various layers of foil and cling wrap to preserve the moisture within the sample. The samples are then taken to the laboratory where it was weighed and left in the oven at 100 °C for 12 hours to dry. After the drying process is complete, the sample is weighed again to obtain the final mass.

3.6.3 Direct shear strength measurement

The vane shear measurements take place at depths of 5, 5-10 and 15-30cm, at three positions on each of the chosen "blocks". The spindle is positioned a distance away from the cracks and the cavity left by the extruded sample. This prevents the fracturing of the material and the rendering of erroneous readings. The size of the spindle that is used depends on the strength of the material as discussed in Section 3.2.8.

3.6.4 measurement of suctions

The measurement of the suction pressures commences with the use of the suction probe and the base plate stabiliser, as discussed in Section 3.2.9. To compare the results obtained from the drying box experiment to actual values, the suctions were also taken at various depths.

Surface suction measurements

The base plate stabiliser is fixed firmly into the tailings material before 5 mm of the surface material is scraped off. This is done to ensure a better hydraulic contact between the probe and the surface. The probe is then clamped into position and kept there for approximately 12 min before a reading was taken. This process is repeated three times at three different locations on the tailings surface. Figure 3.17 illustrates how surface suctions are measured with the use of the base plate stabiliser.

Figure 3.17: Surface suction measurements

Suction measurements at different depths

After the surface suctions have been measured, the material is progressively removed to depths of 5-10, 10-15 and 15-30cm, with the use of a shovel. The base plate stabiliser is, again, firmly fixed into the tailings before the suction pressures are measured. This is achieved by following the same procedure that was stated for the measurement of the surface suctions. Figure 3.18 illustrates how suction measurements were taken at a depth of 5 cm.

Figure 3.18: Suction measurements at 5 cm

3.6.5 Determination of volume-mass relations

The volume mass-relations of the samples extracted insitu have been obtained by following the method outlined in Section 3.4.10, for samples extracted from the drying box.

4. SHEAR STRENGTH OF GOLD MINE TAILINGS

4.1 Introduction

The aim of this chapter is to present the results from the experimental procedures outlined in Chapter 3. The results are given in the form of various tables and graphs.

The chapter is divided into four sections. The first and second section present the results and graphs obtained from the trough test, that were used for the determination of the soil-water characteristics curve and shear strength, respectively. The results obtained from the drying box test are presented in the third section. The field-testing results make up the fifth section. The results will be discussed and evaluated in Chapter 5.

4.2 Soil-water Characteristic Curve

This section present the results obtained from the trough tests as discussed in Section 3.4. During the trough test, measurements of the suction pressures, change in volume, and mass were recorded. Three trough tests were carried out, of which the first test rendered erroneous results, due to the small size of the trough. After the larger troughs were built, two successful tests were carried out.

The data for the two tests, which were conducted on the same material, are tabled in Appendix A-1 and A-2 for trough test 2 and 3, respectively. The measured data was used to determine the moisture content (w), void ratio (e), and degree of saturation (S), using Equations [3.2], [3.3] and [3.4]. The results are illustrated graphically in Figure 4.1, 4.2 and 4.3 as plots of moisture content versus suction, void ratio versus suction, and degree of saturation versus suction for both tests.

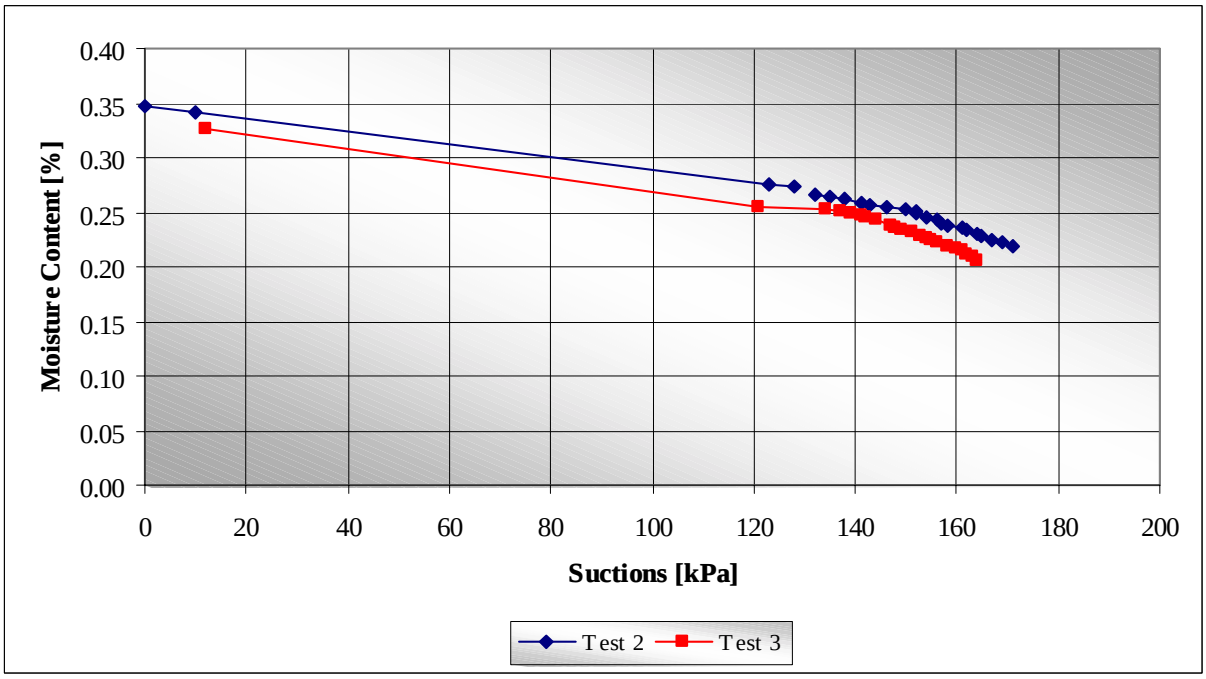

Figure 4.1: Moisture content versus suction

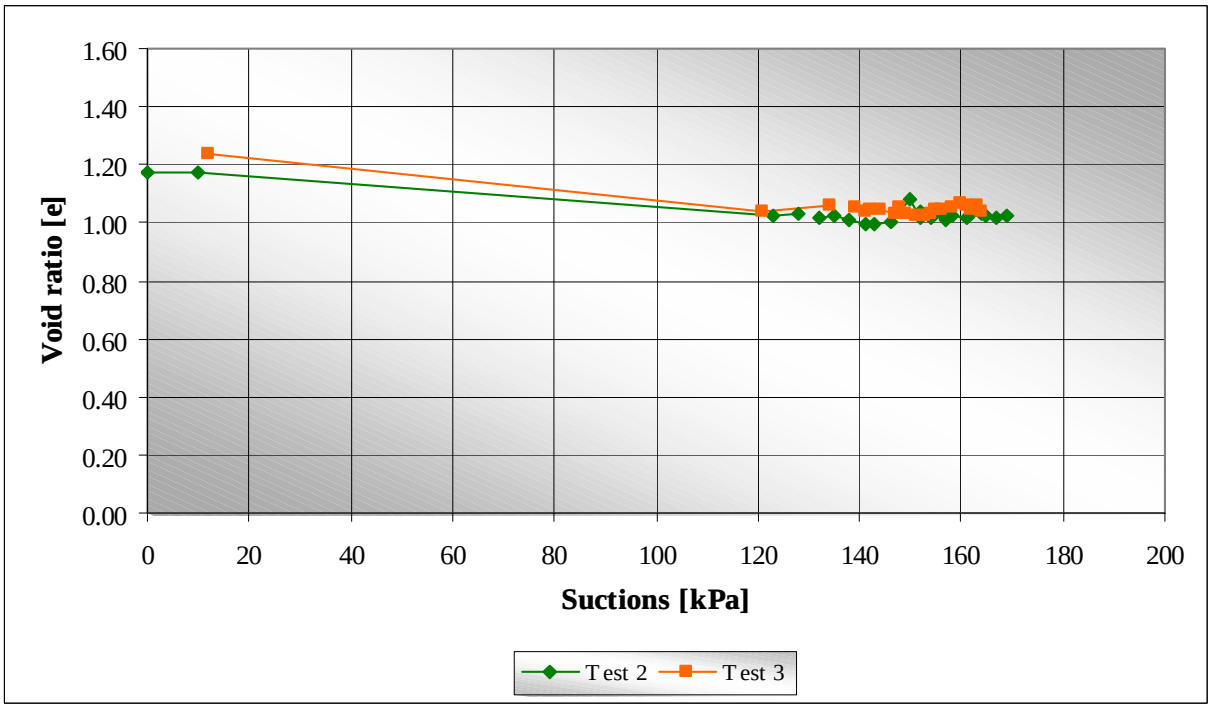

Figure 4.2: Void ratio versus suction

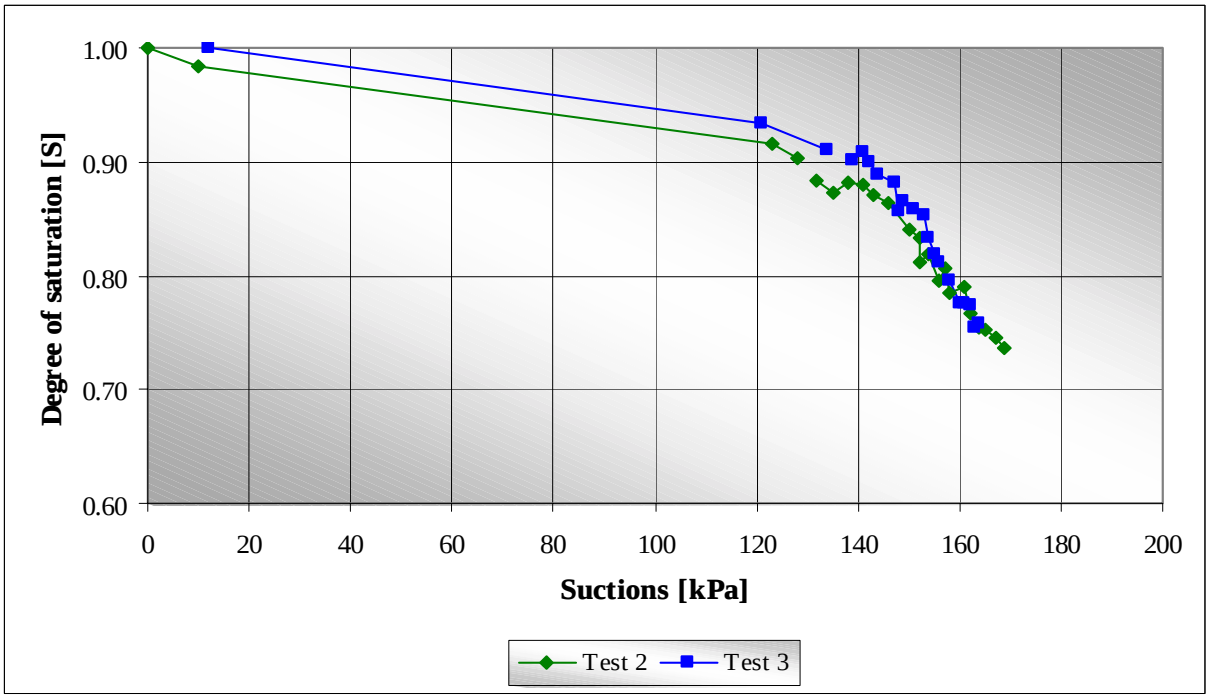

Figure 4.3: Degree of saturation versus suction

Figure 4.4 illustrates the percentage linear shrinkage versus suction relationship, obtained from the results of trough test 2 and 3. The data for the two tests are tabled in Appendix A-3 for both trough tests 2 and 3.

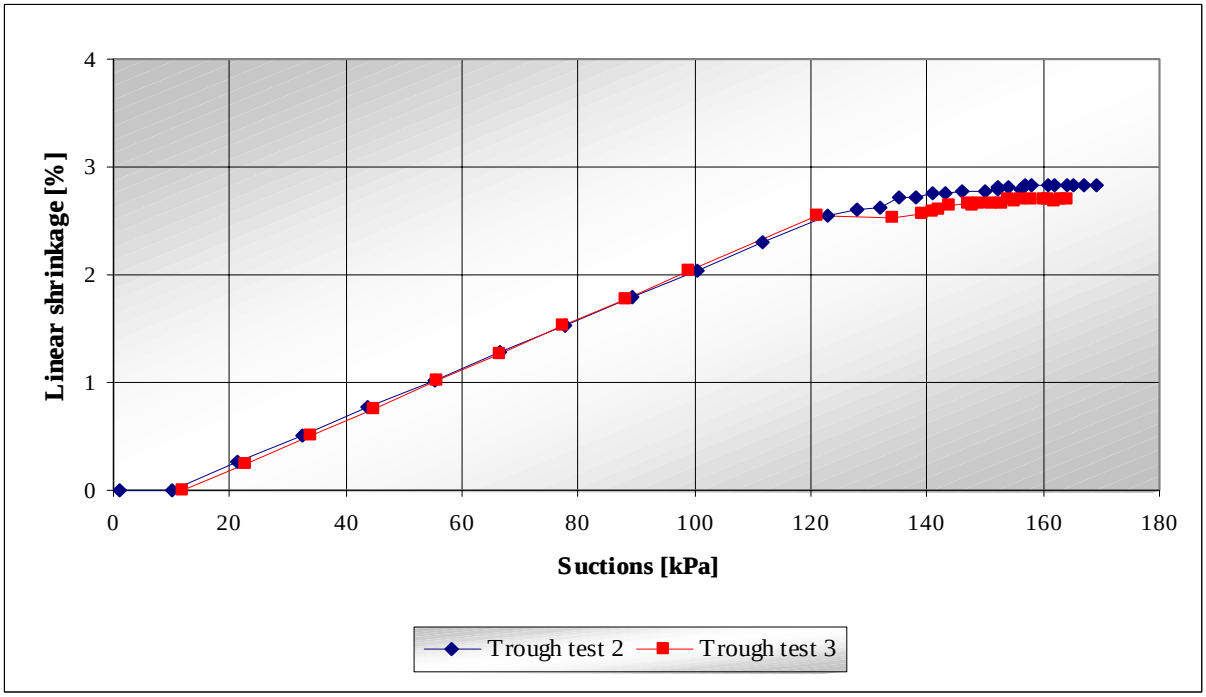

Figure 4.4: Percentage linear shrinkage versus suction

The values determined for the void ratio and the degree of saturation were then substituted into Equation [2.12] to determine the volumetric water content (θ). These results are tabled in Appendix A-3 for trough test 2 and 3. The results are illustrated graphically in Figure 4.5, as a plot of volumetric water content versus suction. These plots represent a portion of the soil water characteristic curve.

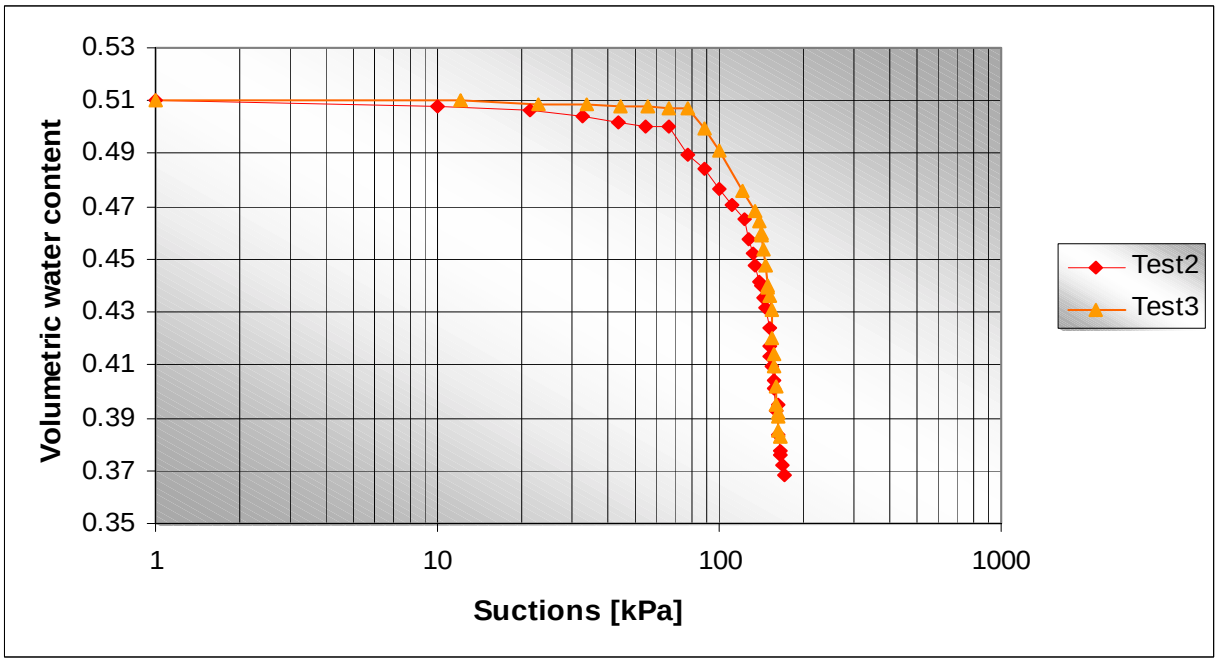

Figure 4.5: Volumetric water content versus suction

An extrapolation of this data was carried out with the use of the graphical method described in Section 3.4.4. The relevant extrapolation parameters are presented in Table 4.1 for trough test 2 and 3, respectively. The extrapolated curves and the data points for trough test 2 and 3 are illustrated in Figure 4.6 and 4.7, respectively. The extrapolated data points are tabled in Appendix A-4 and A-5 for trough test 2 and 3, respectively.

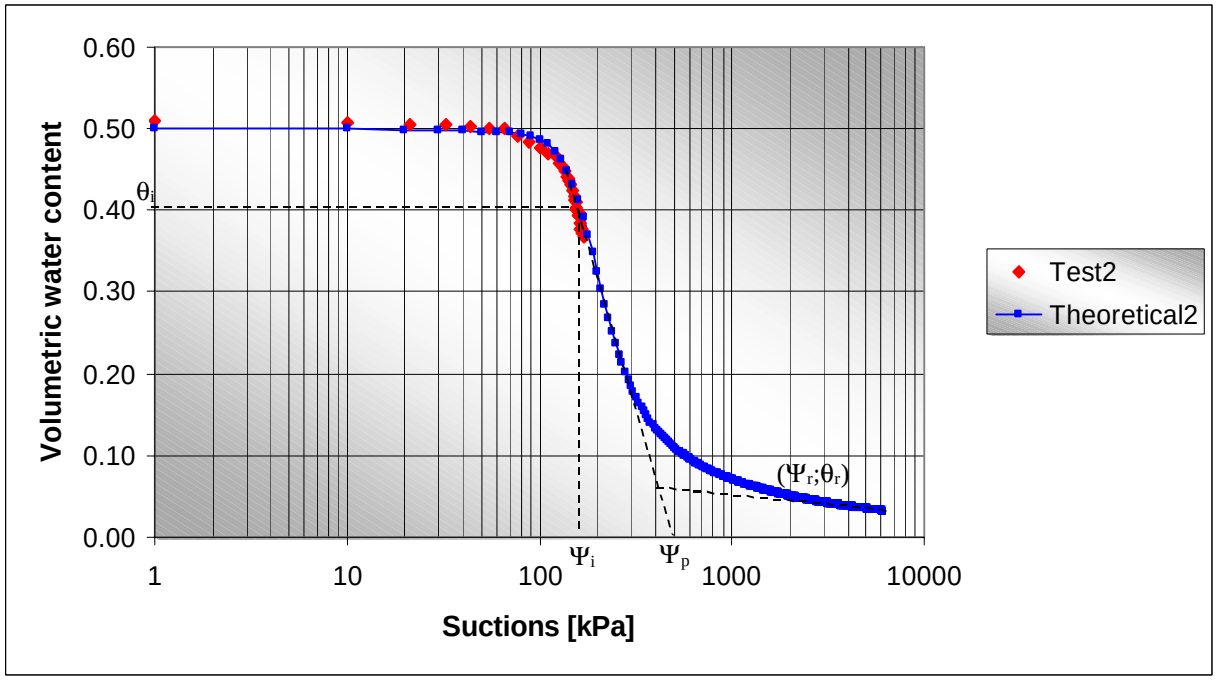

Figure 4.6: Volumetric water content versus suction - Trough Test 2

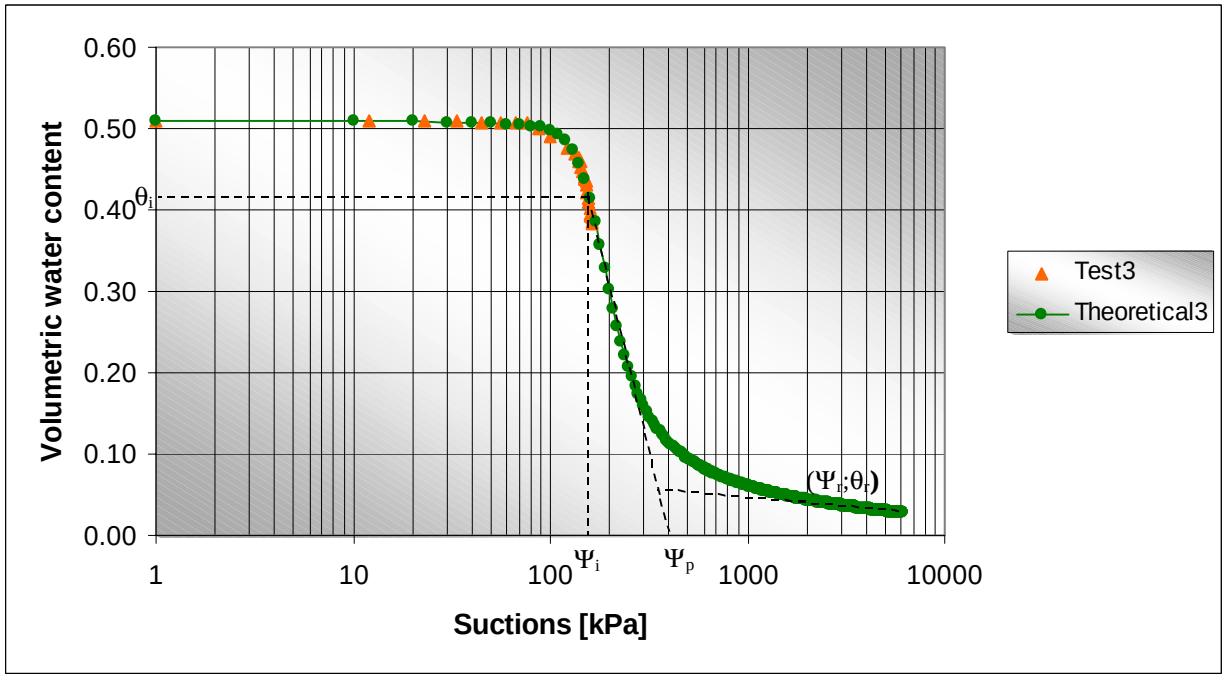

Figure 4.7: Volumetric water content versus suction - Trough Test 3

Table 4.1: Fitting Parameters

Trough test 2		Trough test 3	
ψ_r	2000	ψ_r	3000
θi	0.400	θi	0.410
n	5.503	n	6.618
S	0.371	s	0.452
s^*	0.770	s^*	0.870
E	2.718	e	2.718
M	0.819	m	0.816
Ψ_p	500	Ψ_p	400
θ_s	0.500	θ_s	0.510
θ_r	0.070	θ_r	0.050
ϕ	0.590	ϕ	0.593
a	170	a	165

Figure 4.8 illustrates the two complete soil water characteristic curves.

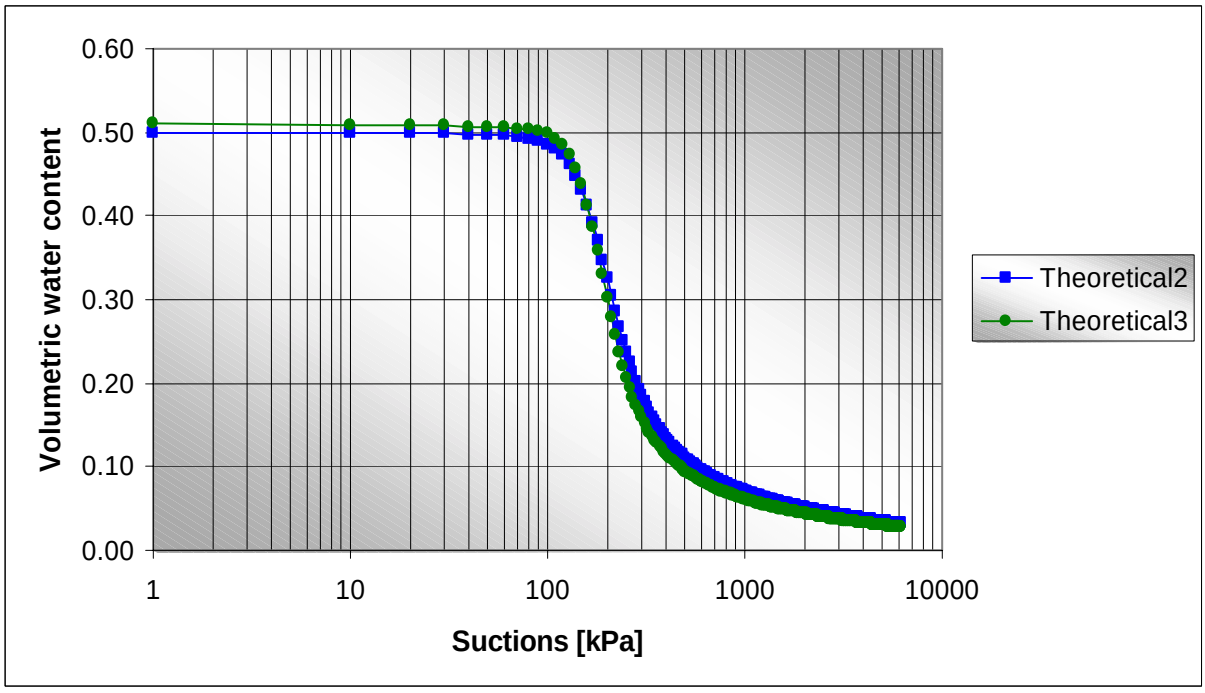

Figure 4.8: Complete soil-water characteristic curves

Figure 4.9 illustrates an average of the two complete soil water characteristic curves obtained from the results of trough test 2 and 3. These data points are presented in Appendix A-6.

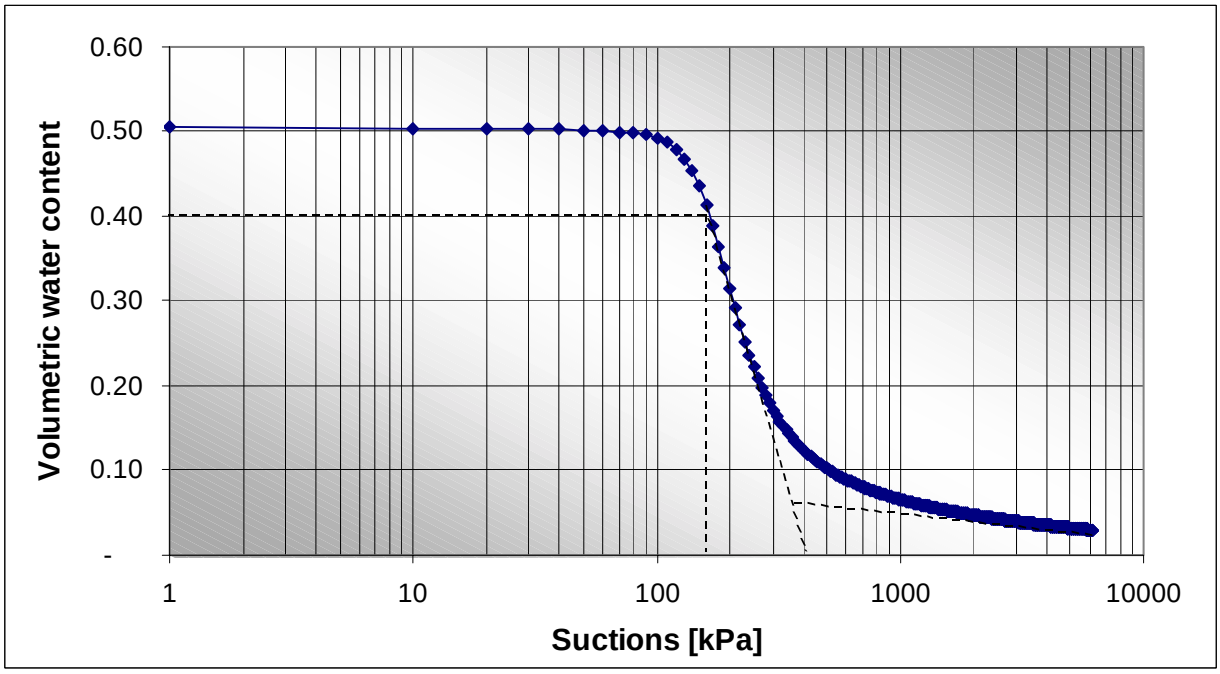

Figure 4.9: Average soil-water characteristic curve

4.3 Shear strength induced by suctions

Using Equation [2.32], the shear strength versus suction relationship, illustrated in Figure 4.10, was determined from the soil-water characteristic curves and the residual volumetric water content, which were determined in Section 4.2 from the results of trough test 2 and 3. The data points calculated from the results of trough test 2 and 3 are presented in Appendix A-3. Appendix A-4 and A-5 presents the data points calculated from the complete soil water characteristic curves.

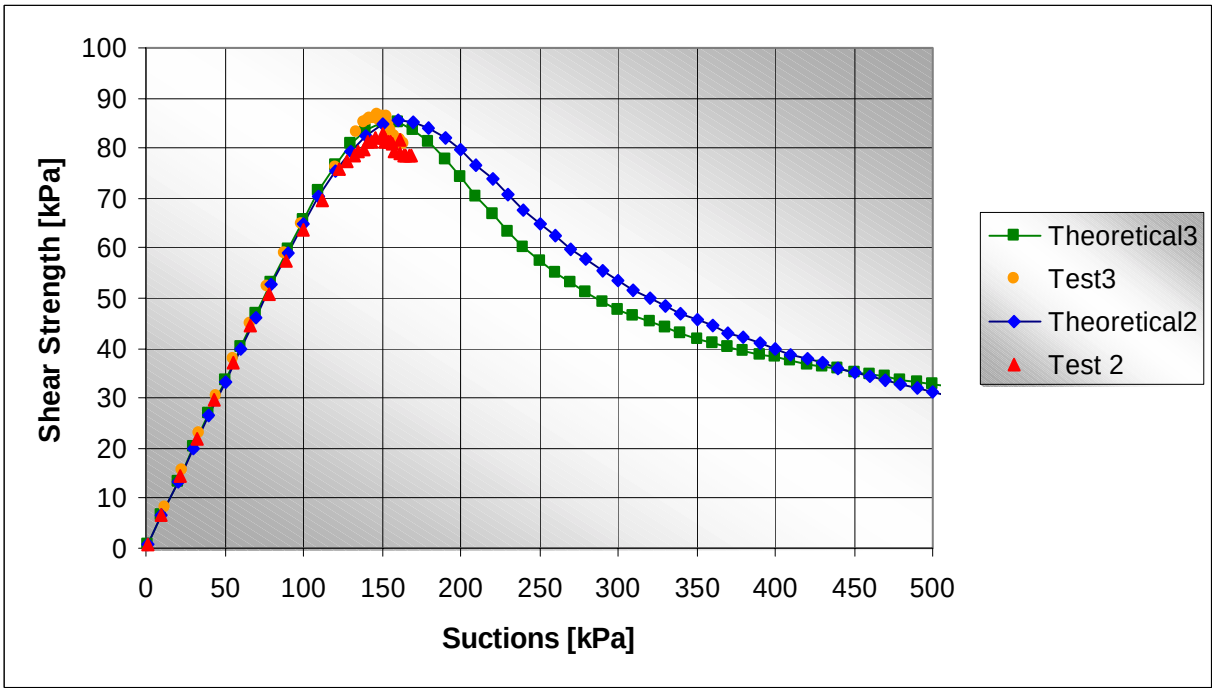

Figure 4.10: Calculated shear strength versus suction

Figure 4.11 illustrates an average calculated shear strength versus suction graph for the results of trough test 2 and 3. These data points are presented in Appendix A-6.

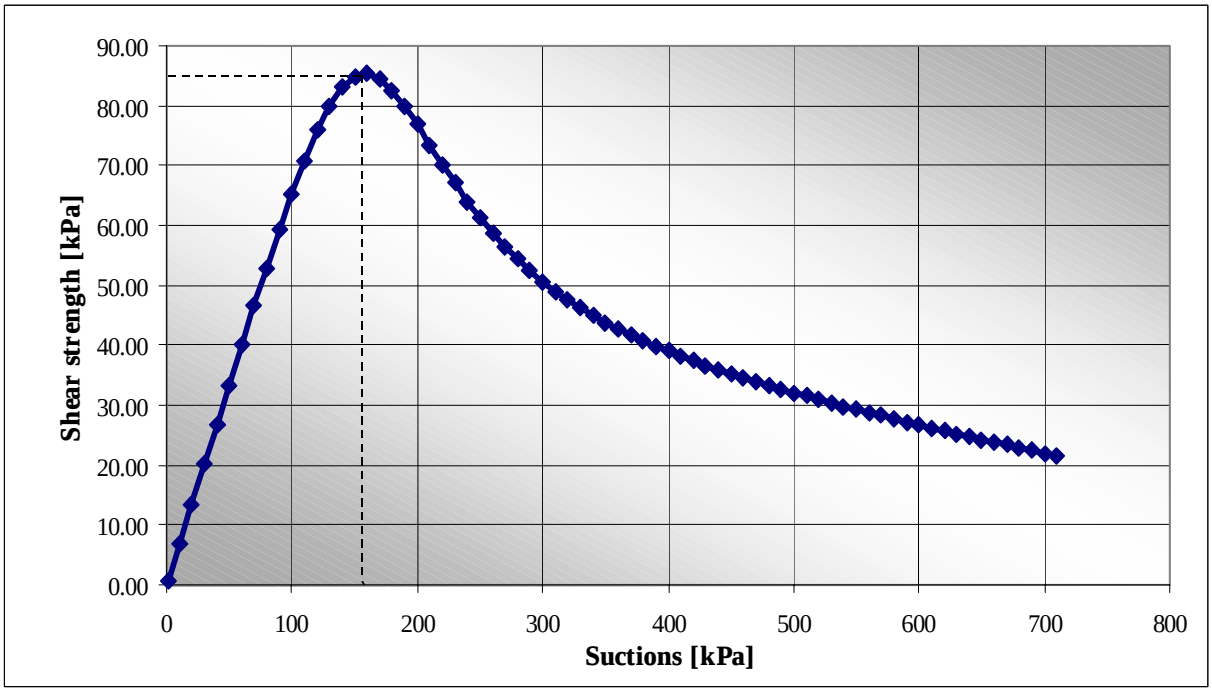

Figure 4.11: Average calculated shear strength versus suction

4.4 Drying and desiccation of gold tailings material

This section presents the results obtained from the drying box test, as discussed in Section 3.5. During the test measurements were taken of the changing water level, settled level, mass, air temperature, insitu shear strength, suction pressures and crack widths in the drying box. Additional measurements were obtained from extracted samples from the drying box. Four drying box tests were carried out, of which the first test rendered erroneous results due to the incorrect calibration of the load cell. This was corrected for drying box test 2, 3 and 4.

Each test was subdivided into a first and second lift. For the first lifts the data is tabled in Appendix B-1, B-2 and B-3 for drying box test 2.1, 3.1 and 4.1, respectively. For the second lifts the data is tabled in Appendix B-4, B-5 and B-6 for drying box test 2.2, 3.2 and 4.2.

From the measured data, the moisture content (w), for both the bulk and sampled material were calculated using Equations [3.5] and [3.6], respectively. Thereafter, the void ratio (e), degree of saturation (S), and volumetric water content (,), were determined with the use of Equations [3.3], [3.4] and [2.12].

These results are tabled in Appendix B-7, B-8 and B-9 for drying box test 2.1, 3.1 and 4.1, respectively and Appendix B-10, B-11 and B-12 for drying box tests 2.2, 3.2 and 4.2. Figure 4.12 and 4.13 illustrates the moisture content versus suction plots for the first and second lift. Figure 4.14 and 4.15 illustrates the void ratio versus suction plots for the first and second lift. Figure 4.16 and 4.17 illustrates the plot of degree of saturation versus suction for the first and second lift respectively.

The percentage linear shrinkage was calculated from the crack measurements taken during the drying of the bulk material inside the drying box. Figure 4.18 and 4.19 illustrates the percentage linear shrinkage versus suction plots for the first and second lifts, respectively.

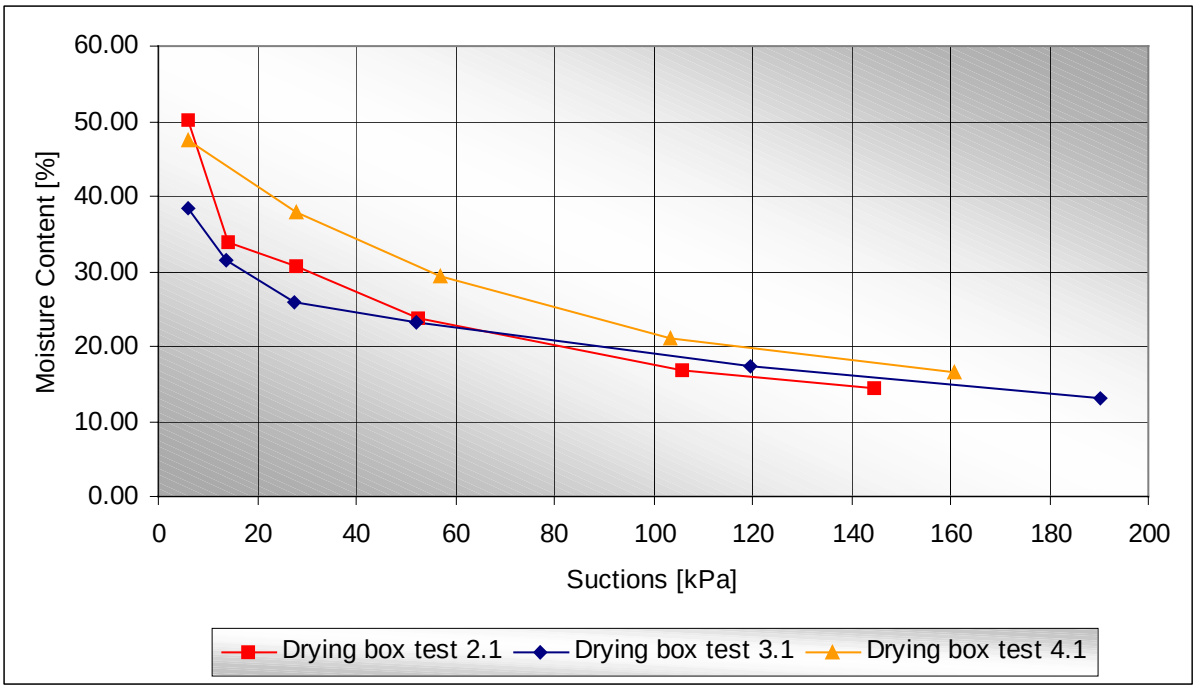

Figure 4.12: Average moisture content versus suction – Lift 1

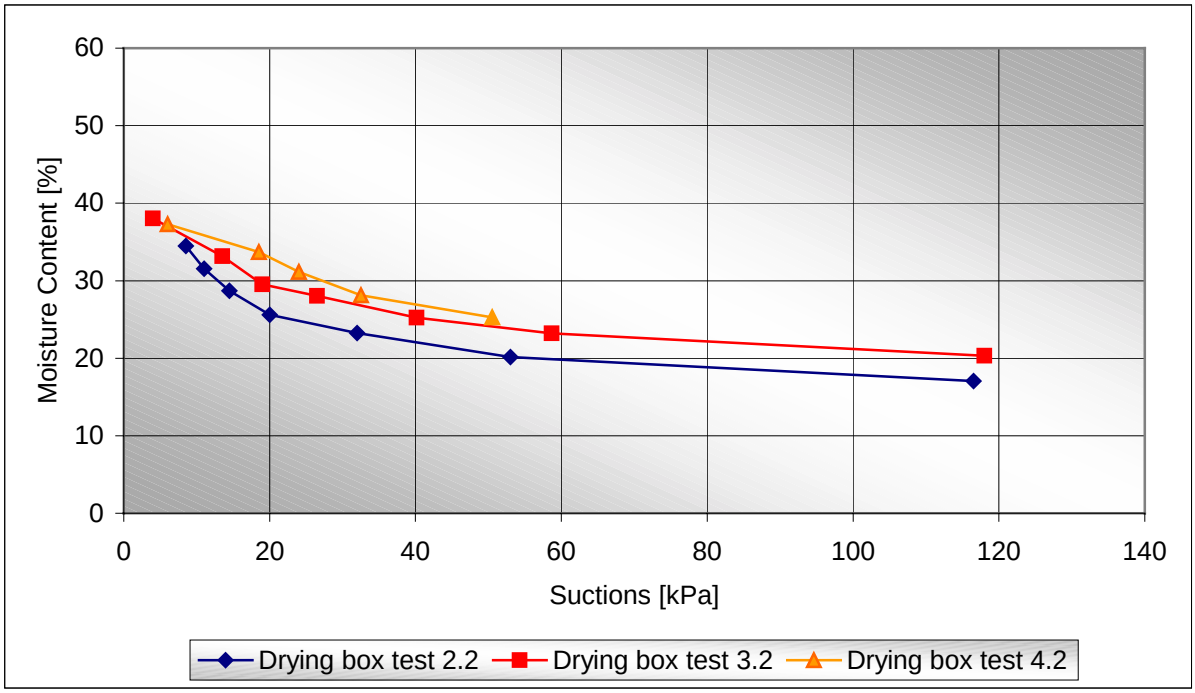

Figure 4.13: Average moisture content versus suction – Lift 2

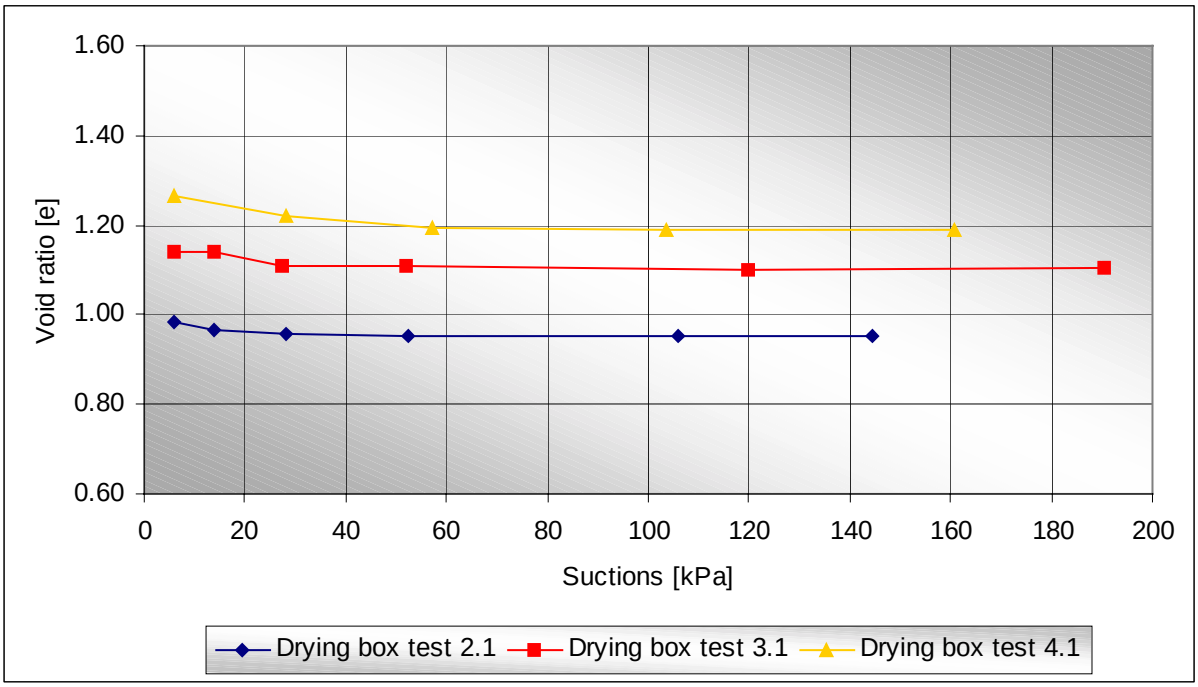

Figure 4.14: Average void ratio versus suction – Lift 1

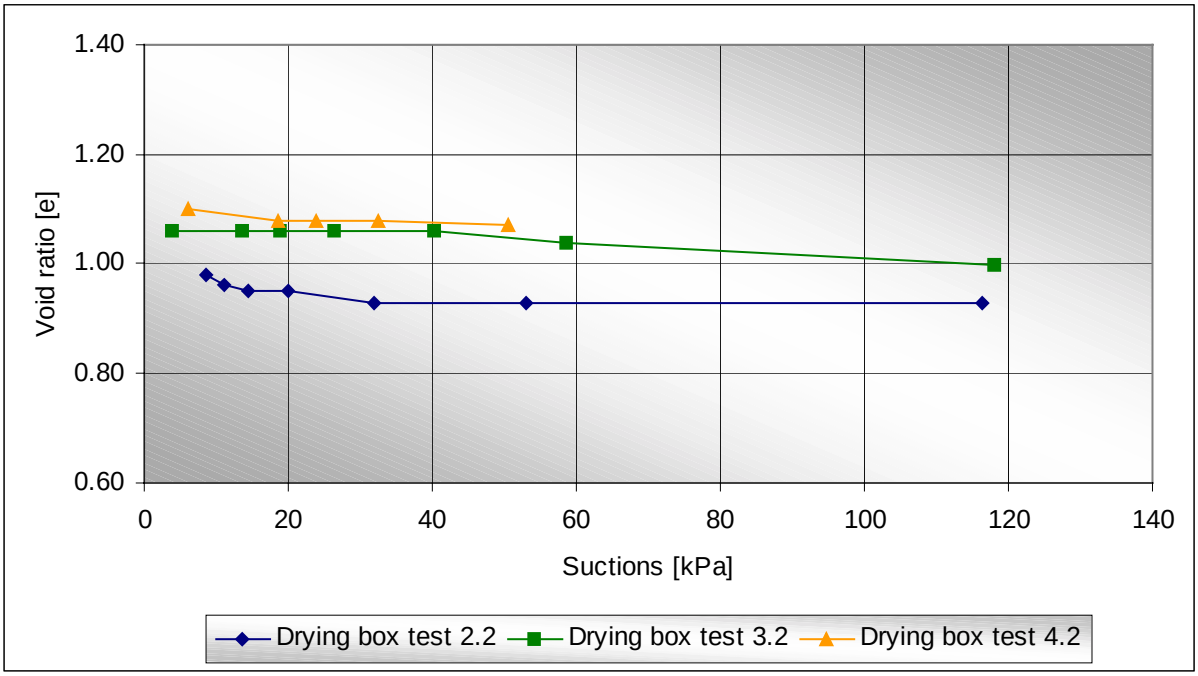

Figure 4.15: Average void ratio versus suction – Lift 2

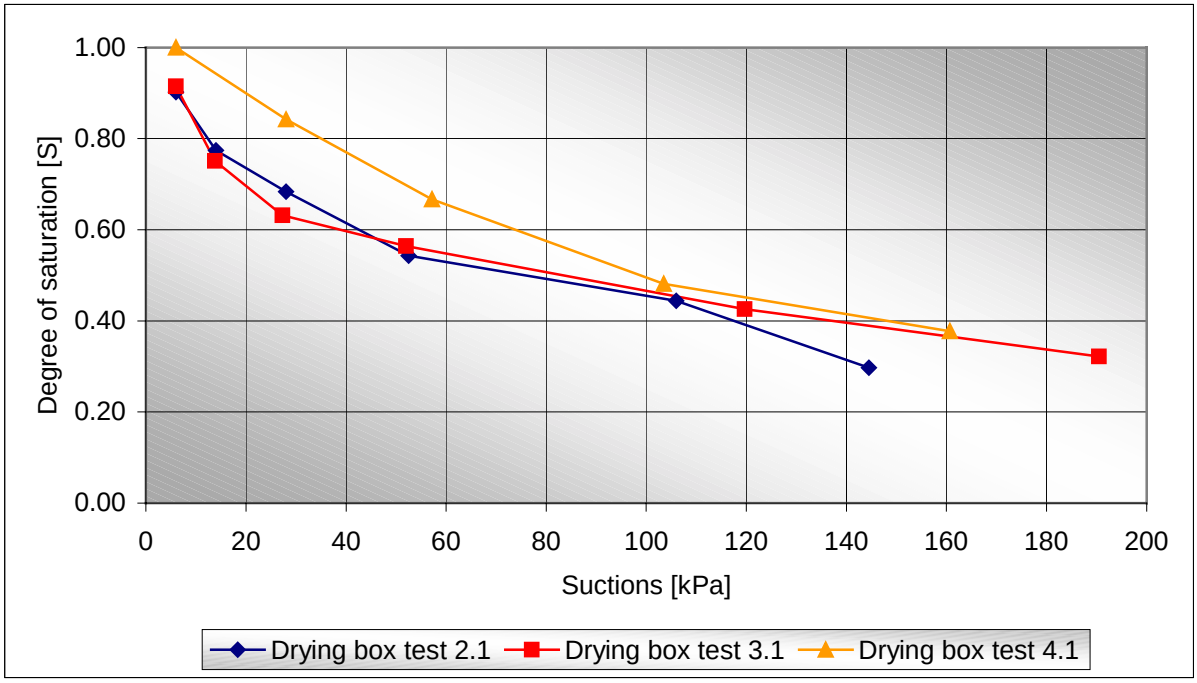

Figure 4.16: Average degree of saturation versus suction – Lift 1

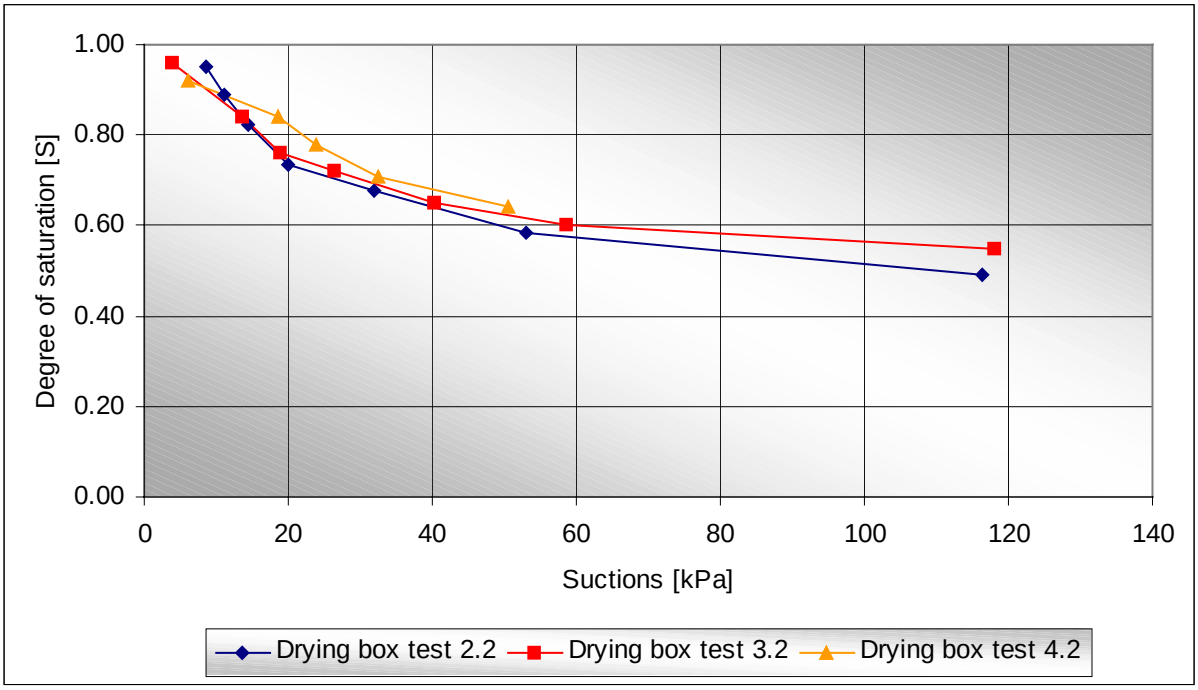

Figure 4.17: Average degree of saturation versus suction – Lift 2

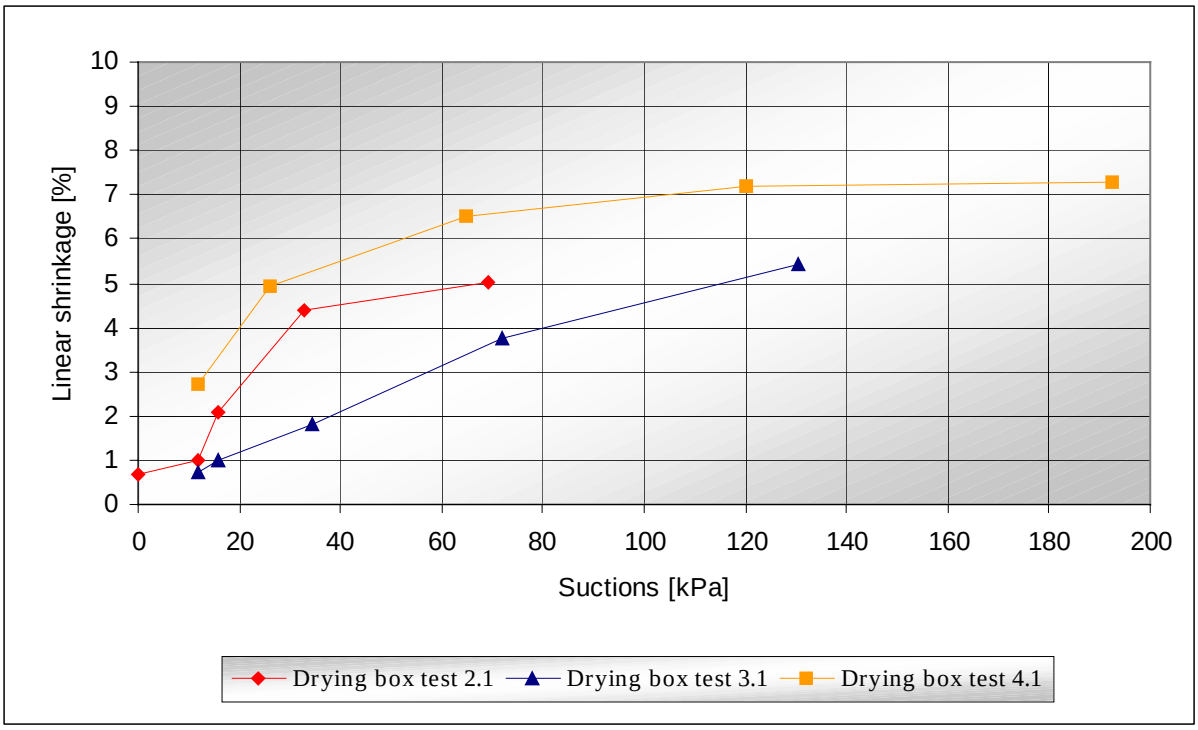

Figure 4.18: Percentage linear shrinkage versus suction – Lift 1

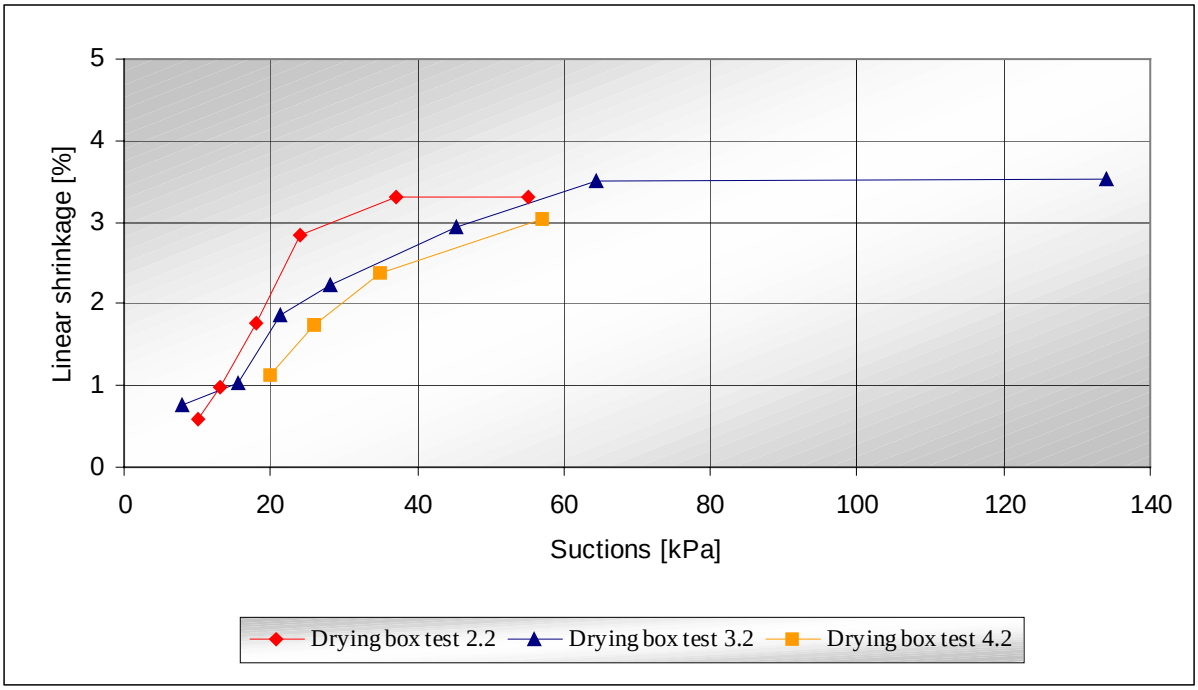

Figure 4.19: Percentage linear shrinkage versus suction – Lift 2

From these results the shear strength, at various positions during the commencement of the first and second lifts, were calculated using Equation [2.32]. For the first lifts the data is tabled in Appendix B-13, B-14 and B-15 for drying box test 2.1, 3.1 and 4.1, respectively. For the second lifts the data is tabled in Appendix B-16, B-17 and B-18 for drying box test 2.2, 3.2 and 4.2.

Figure 4.20 and 4.21 illustrates the relationship between calculated shear strength and suction, at 0 cm and 8 cm during the first lift. Figure 4.22, 4.23 and 4.24 illustrates the calculated shear strength versus suction relationship for 0 cm, 10 cm and 20 cm during the second lift.

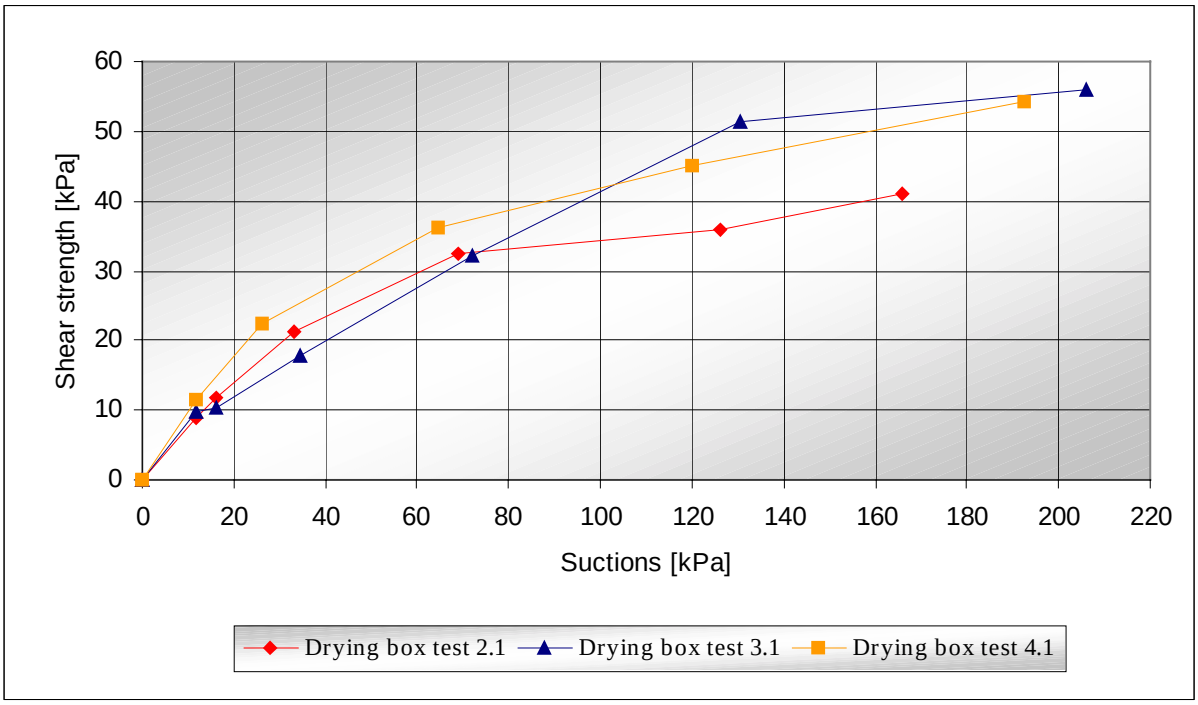

Figure 4.20: Calculated shear strength versus suction at 0 cm – Lift 1

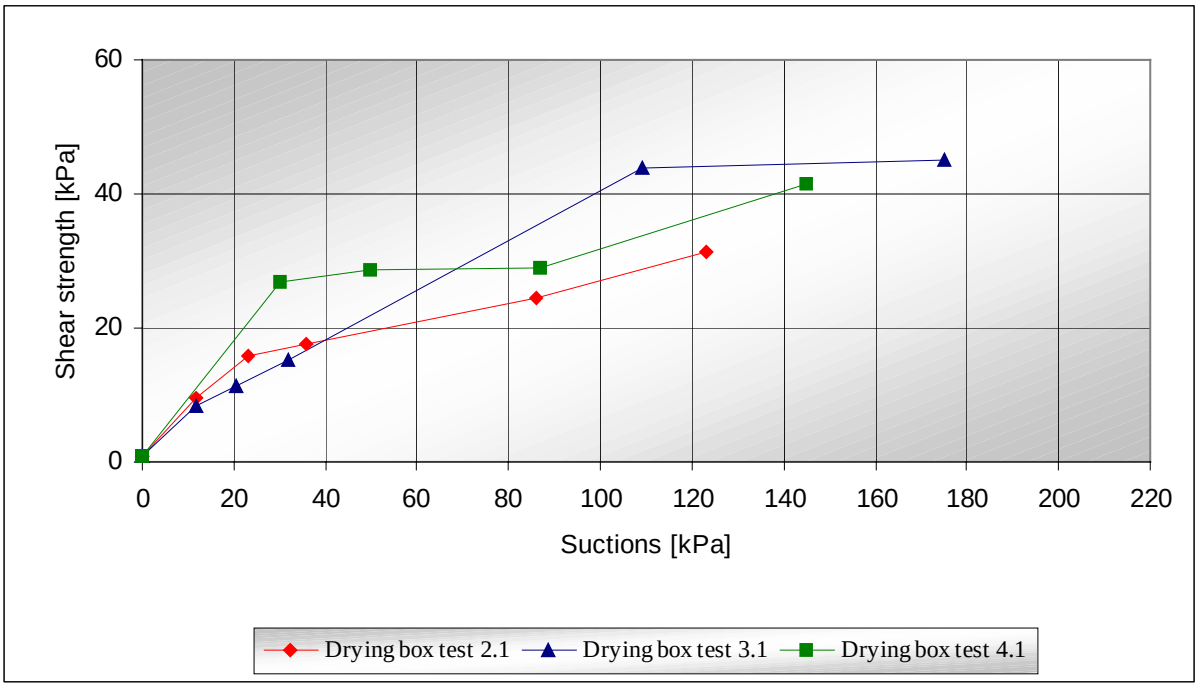

Figure 4.21: Calculated shear strength versus suction at 8 cm – Lift 1

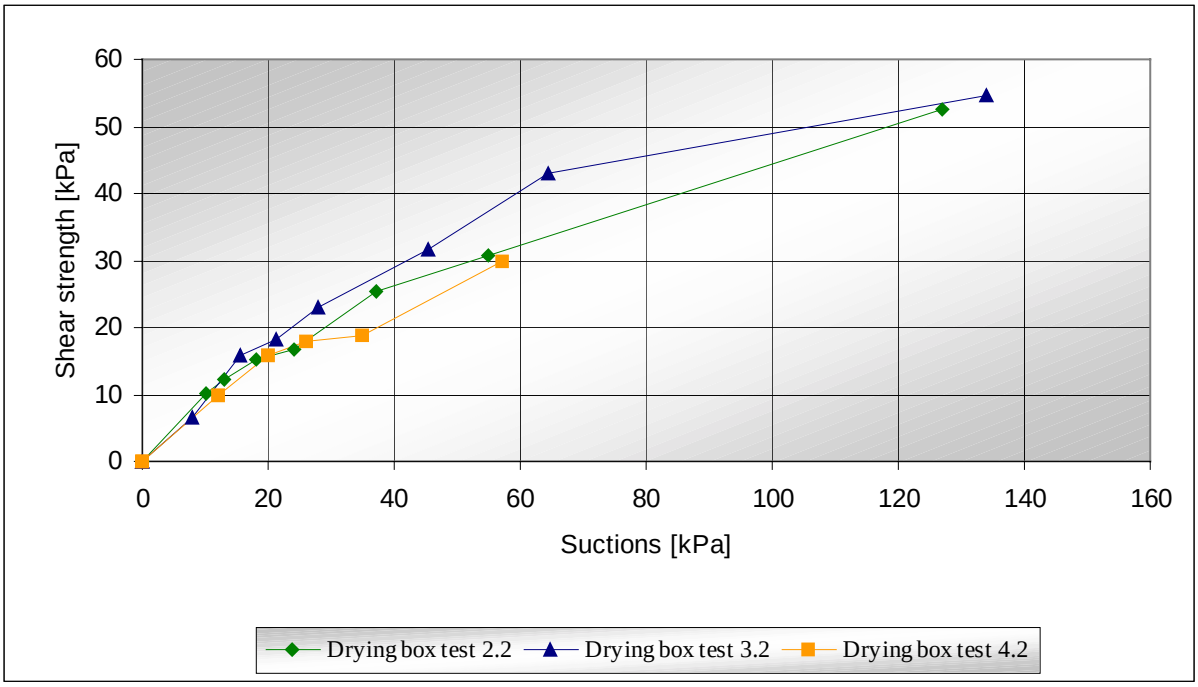

Figure 4.22: Calculated shear strength versus suction at 0 cm – Lift 2

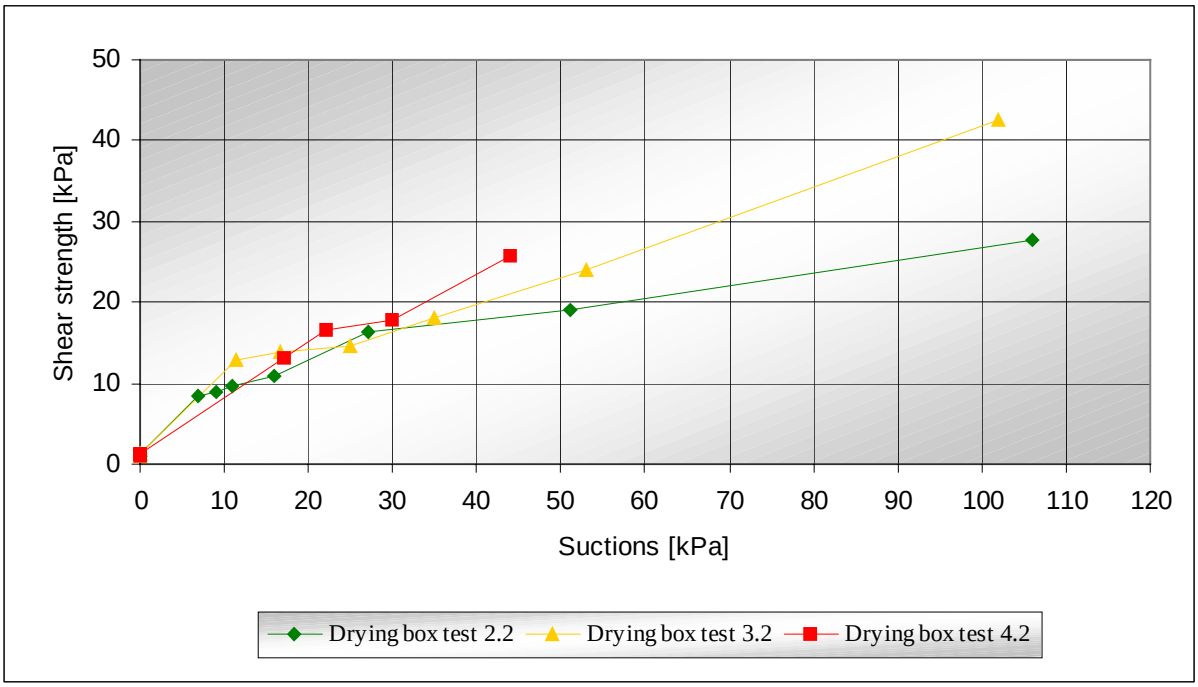

Figure 4.23: Calculated shear strength versus suction at 10 cm – Lift 2

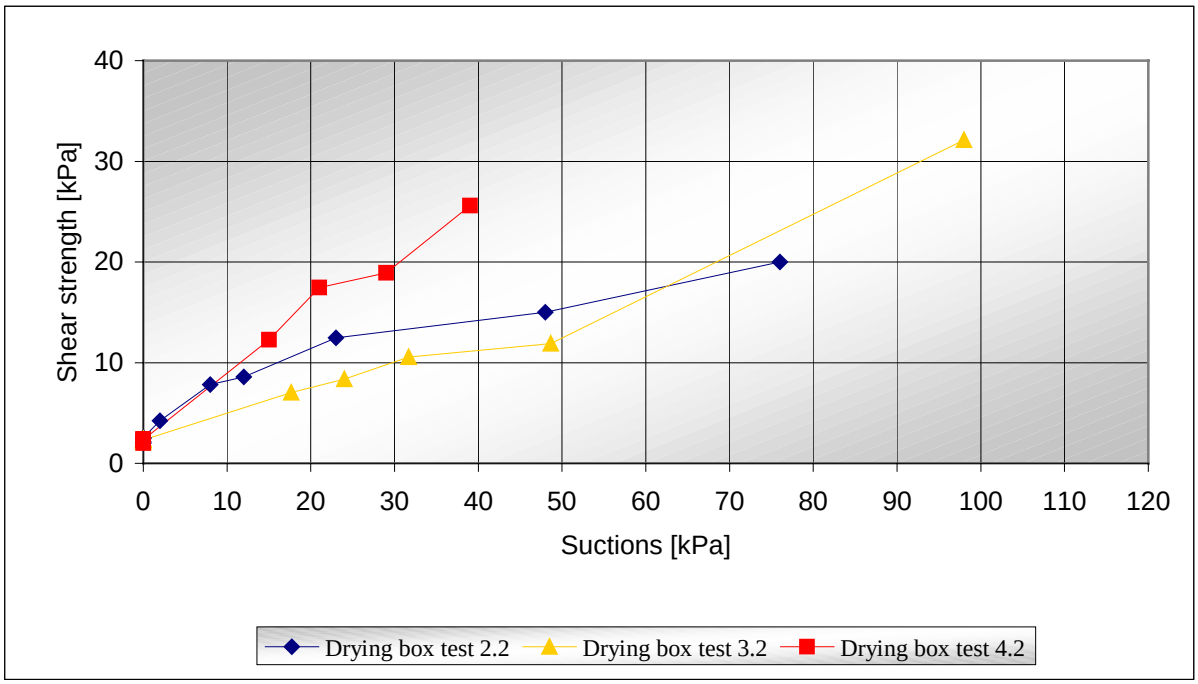

Figure 4.24: Calculated shear strength versus suction at 20 cm – Lift 2

To compare the calculated shear strength results with the vane shear readings, taken at the corresponding depths, an average line was drawn through the shear strength data points. Figure 4.25 and 4.26 compares the shear strength results at 0 cm and 8 cm, with the vane shear readings taken at 0-5 cm and 5-10 cm, during the first lift. Figure 4.27, 4.28 and 4.29 compares the calculated shear strength results at 0 cm, 10 cm and 20 cm with the vane shear readings taken at 0-5 cm, 5-10 cm and 15-20cm during the second lift.

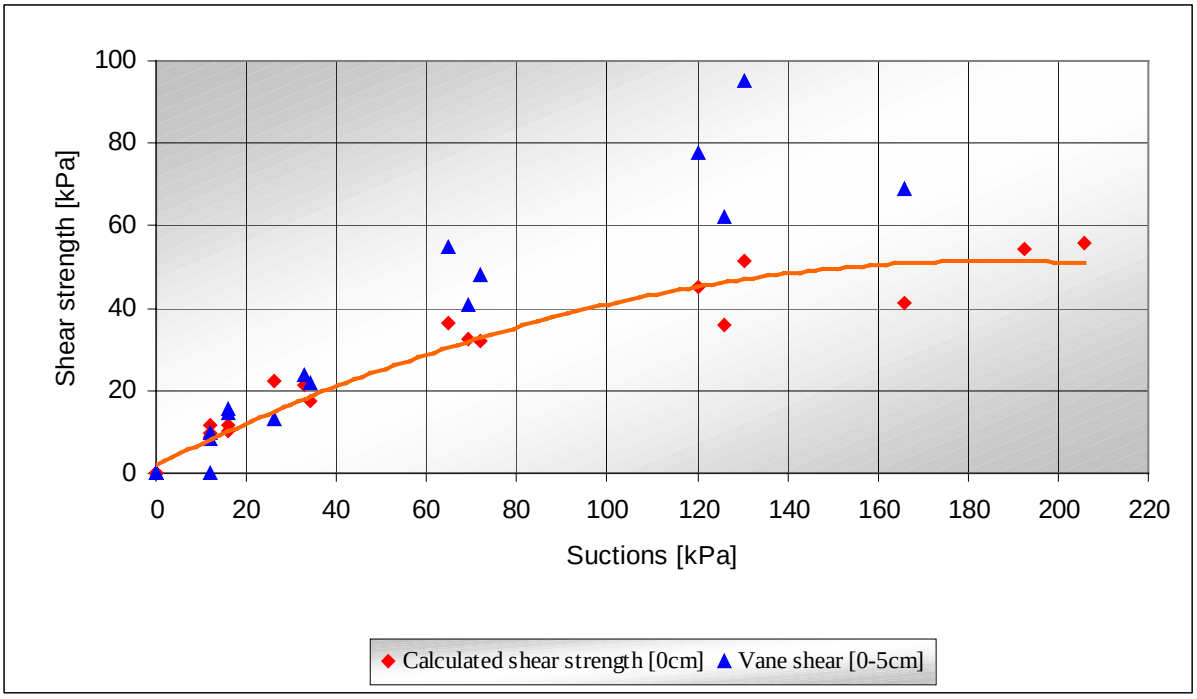

Figure 4.25: Comparison of calculated shear strength and vane shear readings at 0 cm – Lift 1

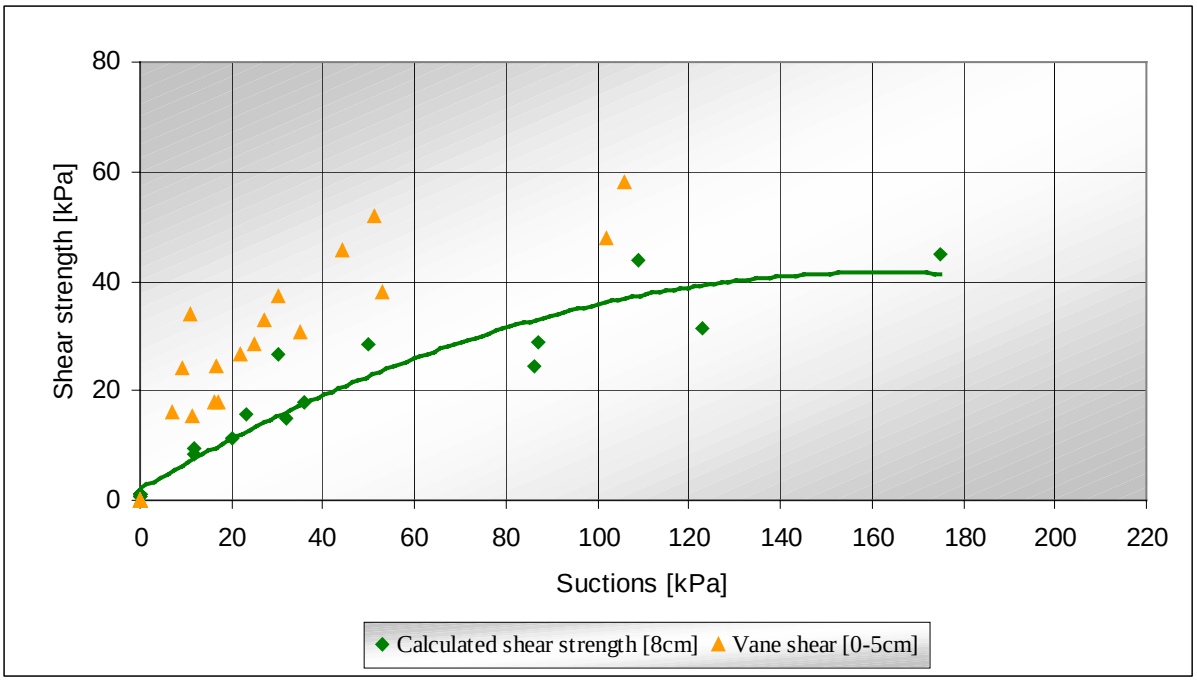

Figure 4.26: Comparison of calculated shear strength and vane shear readings at 8 cm – Lift 1

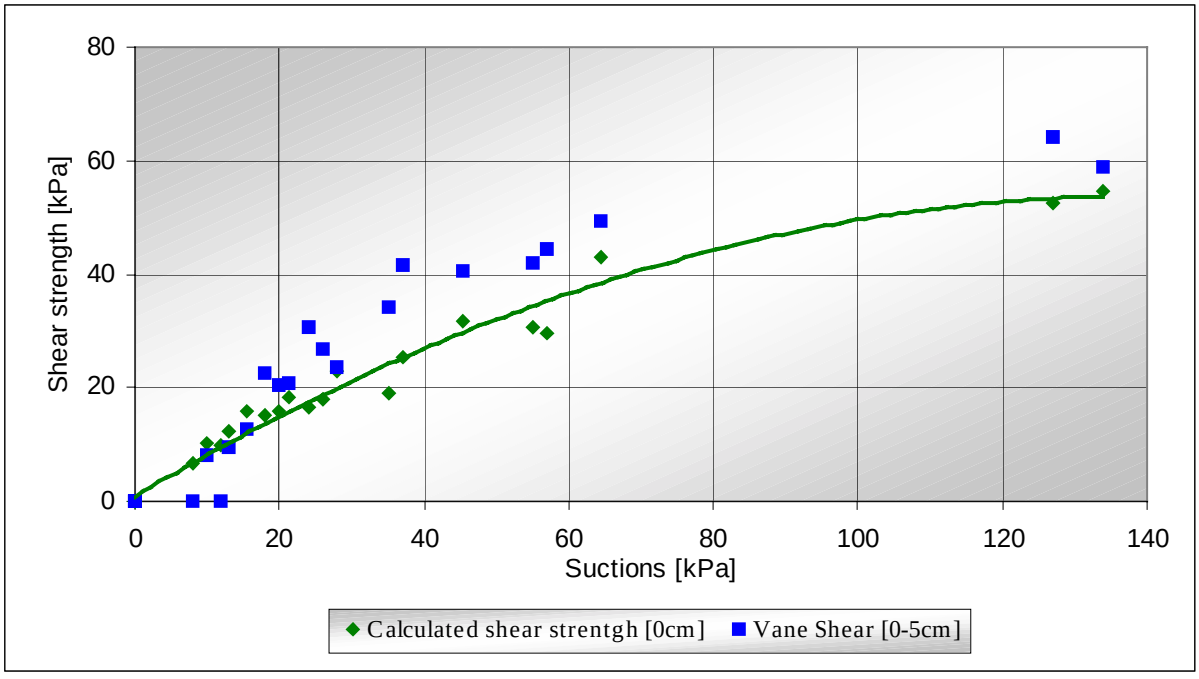

Figure 4.27: Comparison of calculated shear strength and vane shear readings at 0 cm – Lift 2

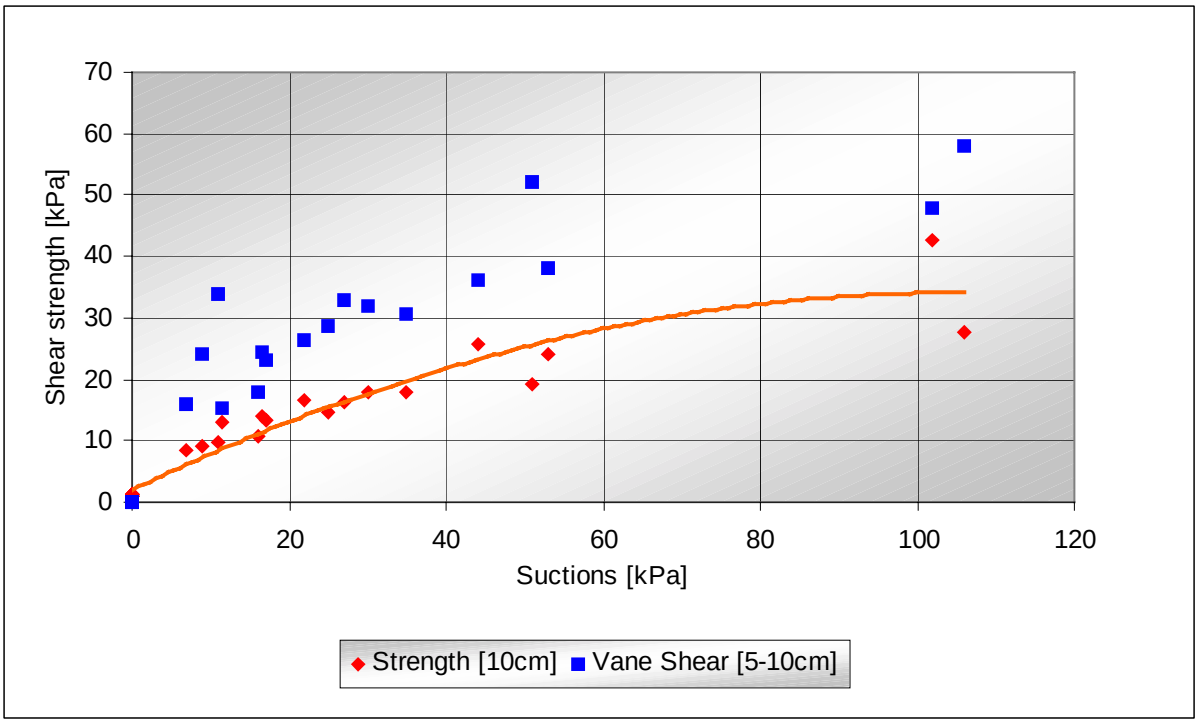

Figure 4.28: Comparison of calculated shear strength and vane shear readings at 10 cm – Lift 2

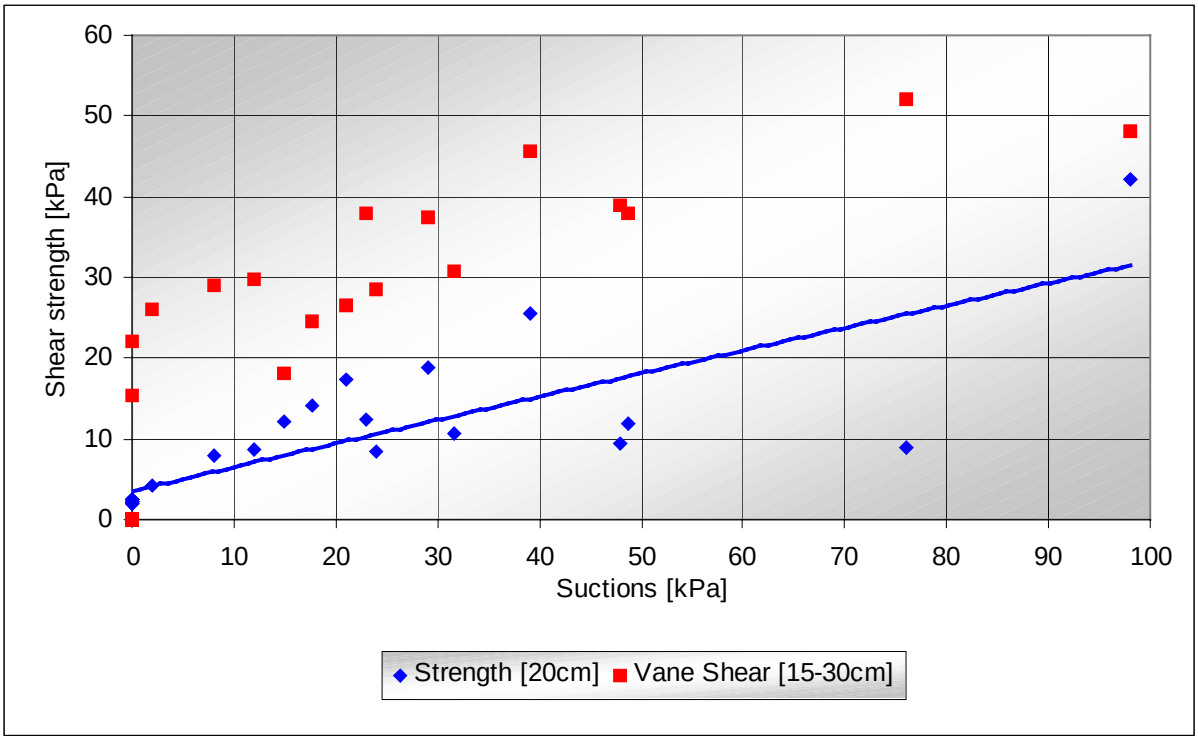

Figure 4.29: Comparison of calculated shear strength and vane shear readings at 20 cm – Lift 2

To establish the influence of sampling errors on the magnitude of the calculated shear strength, the volumetric water content obtained by sampling from the drying box was replaced with volumetric water content values from the SWCC illustrated in Figure 4.10. Thus the second part of Equation [2.32] was calculated by obtaining the volumetric water content at the various suction pressures from Figure 4.10. Thus a theoretical shear strength was calculated based on the results from the trough tests.

For the first lifts the theoretical shear strength values is tabled in Appendix B-13, B-14 and B-15 for drying box test 2.1, 3.1 and 4.1, respectively. For the second lifts this data is tabled in Appendix B-16, B-17 and B-18, for drying box test 2.2, 3.2 and 4.2.

The relationship between theoretical shear strength and suction, at 0 cm and 8 cm, during the first lift and 0, 10 and 20cm, during the second lift, are illustrated graphically in Figure 4.30, 4.31, 4.32, 4.33 and 4.34, respectively.

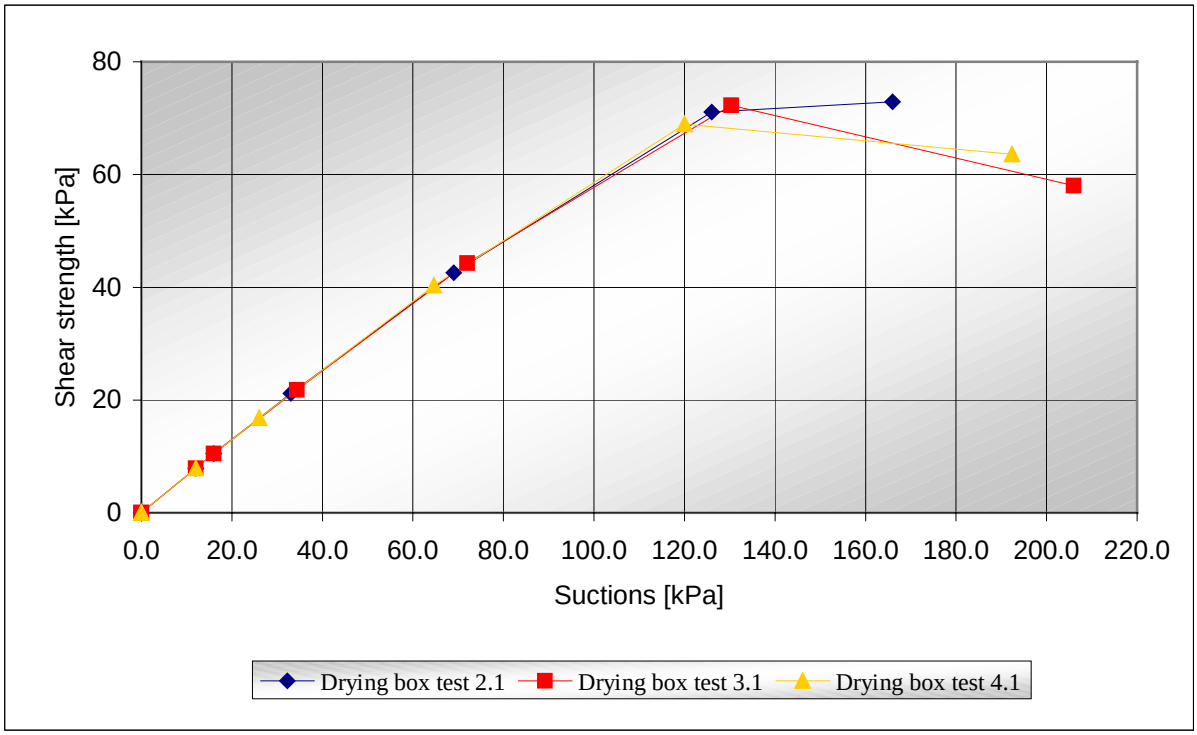

Figure 4.30: Theoretical shear strength versus suction at 0 cm – Lift 1

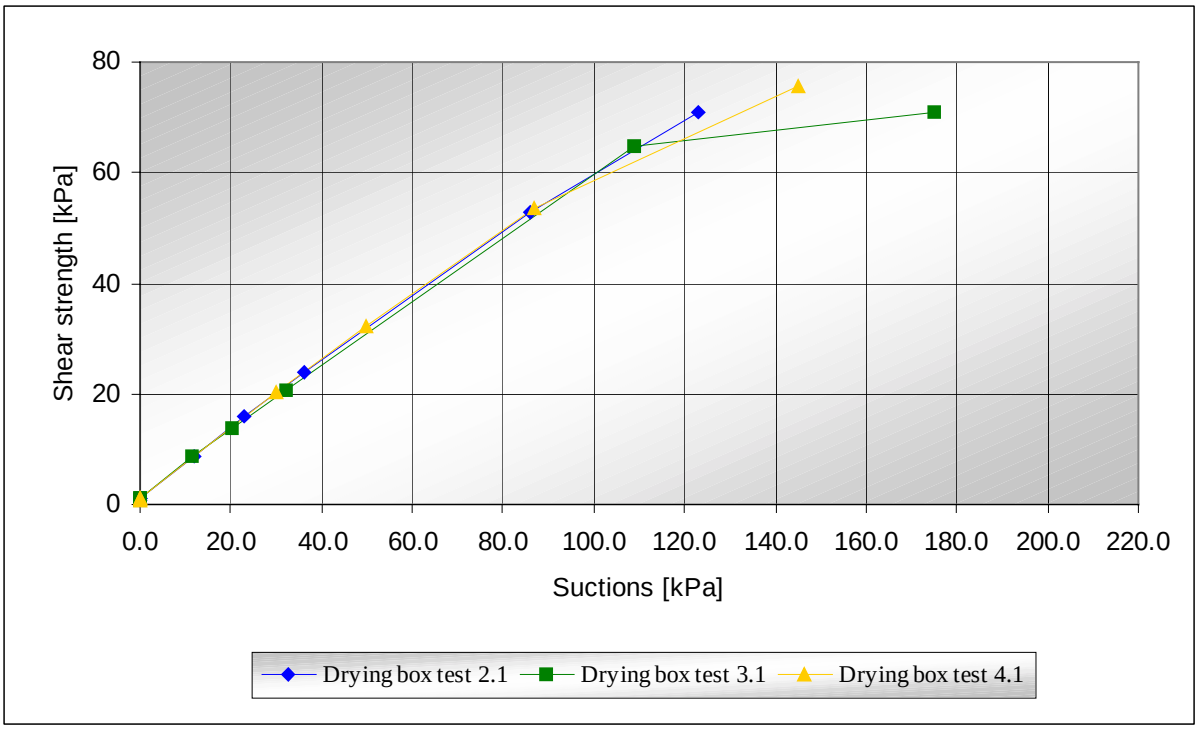

Figure 4.31: Theoretical shear strength versus suction at 8 cm – Lift 1

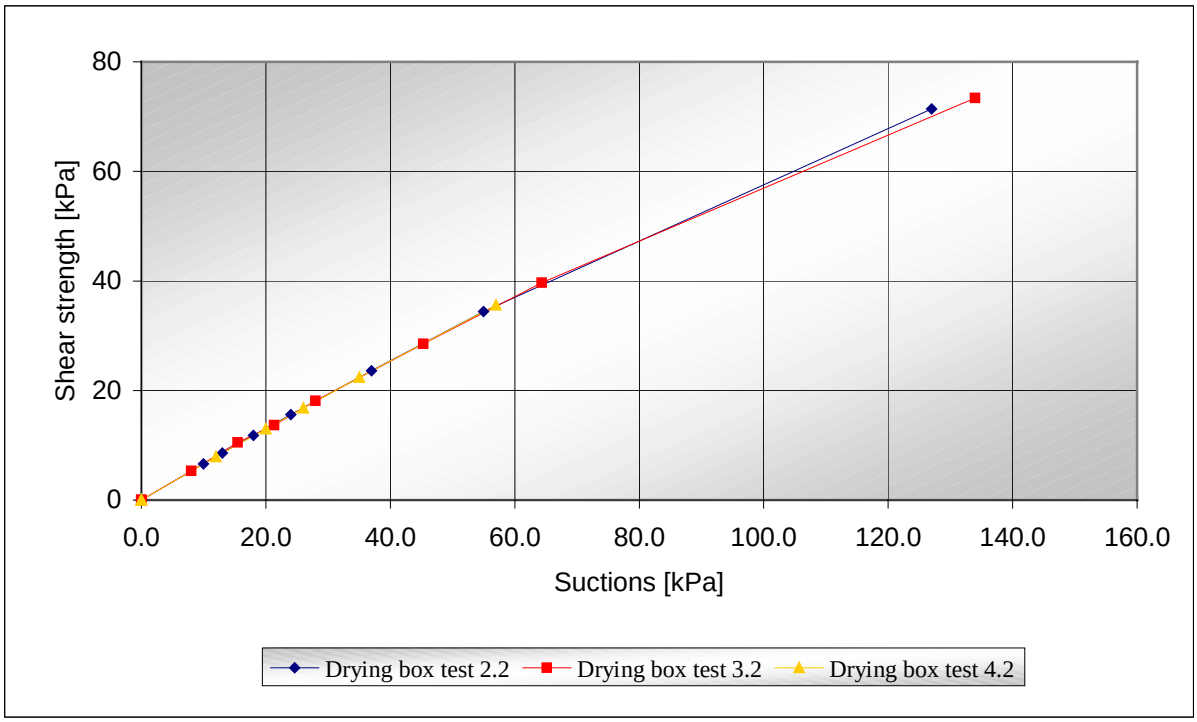

Figure 4.32: Theoretical shear strength versus suction at 0 cm – Lift 2

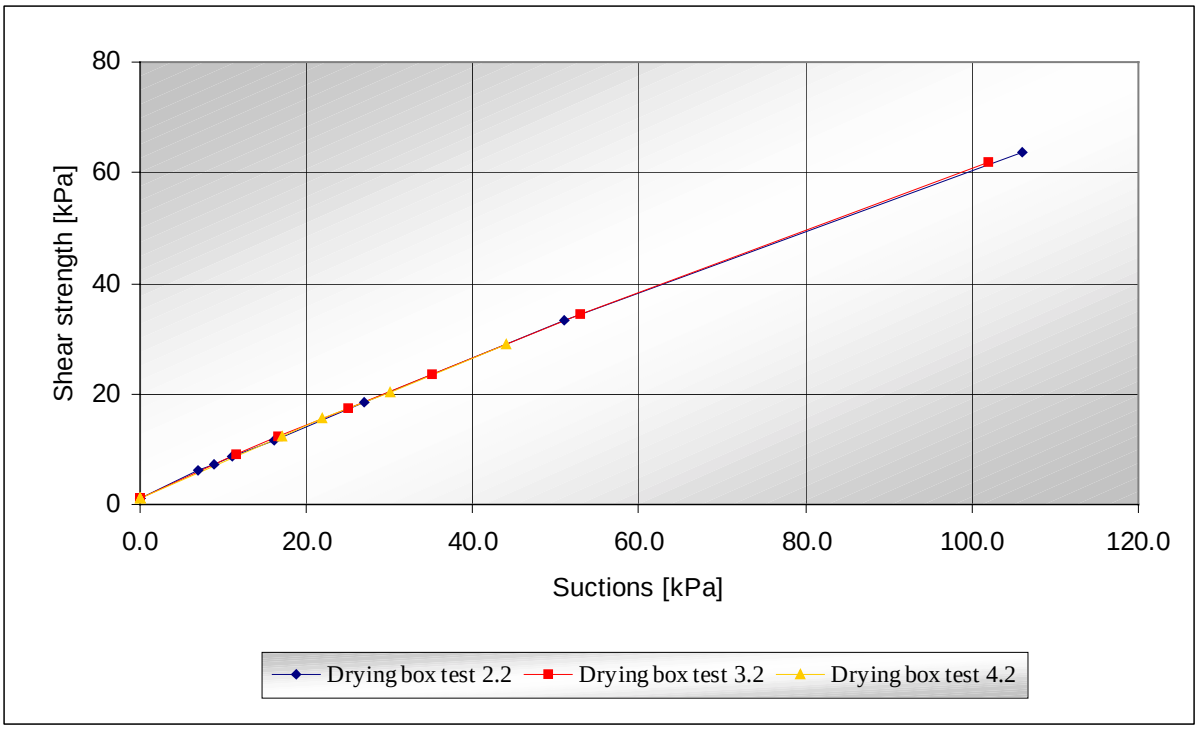

Figure 4.33: Theoretical shear strength versus suction at 10 cm – Lift 2

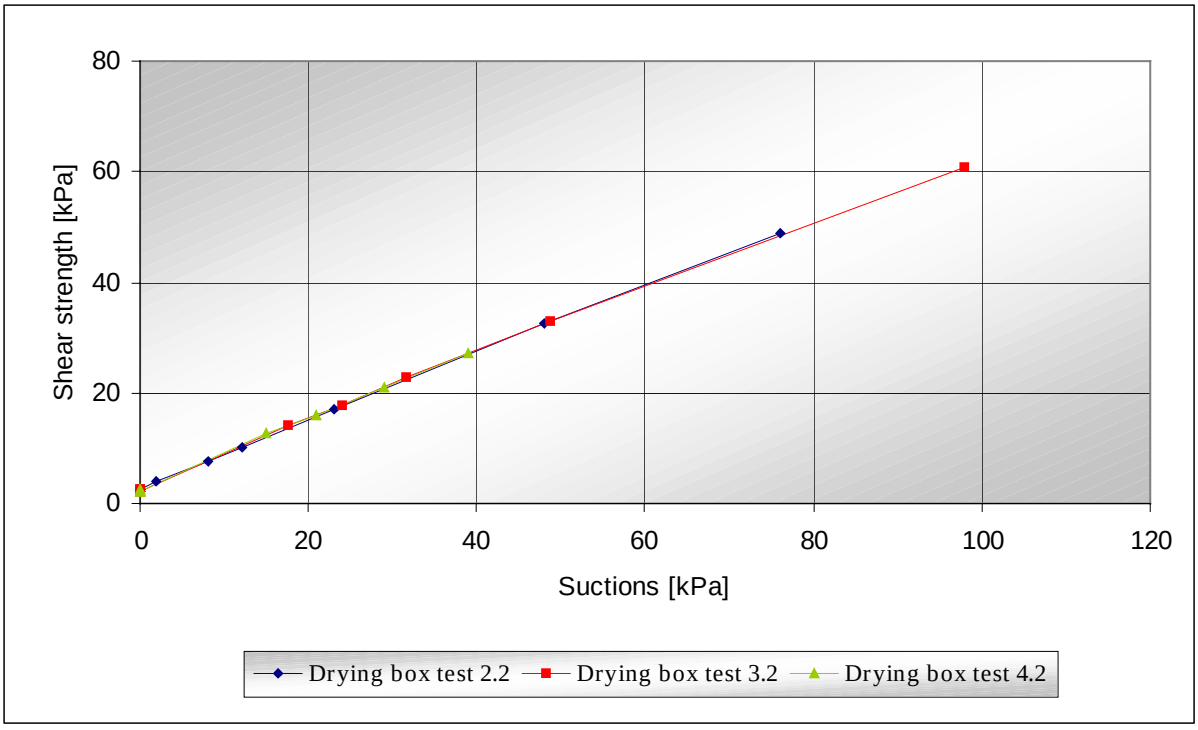

Figure 4.34: Theoretical shear strength versus suction at 20 cm – Lift 2

To compare the theoretical shear strength results with the vane shear readings taken at the corresponding depths, an average line was again drawn through the shear strength data points. Figure 4.35 and 4.36 compares the theoretical shear strength results at 0 cm and 8 cm, with the vane shear readings taken at 0-5 cm and 5-10 cm, during the first lift. Figure 4.37, 4.38 and 4.39 compares the theoretical shear strength results at 0 cm, 10 cm and 20 cm with the vane shear readings taken at 0-5 cm, 5-10 cm and 15-20cm during the second lift.

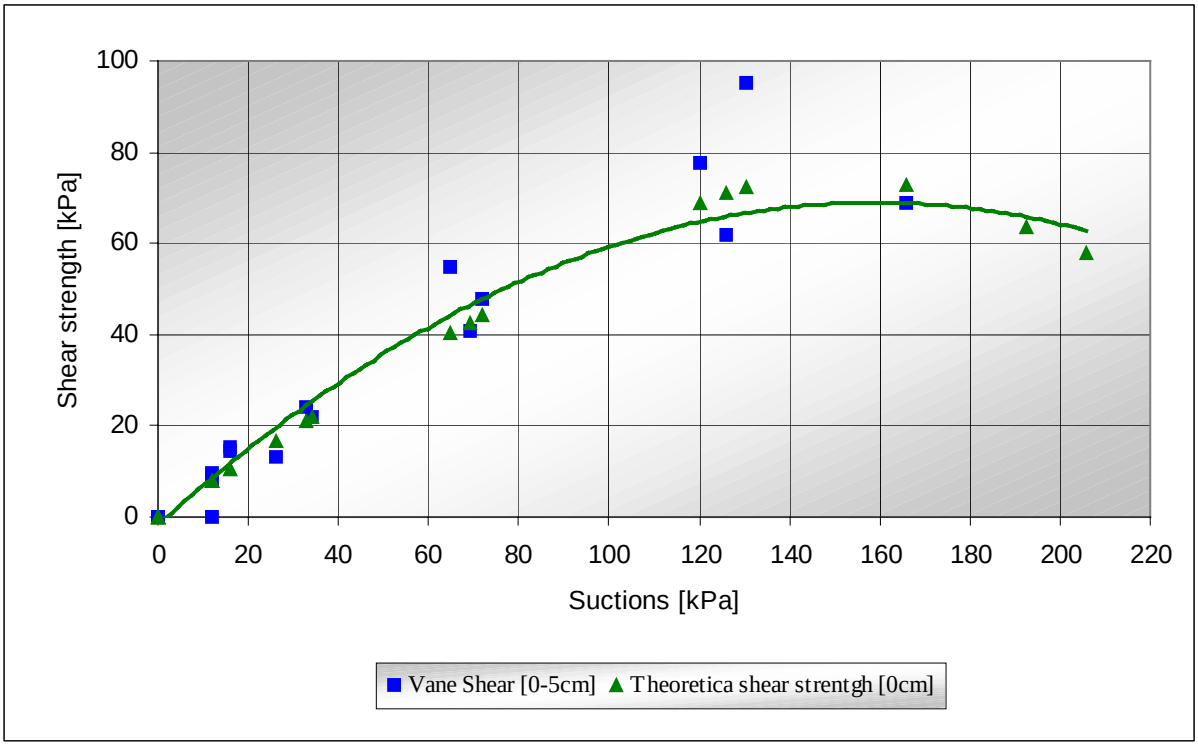

Figure 4.35: Comparison of theoretical shear strength and vane shear readings at 0 cm – Lift 1

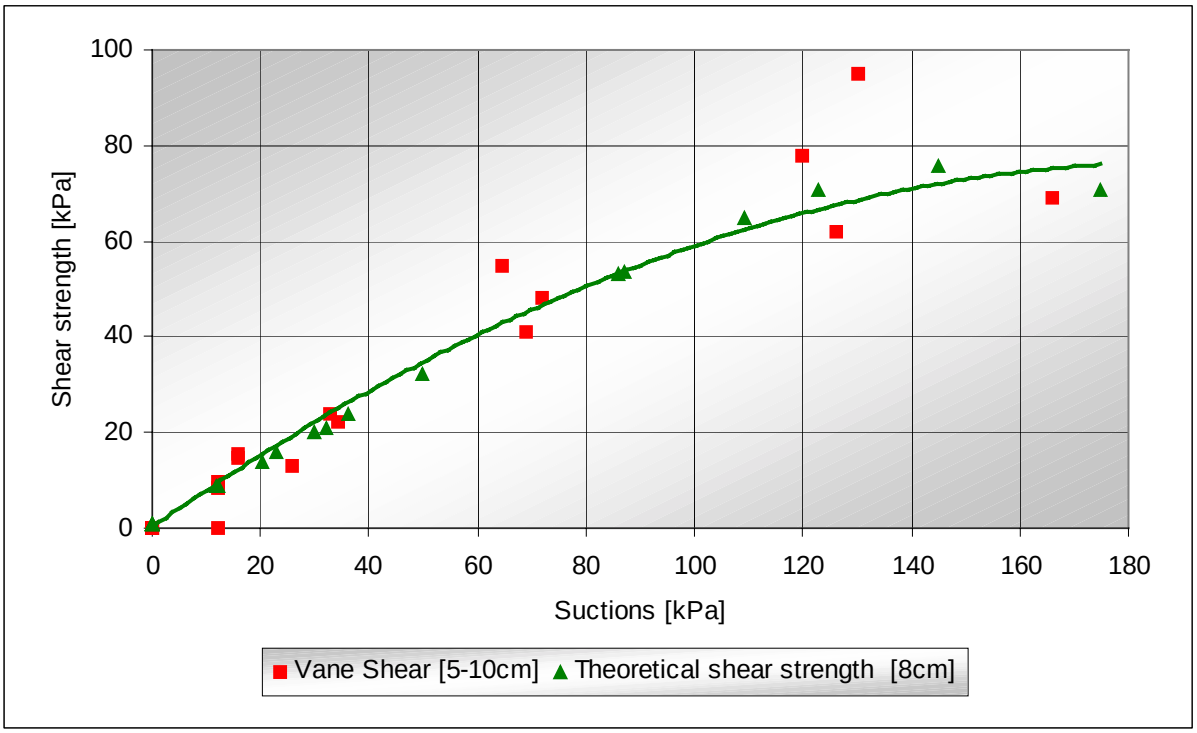

Figure 4.36: Comparison of theoretical shear strength and vane shear readings at 8 cm – Lift 1

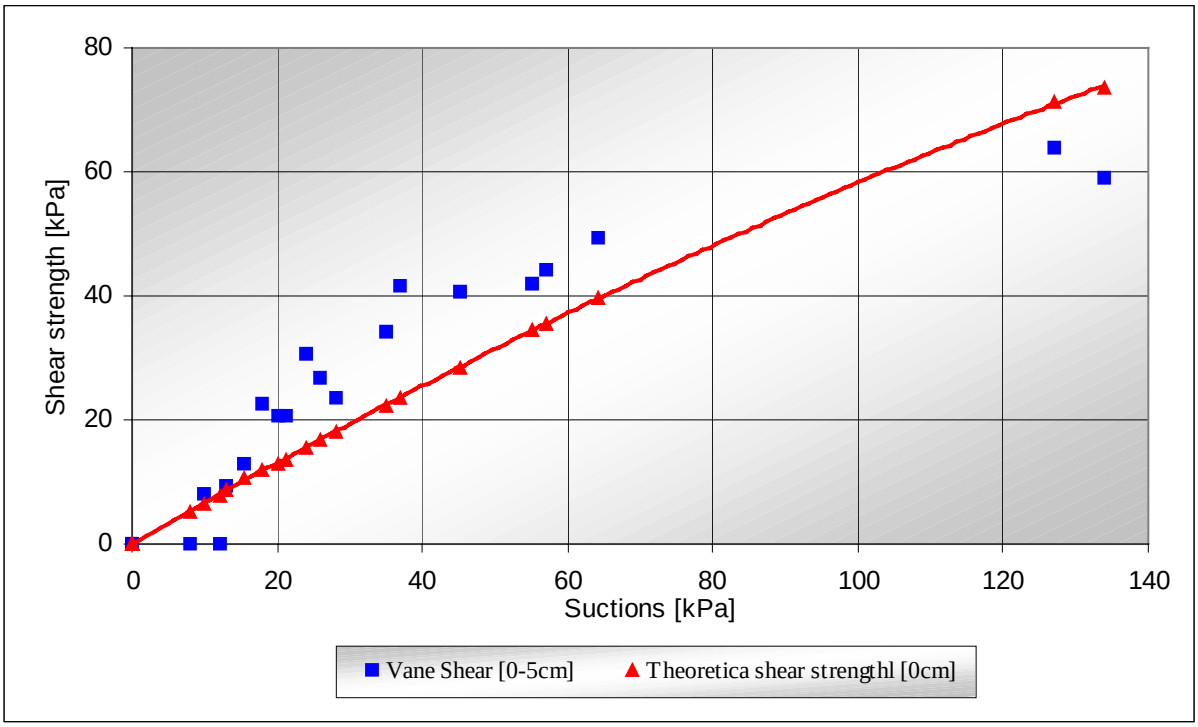

Figure 4.37: Comparison of theoretical shear strength and vane shear readings at 0 cm – Lift 2

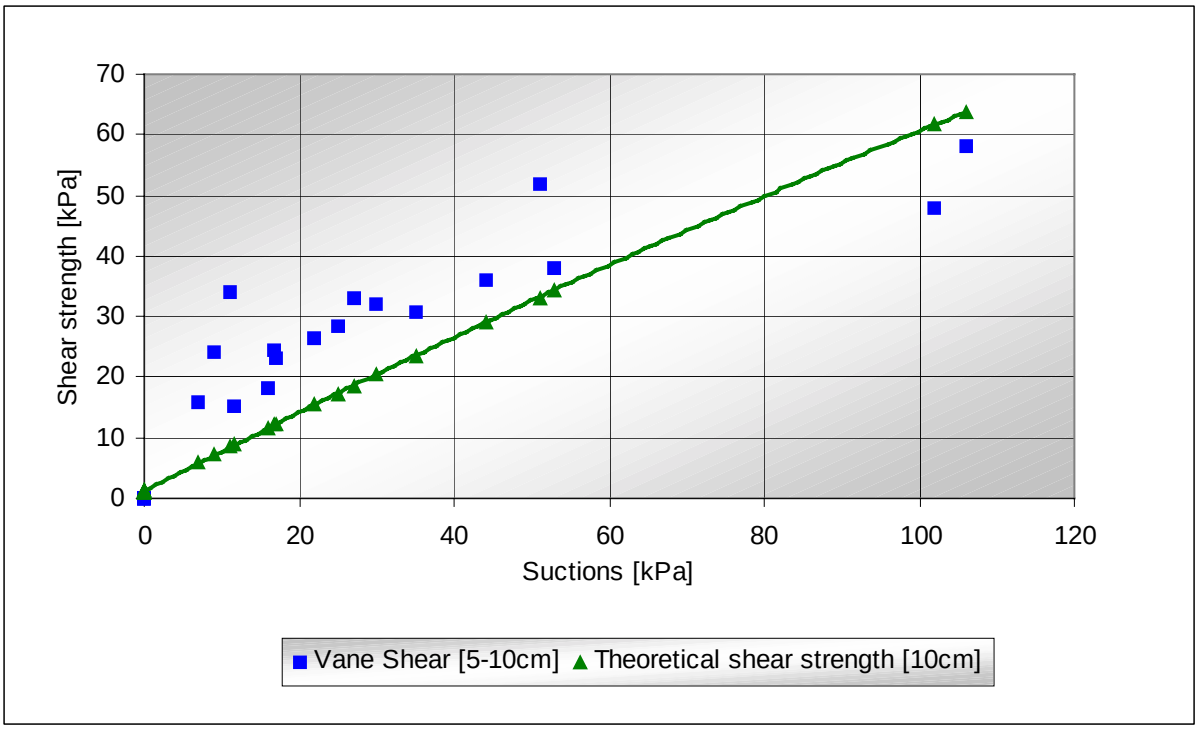

Figure 4.38: Comparison of theoretical shear strength and vane shear readings at 10 cm – Lift 2

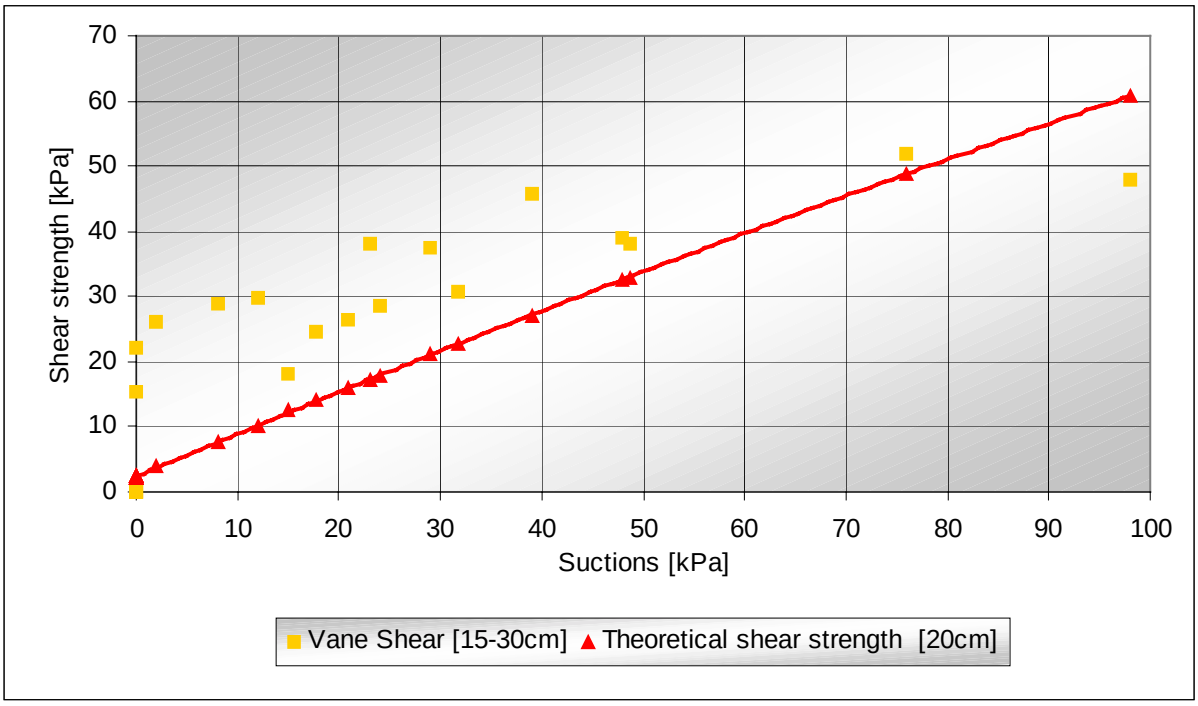

Figure 4.39: Comparison of theoretical shear strength and vane shear readings at 20 cm – Lift 2

4.5 Field Testing

This section presents the results obtained from the field tests, which were carried out on the daywall of Mispah residue dam, as discussed in Section 3.6. Measurements of the cracked block size, crack widths and air temperature were made before the insitu shear strength and suction pressures were measured at different depths within different blocks. Additional measurements were obtained from samples that were extracted from the cracked blocks.

The results of the three field testing sessions are given in Appendix C-1, C-2 and C-3 for site visit 1, 2 and 3 respectively. Figure 4.40, 4.41 and 4.42 illustrates the depth versus suction relationship obtained at the different cracked blocks during site visit 1, 2 and 3, respectively.

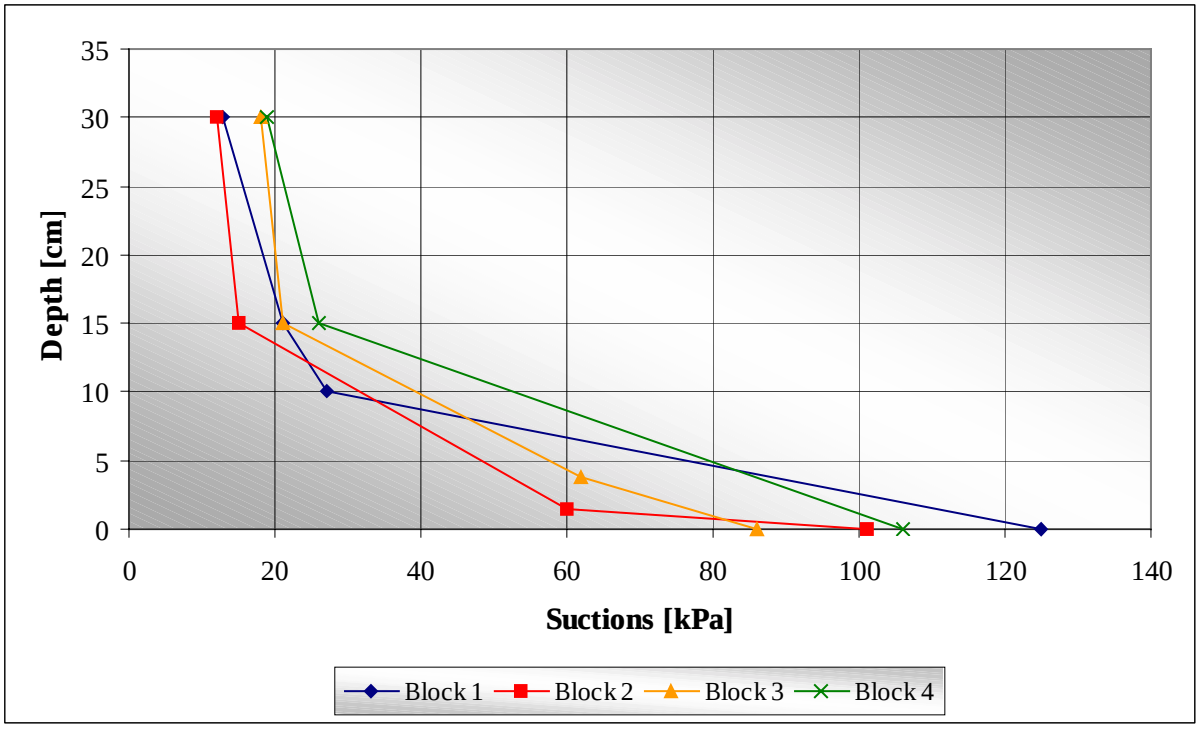

Figure 4.40: Depth versus suction – Site visit 1

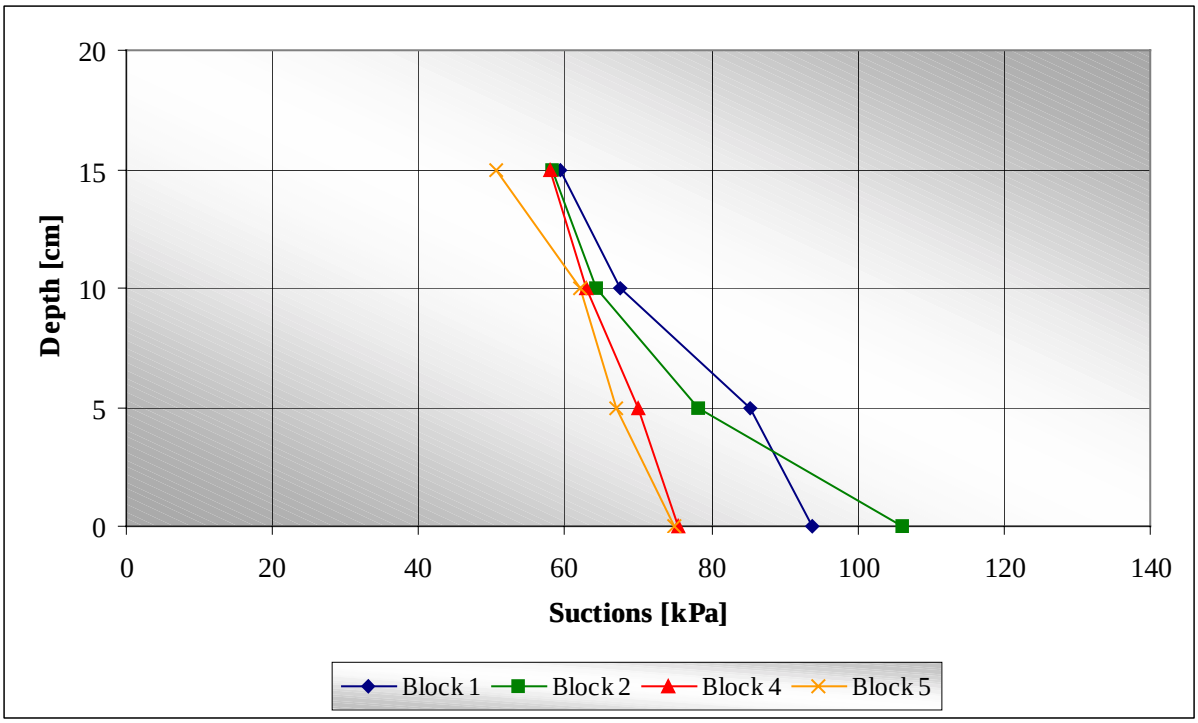

Figure 4.41: Depth versus suction – Site visit 2

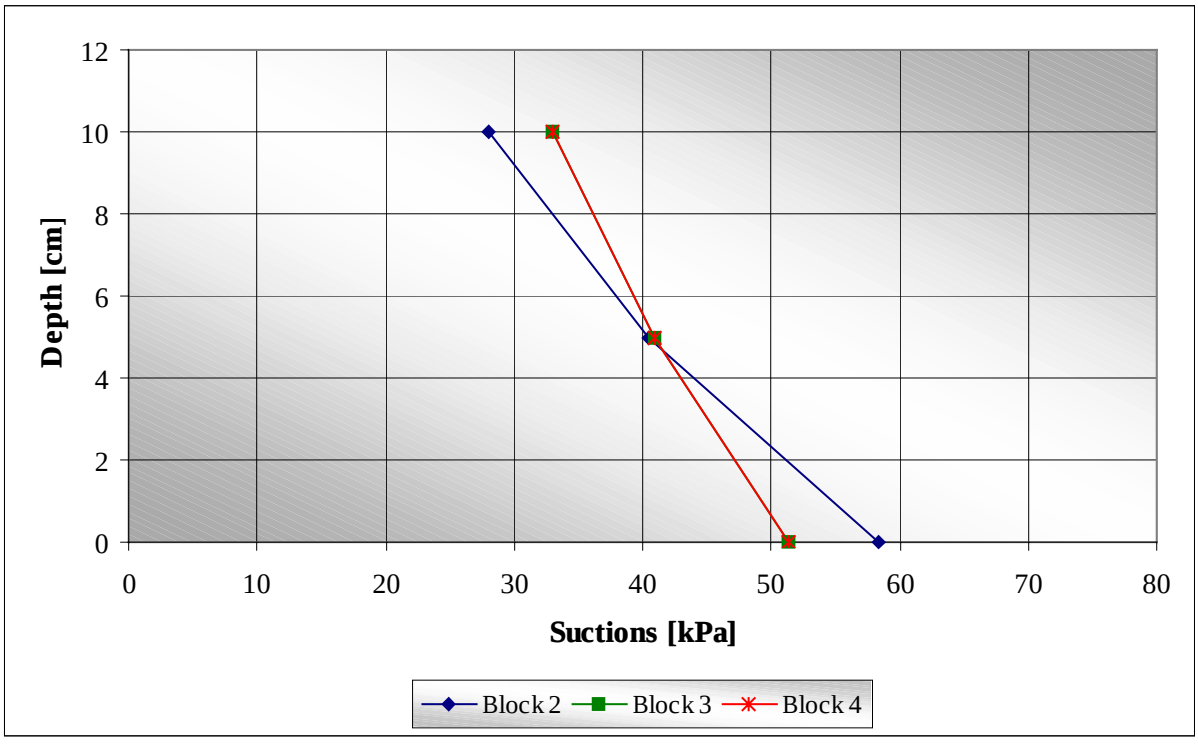

Figure 4.42: Depth versus suction – Site visit 3

From the extracted samples it was possible to determine the moisture content (w), of the tailings material in the daywall using Equation [3.6]. Thereafter the void ratio (e), degree of saturation (S), and volumetric water content (θ), were determined with the use of Equations [3.3], [3.4] and [2.12] respectively. These results are tabled in Appendix C-4, C-5 and C-6 for site visit 1, 2 and 3, respectively.

Figure 4.43 and 4.44 compares the average volumetric water content from the drying box tests, lift 1 and 2, with the results obtained from the field testing.

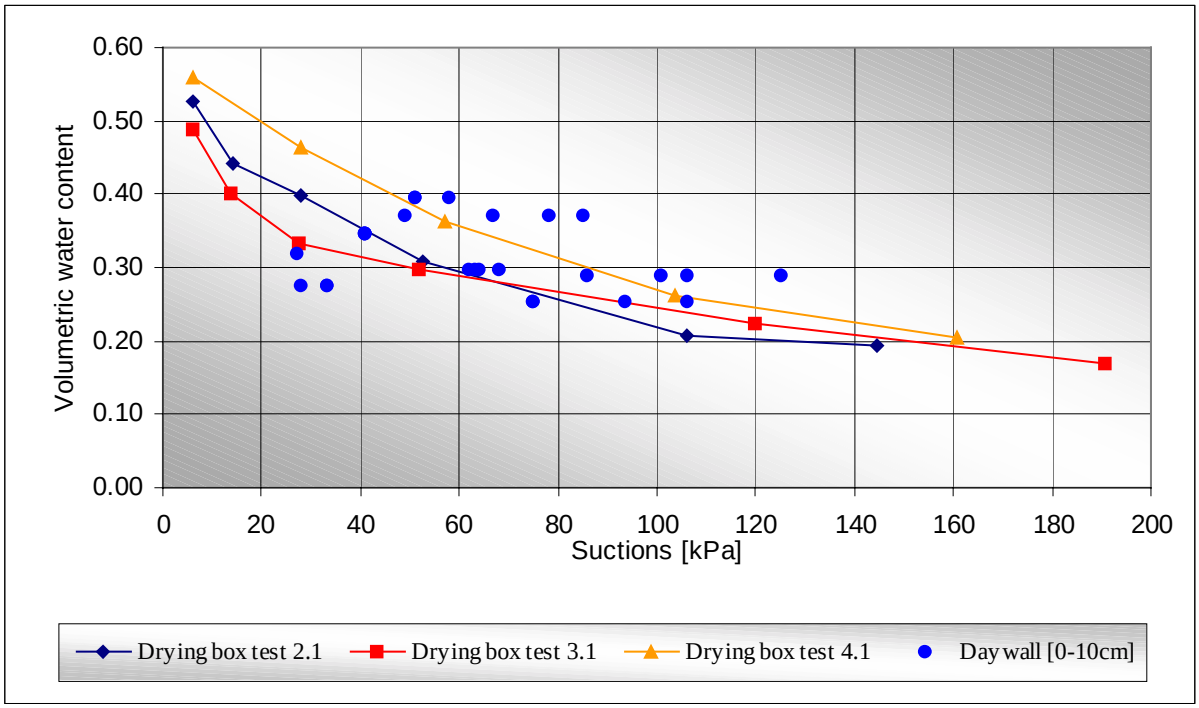

Figure 4.43: Volumetric water content versus suction – Lift 1 and field tests

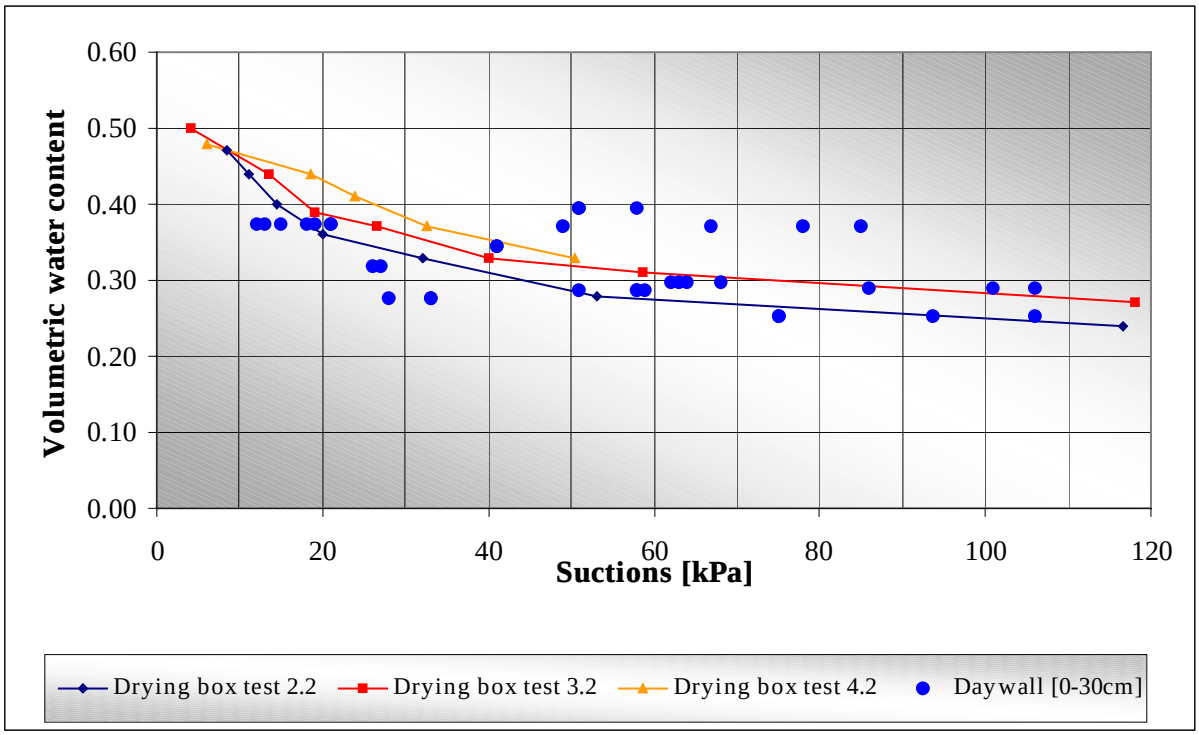

Figure 4.44: Volumetric water content versus suction – Lift 2 and field tests

Figure 4.45 and 4.46 compares the calculated shear strength, theoretical shear strength and vane shear readings from the drying box, at 0-5cm and 5-10cm during the first lift with the vane shear readings from the field testing, at 0-5cm and 5-10cm, respectively. Figure 4.47, 4.48 and 4.49 compares the calculated shear strength, theoretical shear strength, and vane shear readings from the drying box at 0-5cm, 5-10cm and 15-30cm during the second lift with the vane shear readings from the field testing at 0-5cm, 5-10cm and 15-30cm, respectively.

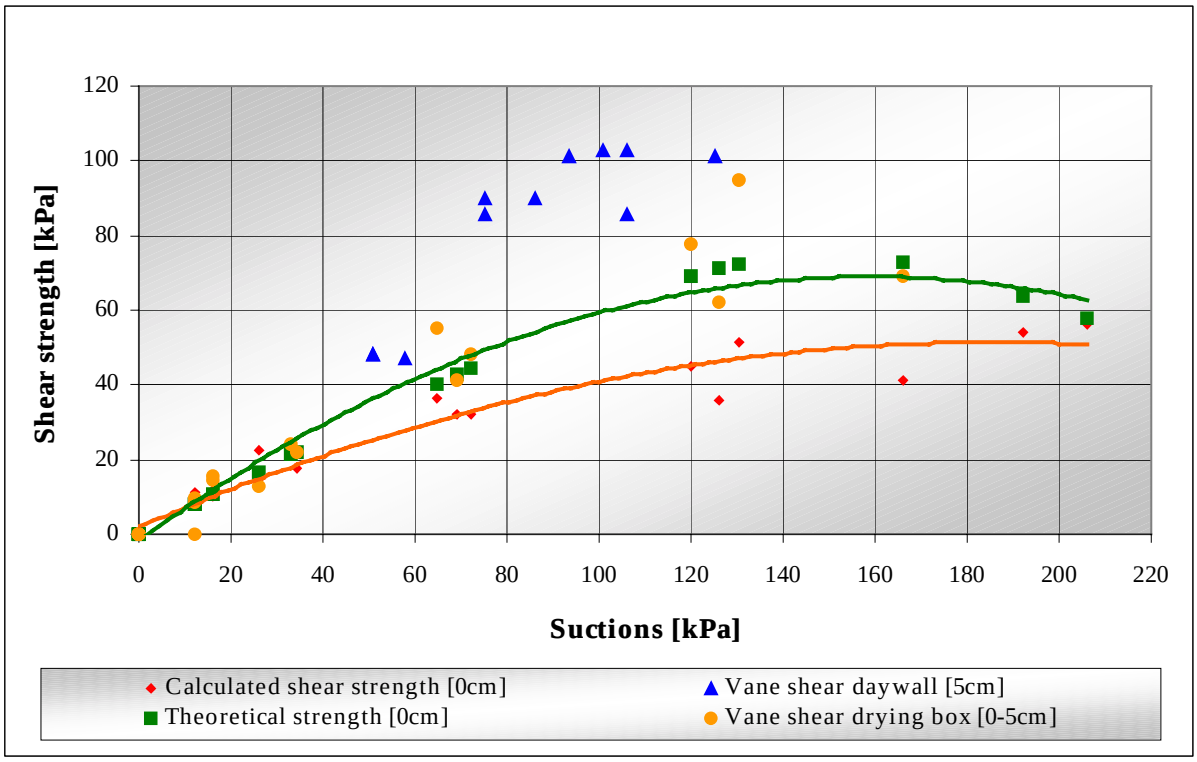

Figure 4.45: Comparison of shear strengths [0-5cm] – Lift 1

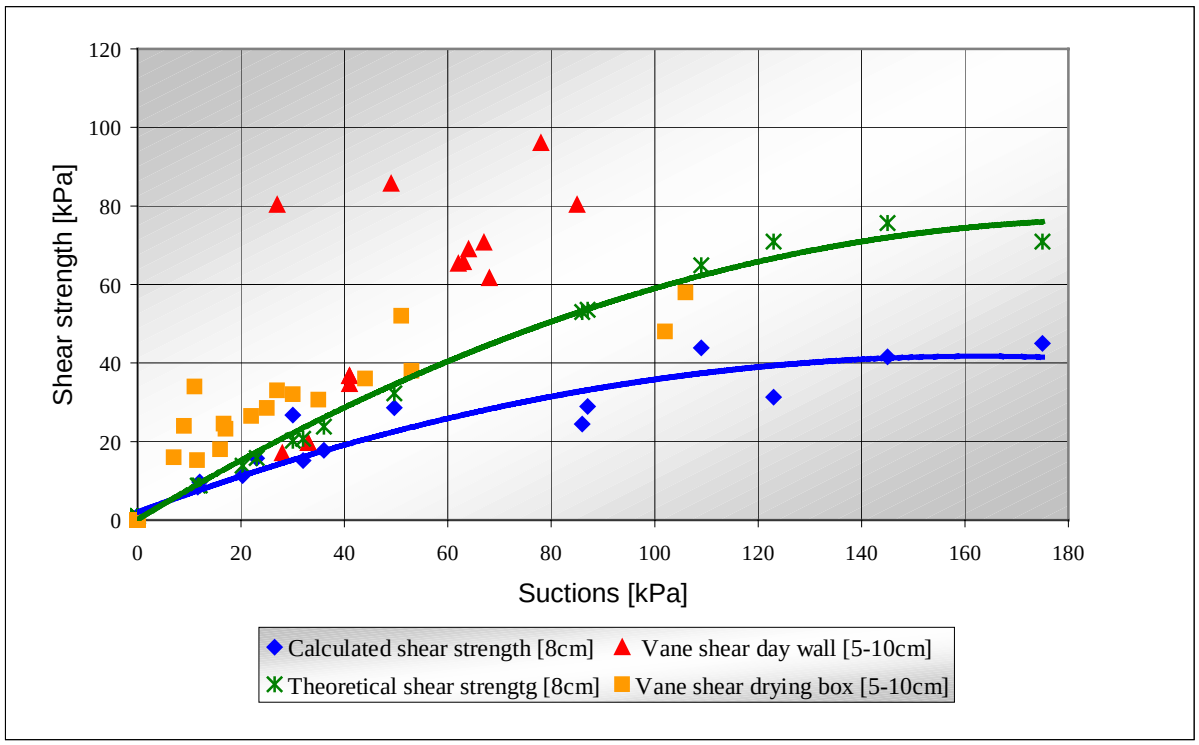

Figure 4.46: Comparison of shear strengths [5-10cm] – Lift 1

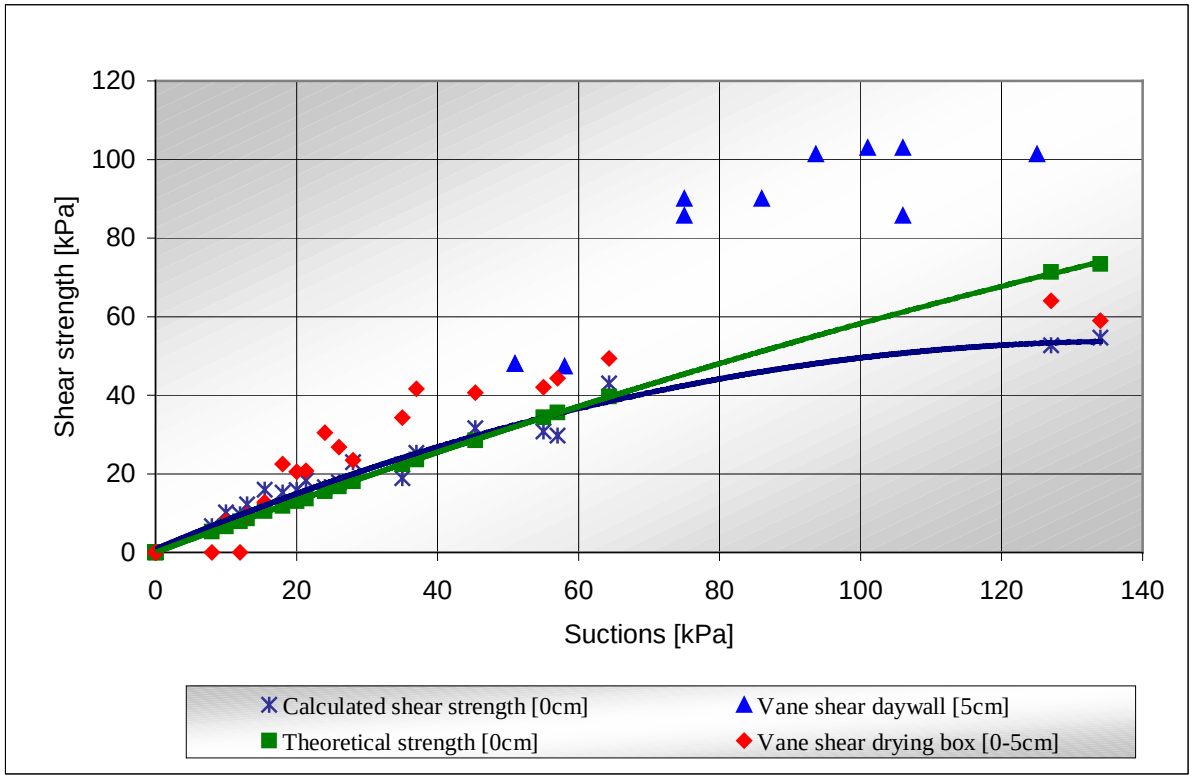

Figure 4.47: Comparison of shear strengths [0-5cm] – Lift 2

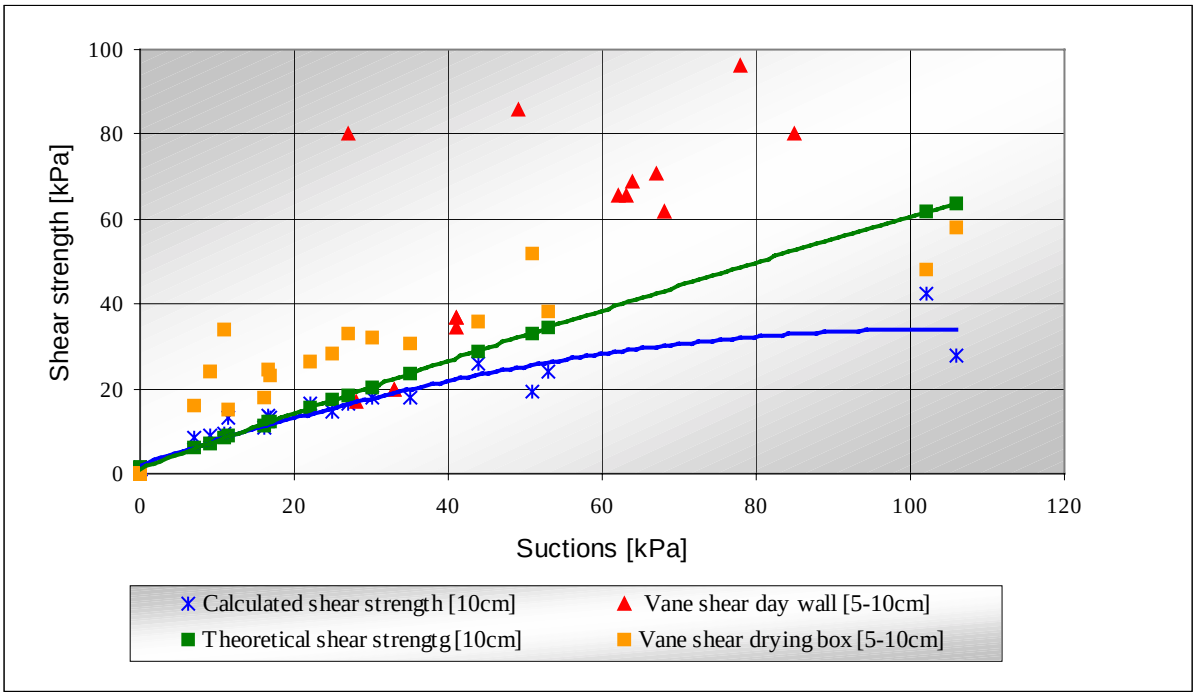

Figure 4.48: Comparison of shear strengths [5-10cm] - Lift 2

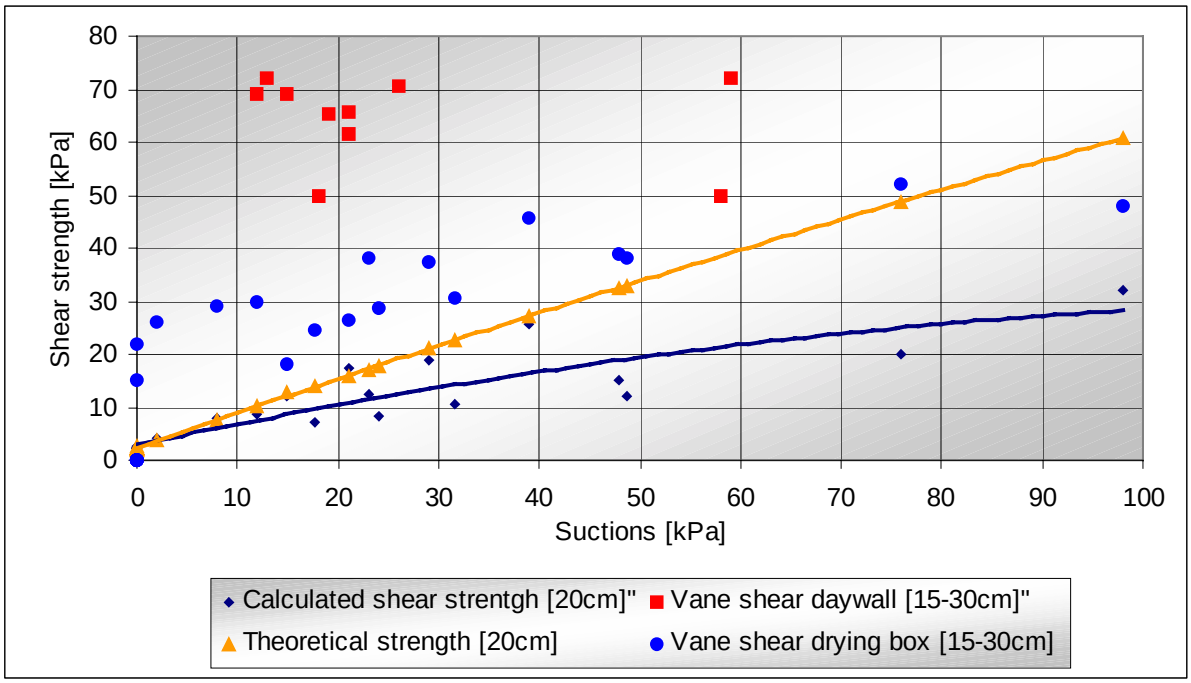

Figure 4.49: Comparison of shear strengths [15-30cm] – Lift 2

5. DISCUSSION

5.1 Introduction

Experimental tests were conducted in order to investigate three different methods of quantifying suction induced shear strength, in gold mine tailings. It is the aim of this chapter to discuss the results given in Chapter 4, and to compare the results of the three different methods. There were various shortcomings in the experimental equipment and procedures used, which influenced the results obtained.

The measurement of volume changes during the trough test, the volume of samples extracted from the daywall, and the measurement of crack widths could not be done accurately. This was due to the inherent limitations of the measuring equipment used and due to the sloughing of the very wet samples and the shattering of the dry samples after it had been extracted. These limitations caused some inaccuracy in the calculations of degree of saturation (S), void ratio (e) and volumetric water content (θ) of the material tested.

The tailings material used during the test were gathered at different positions and depths on the daywall of Mispah residue dam. This causes variation in the results obtained for the various drying box tests since different material was used during the construction of each lift. With only a small quantity of material used, it is assumed that the behavior exhibited through the results would be representative of the behavior of the bulk of the material on Mispah residue dam.

The drying box tests were conducted with simulated continuous daytime conditions, except for the 15min periods in which the lights cooled down. Thus, the drainage of excess water that usually takes place during the nighttime, was not taken into consideration. This was compensated for with the free draining Bidim filter that caused a higher drainage flux to the bottom of the layer.

The drying box only represents the behavior of a small portion of the daywall and did not allow for the simulation of surplus surface water runoff, horizontal seepage, and changes in the climatic conditions. The very short drainage length and the higher drainage flux, due to the free draining surface, compensated for this.

Due to the anisotropy of the deposited tailings material, and the presence of silt, the vane shear readings obtained were erroneous to some degree. But since the vane shear would only be used as a direct method to validate the calculated shear strengths, it was assumed to be negligible.

5.2 Soil-water Characteristic Curve

The results obtained from the trough tests are illustrated in Figure 4.1 – 4.5. Figure 4.1 illustrates the moisture content versus suction relationship for trough tests 2 and 3. Both curves follow the same trend with a 2% difference between the two plots. These results are compared in Figure 5.1 with the results obtained by Van Heerden (2001) for various particle ranges of Mispah gold tailings. These ranges are given in the following table:

Table 5.1: Particle range used by Van Heerden (2001)

Code	Particle size
B	20<63µm
C	6<20µm
D	2<6µm
E	<2µm

From Figure 5.1 it can be seen that the two plots of trough test 2 and 3 falls between the plots of particle range C and D. With the plots not exhibiting a common trend, it is not possible to find a comparison between the results.

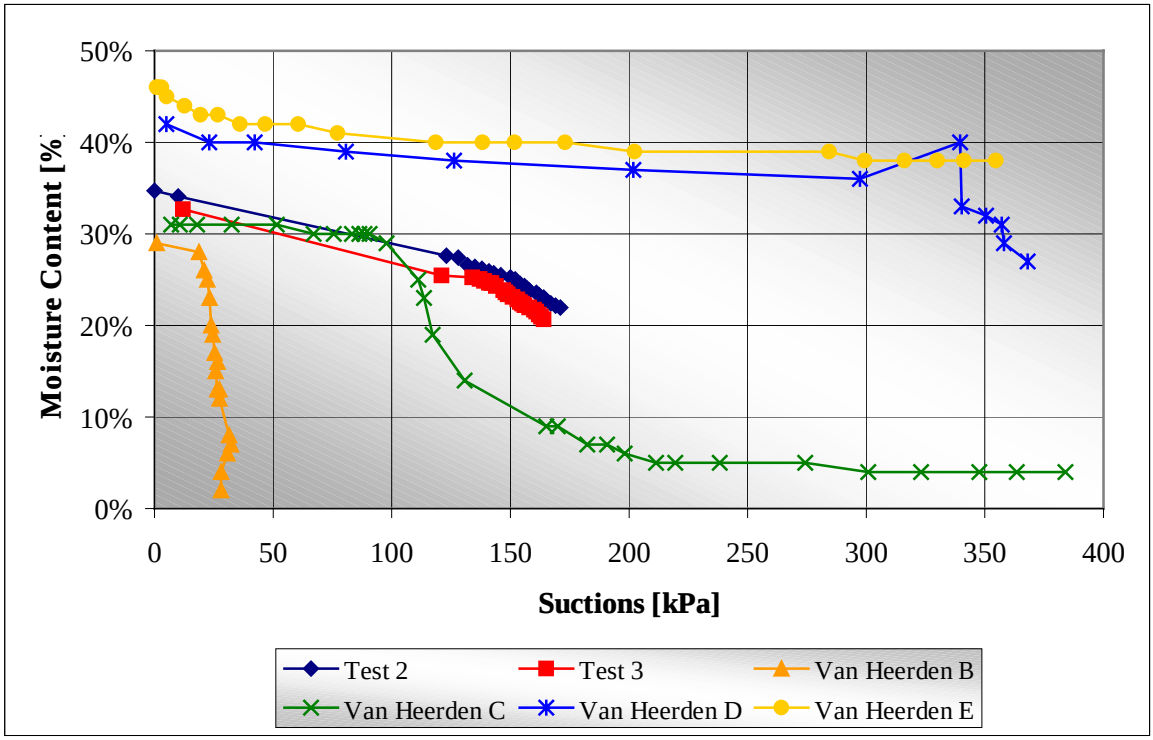

Figure 5.1: Comparison of moisture content versus suction

Figure 4.2 illustrates the void ratio versus suction relationship of both trough tests. The trends of the plots correlate well with each other, with a maximum difference of 0.1 at 10kPa suction pressure. At suction pressures of between 120kPa and 160kPa, the two plots coincided, rendering a void ratio of between 1 and 1.05. The small variations in the void ratios are mainly as a result of measurement inaccuracies during the volume measurement.

Figure 5.2 compares the void ratio versus suction plots of trough test 2 and 3, with the plots obtained by Van Heerden (2001). The trend of the plots of trough test 2 and 3 correlates best with the plots of particle range E and D, where there is a small decrease in void ratio that takes place before a constant value is reached. The range of void ratios in Figure 5.2 is between 0.7 and 1.2 for all the particle ranges, with trough test 2 and 3 exhibiting a void ratio of between 1 and 1.05.

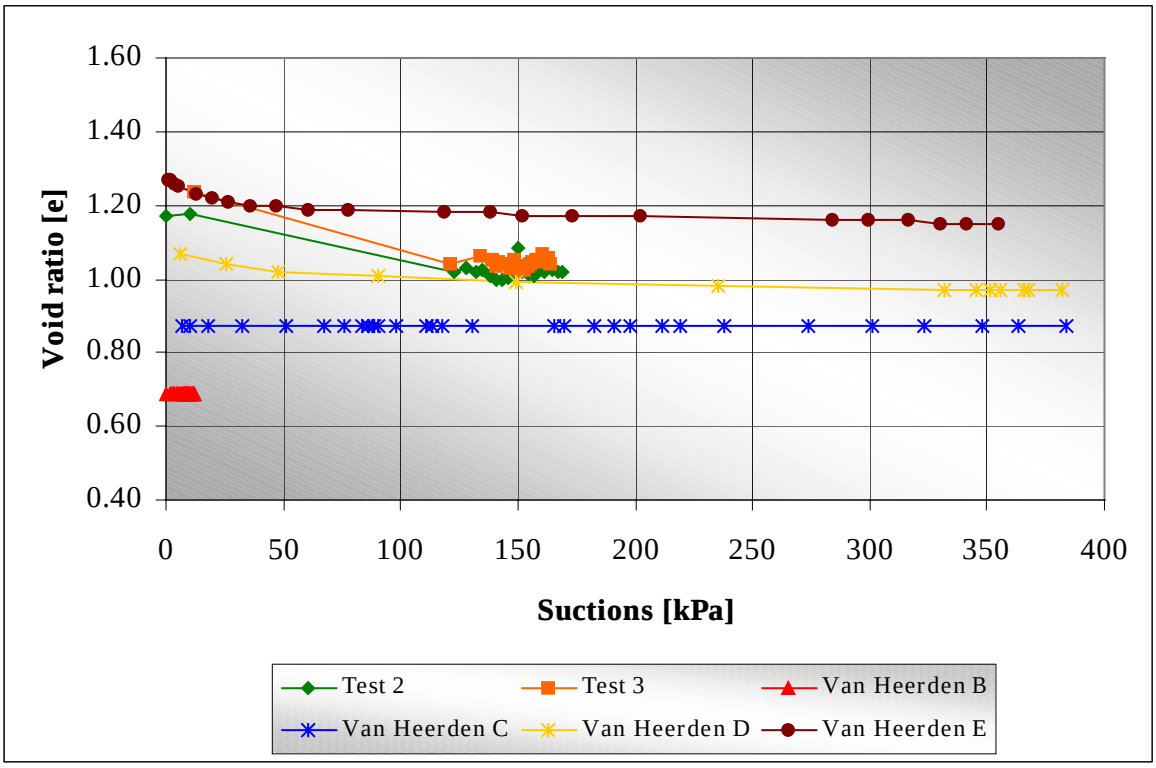

Figure 5.2 Comparison of void ratio versus suction

The degree of saturation versus suction plot for trough tests 2 and 3 are illustrated in Figure 4.3. The two plots exhibit the same trend with an initial difference of 0.2 over the suction range of 0 – 140kPa between the two plots. Above 140kPa suction pressures the two plots starts to coincide.

Figure 5.3 compares the degree of saturation versus suction plots, of the two trough tests with the plots obtained by Van Heerden (2001). All the plots follow the same trend, with an initial near linear portion over which the degree of saturation decreases slightly. This is followed by a sharp decrease as the air entry suction pressure is reached. The results of trough tests 2 and 3 falls between the plots of particle range C and E, indicating that the material used for the two trough tests exhibits the behavior of a well graded mixture of tailings material.

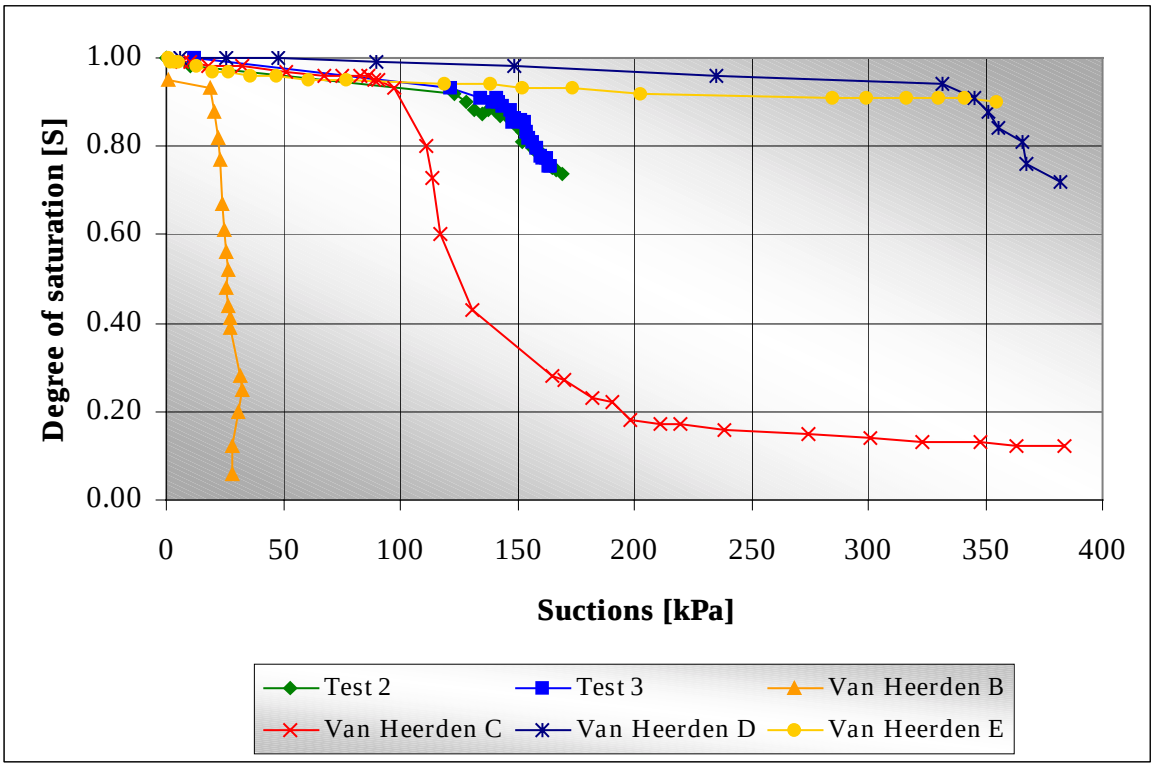

Figure 5.3: Comparison of degree of saturation versus suction

Figure 4.4 illustrates the percentage of linear shrinkage versus suction plots for trough test 2 and 3. The plots show a linear increase in shrinkage over suction pressures of between 0kPa and 120kPa. Above 120kPa the plots become asymptotic at 2.6% and 2.8% linear shrinkage. The results from Van Heerden (2001) indicate an average percentage linear shrinkage of 2.4%, which correlates well with the results obtained from the two trough tests.

The soil-water characteristics curve for the Mispah residue whole tailings material is represented in Figures 4.6 and 4.7. The associated values of suction at residual saturation (ψ_r), saturated volumetric water content (θ_s), and the residual volumetric water content (θ_r), along with the other SWCC-fitting parameters is summarised in Table 4.1.

The results obtained from the trough tests were used to obtain two partial SWCC plotted on an axis of volumetric water content versus suction, as illustrated in Figure 4.5. The saturated volumetric water content was approximately 0.51 for trough test 2 and 3. This value corresponds to the saturated volumetric water contents of 0.44 and 0.39 obtained for tailings material by Fredlund et al. (1997) and Rassam et al. (2000), as illustrated in Figure 5.4 and 5.5 respectively.

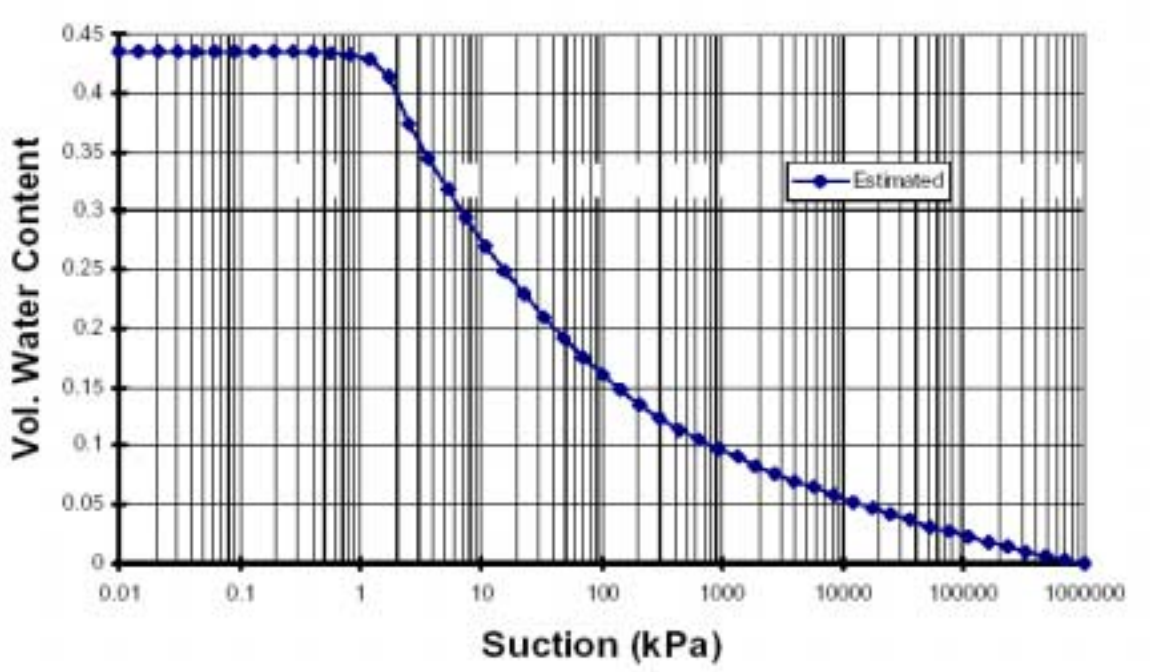

Figure 5.4: Estimated soil-water characteristic curve for mine tailings (Fredlund et al., 1997)

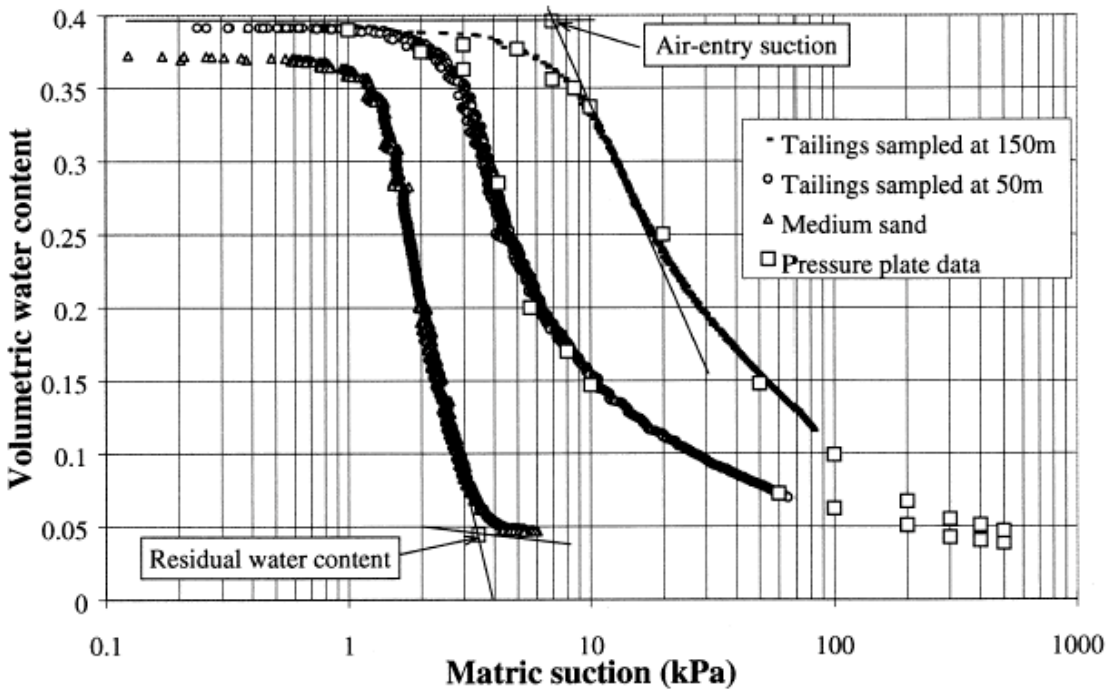

Figure 5.5: Water characteristic curves (Rassam et al., 2000)

The difference between the two partial plots is the result of measurement inaccuracies and poor mixing of the slurry, which rendered non-homogeneous samples. The partial plots, illustrated in Figure 4.5, indicate that air entry occurs at a suction of between 130kPa and 140kPa.

This compares well with the air entry values of 130kPa and 100kPa observed by Fredlund et al. (1994) as illustrated in Figure 5.6. This high value of air entry is to be expected as the Mispah whole tailings is predominantly clayey silt. The tailing material used to obtain the SWCC in Figure 5.4 and 5.5, were predominantly sandy silt material due to the cycloning discharging method used.

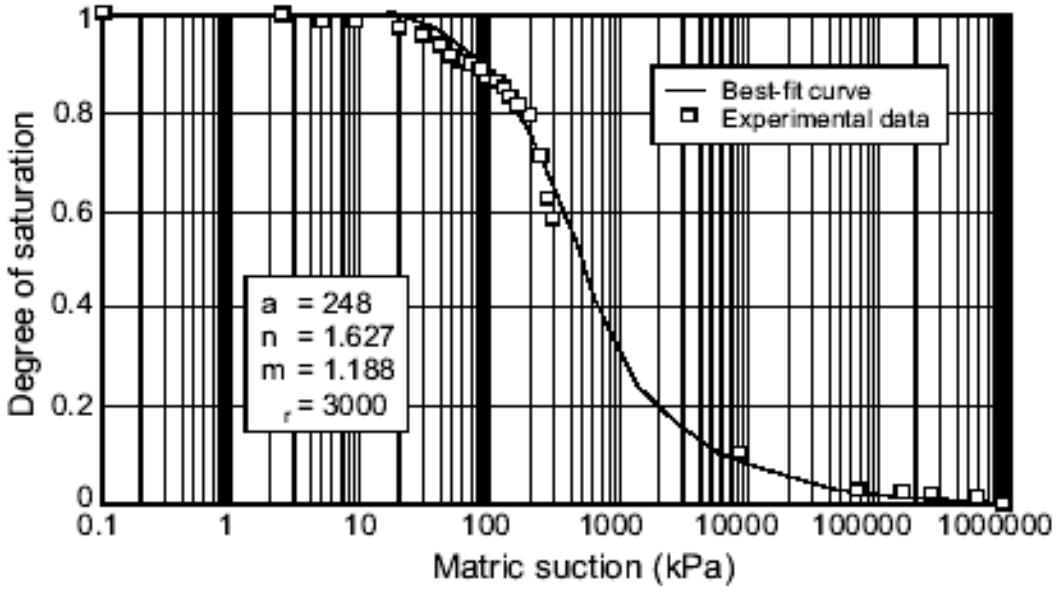

Figure 5.6: A best-fit curve to the experimental data of Kidd Creek tailings (Fredlund et al., 1994)

The SWCC illustrated in Figure 4.6 and 4.7, were constructed using the method described in Section 3.4.4. The excellent correlation of the data points measured with the suction probe between 0 and 200kPa, with the expected theoretical shape of the SWCC allowed the data points at greater suctions to be extrapolated with confidence.

The SWCC gives an indication of the residual volumetric water content of the Mispah tailings material. The residual volumetric water content determined from the extrapolated graphs for trough test 2 and 3, were 0.07 and 0.05, respectively. It can be noted from Figure 4.8 that the two SWCC plots for trough test 2 and 3 coincide at the point of inflection, as well as over the linear portions of the graphs. The maximum variation between the two plots can be found at the maximum points of curvature, with both plots converging as it approaches the residual suction value.

Figure 4.9 illustrates the average SWCC obtained through curve fitting and it can be seen that the shape of the average SWCC corresponds well to the shape of the SWCC illustrated in Figure 5.4, 5.5 and 5.6.

5.3 Shear Strength Induced By Suctions

Figure 4.10 illustrates the relationship between the shear strength, calculated with the volumetric water content and residual degree of saturation from the SWCC, as well as suction pressures. This graph shows the data points calculated from the partial SWCC, which were obtained from the results of trough test 2 and 3, as well as the complete plots, which were obtained from the extrapolated SWCC .

For the suction pressure range between 0kPa and 150kPa, the plots correlate well with each other, with all four plots exhibiting near linear behavior. The maximum point of curvature for all four plots is at 150kPa with a maximum calculated shear strength of between 75kPa and 80 kPa. Above 150kPa suction pressures, the calculated shear strength plots start to decrease rapidly up to 300kPa suction pressure. Beyond this point, the plots start to flatten. The maximum difference between the plots are at 150kPa suction pressure, with a 5kPa difference in the calculated shear strengths.

The decrease in shear strength as the suction pressures increase beyond 150kPa, is due to air entry taking place. The continuity of the pore fluid is broken with entry of occluded air bubbles as the largest pores start to drain. This leads to a decrease in the surface area over which the pore pressure can act, and causes a decrease in the suction induced shear strength. As the pore fluid decreases the suction induced shear strength would decrease even further.

Figure 4.11 illustrates an average calculated shear strength curve, obtained from the average SWCC shown in Figure 4.9. The same decrease in the calculated shear strength can be seen beyond 150kPa. At 700kPa suction pressures, the pore fluid is insufficient to transmit any pressure to the soil particles, and the suction induced shear strength becomes zero.

5.4 Drying and Desiccation

The moisture content versus suctions relationships of drying box test 2.1, 3.1 and 4.1 correlates well with each other, as illustrated in Figure 4.12. This relationship is taken as the average moisture content versus suction, throughout the duration of the drying box tests and applies to the bulk mass of material and not just to material at a specific depth. Between 0 and 80kPa suction the moisture content decreases rapidly. Above 80kPa the curves flatten until it reaches an asymptote at approximately 10%.

The maximum variation between the plots (drying box test 2.1, 3.1 and 4.1) is approximately 10% at the points of maximum curvature (30kPa). The plots for drying box test 3.1 and 4.1 follow the expected trend, except for the plot drying box test 2.1, which shows an offset of the data points from the expected trend at 10kPa suction pressure. This data offset can be attributed to inaccuracy of the load cell used to weigh the drying tailings material.

Figure 4.13 illustrates the moisture content versus suction relationship for drying box tests 2.2, 3.2 and 4.2. The shape of the plots for the three individual tests correlates better with each other, than the shape of the plots illustrated in Figure 4.12. The graphs have a steep decrease in moisture content for suction pressures up to 70kPa. Above 70kPa the curves flatten out and become asymptotic at 20% moisture content. The maximum variation between the plots is also at the maximum points of curvature.

Figure 5.7 illustrates the moisture content versus suction plots for the first and second lifts. From these plots it can be concluded that the maximum moisture loss occurs as the suction pressures increase from 0-80kPa. Above 80kPa the moisture content approaches a constant value of 16% as the suction pressures increases.

The moisture loss over the first portion of the plots, between 0kPa and 80kPa suction pressures, is about 25%, with loss in moisture over the rest of the suction range being less than 10%. From the average moisture loss of 35% over the range 0kPa to 200kPa suction pressures, 72% of the losses occur over the range 0 - 80kPa suction pressure and only 28% of the losses take place over the rest of the suction range.

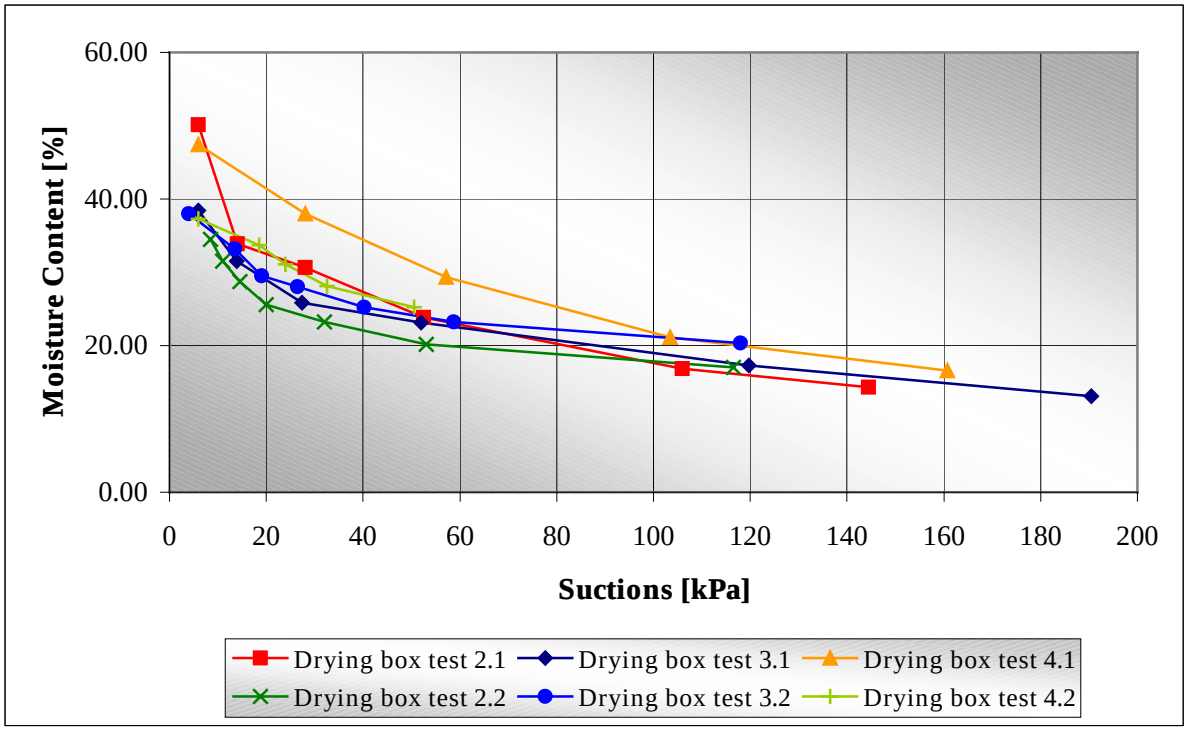

Figure 5.7: Average moisture content versus suction – Lift 1 & Lift 2

Figure 4.13 illustrates the relationship between void ratio and suctions for drying box test 2.1, 3.1 and 4.1. The shape of the plots correlate well with each other, with a gradual decrease in void ratio occurring over the fist 60kPa of suction pressures. Above 60kPa the void ratio remains constant as the suction pressures increases.

The difference in void ratio between drying box test 2.1 and 3.1 is about 0.2, with the difference between drying box test 2.1 and 4.1 being 0.3. The difference between drying box test 3.1 and 4.1 is only 0.1. The variation of void ratios between the three tests can be attributed to the difference in grading of the tailings material used for the individual tests, as the material were gathered from different positions on the daywall of Mispah residue dam.
The plots in Figure 4.15 follow the same trend, with a slight decrease in void ratio over the first 60kPa of suction pressures. Above 60kPa, the plots approach a constant value of between 0.9 and 1. The plots for drying box test 3.2 and 4.2, coincide with the plot of drying box test 2.2, varying with 0.2 over the whole range of suction pressures. This variation is again the result of a variation in the grading of the material used during the tests.

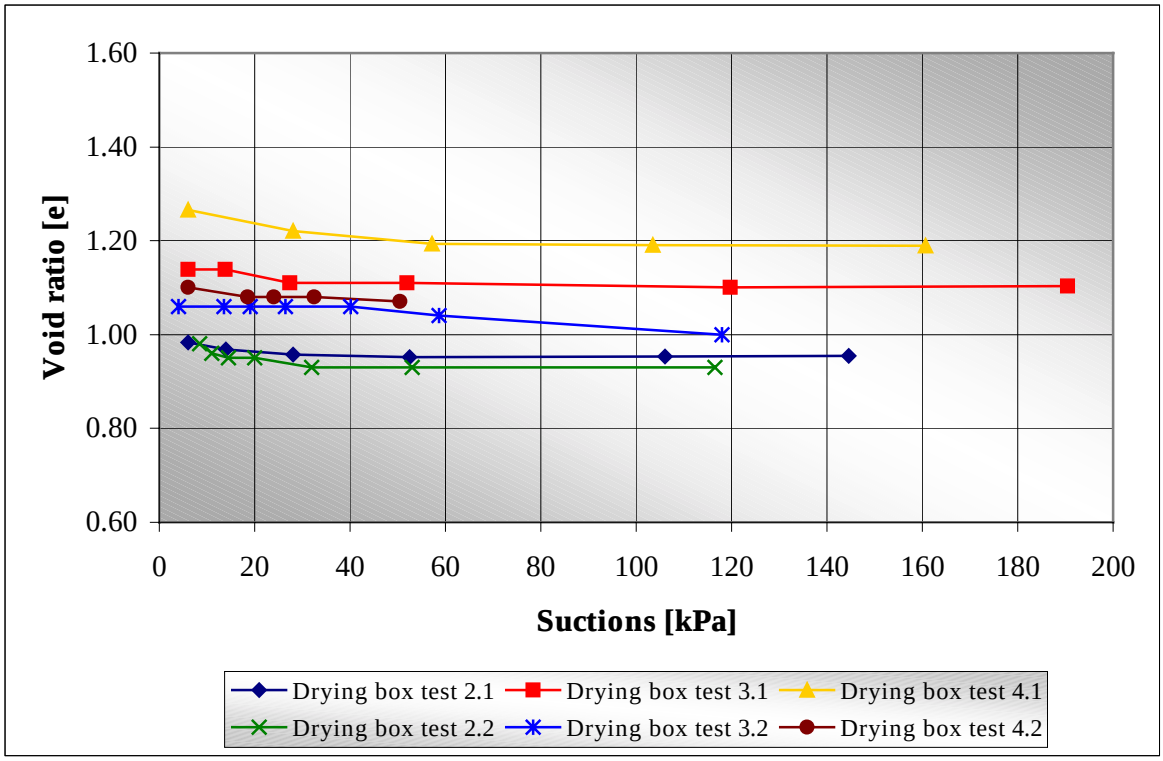

Figure 5.8: Average void ratio versus suction- Lift 1 and Lift 2

Figure 5.8 illustrates the void ratio versus suction results for both the first and second lift. It can be seen that all the graphs fall within the range of 0.9 – 1.2, following the same trend. The relationship between degree of saturation and suction pressures for drying box test 2.1, 3.1 and 4.1 are shown in Figure 4.16. For drying box test 2.1 and 3.1 the degree of saturation decreases rapidly over the range of 0 - 60kPa suction pressures. Above 60kPa the plots approach a constant value of between 0.3 and 0.4. The results from drying box test 4.1, indicate a more linear decrease in degree of saturation, with an increase in suction pressures up to 80kPa, after which it also becomes asymptotic.

The maximum difference in degree of saturation between the three graphs is 0.3, with tests 2.1 and 3.1 coinciding over the largest portion of the measured suction range. The variation of results from the individual tests, can be the consequence of inaccuracies during the volume measurement of the samples. This is due to the sloughing of the very wet samples, and the shattering of the dry samples.

The plots in Figure 4.17 for the three drying box tests during the second lift coincide well, with a maximum difference of 0.05 between the three graphs. All three plots experience a drastic decrease in degree of saturation over the range of 0 – 60kPa suction pressures, with the plots flattening as the suction pressures increases above 60kPa.

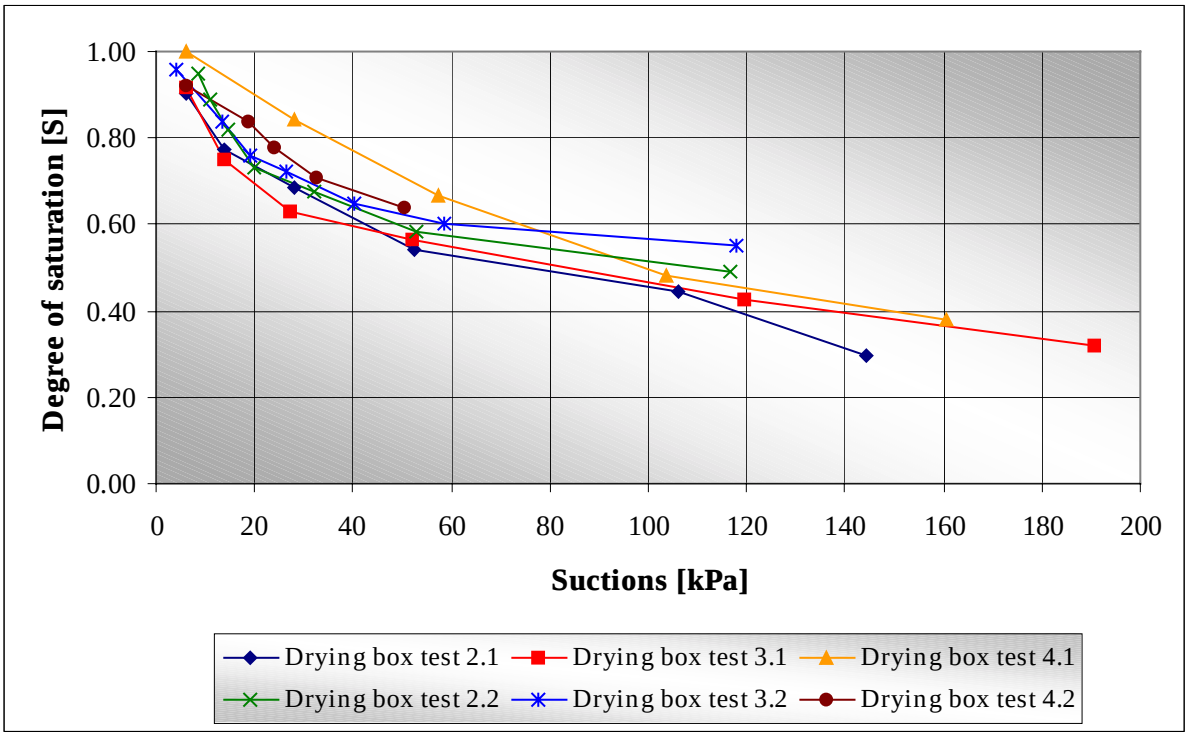

Figure 5.9: Average degree of saturation versus suction – Lift 1 and Lift 2

Figure 5.9 shows the degree of saturation plots for both lifts. Most of the plots coincide well, with the deviations being the results of measurement inaccuracies.

Figure 4.18 shows the relationship between suction pressures and percentage linear shrinkage, which was determined from the crack measurements taken over the length of the drying box on a daily basis. The plots for drying box test 2.1 and 4.1 follow the same trend, with the largest percentage shrinkage occurring between 0kPa and 60kPa suction pressure. Above 60kPa the plots approach constant values of between 5% and 7%. The variation of the results obtained from drying box test 3.1 can be the result of inaccurate measurement of the crack widths due to disturbances caused by the daily sampling.

The three plots for drying box test 2.2, 3.2 and 4.2 are shown in Figure 4.19. The three plots correlate better than the results discussed in the previous paragraph. All three plots indicate a maximum increase in percentage linear shrinkage over the range of 0 – 50kPa suction pressures. The plots reach a constant value of between 3% and 3.5% linear shrinkage after 50kPa suction pressure.

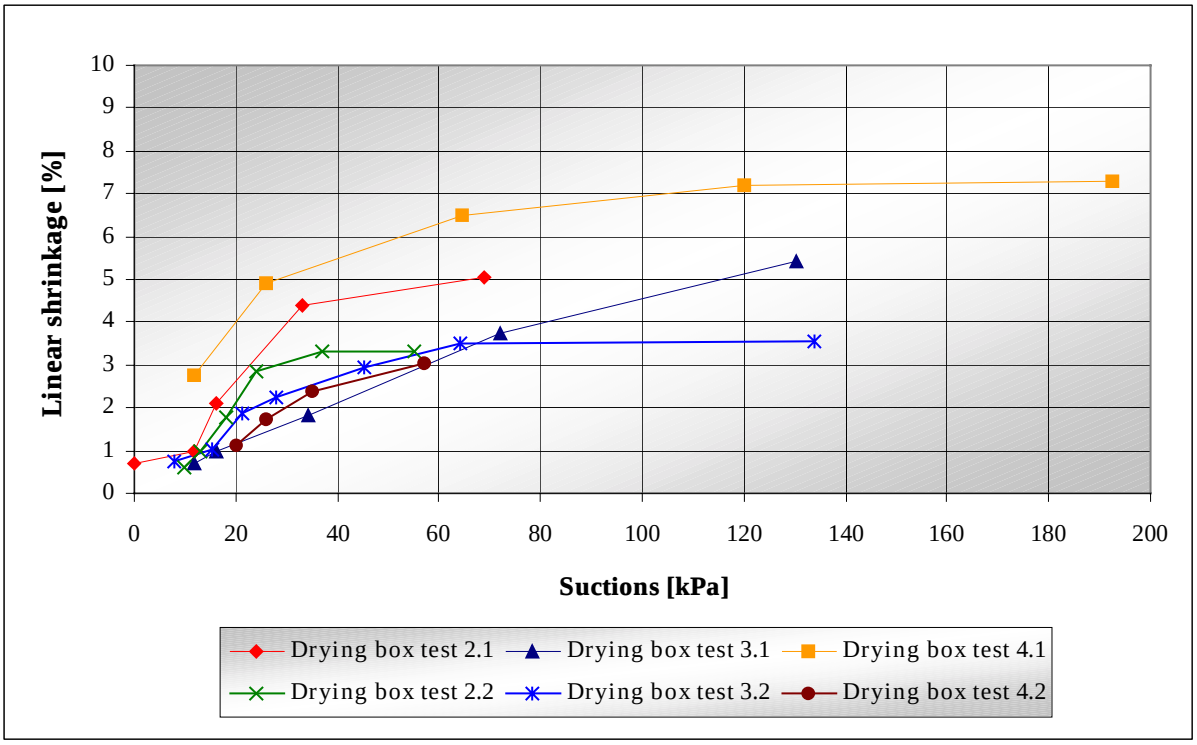

Figure 5.10: Percentage linear shrinkage versus suction – Lift 1 and Lift 2

Figure 5.10 is a compilation of all six drying box test results, from which it is evident that the linear shrinkage measured during the first lift is approximately double that of the second lift. This relationship indicates the decrease in linear shrinkage with an increase of the depth of drying tailings material.

The difference in percentage linear shrinkage between the trough tests, and the drying box tests, is the result of the different methods of material preparation used. For the trough test thickened tailings is used, which is thoroughly mixed before it is poured into the trough. Due to the lower water content, the tailings in the trough is at a denser state, which does not allow much sedimentation to take place. This results in a nearly homogeneous material. With the drying box tests, the tailings is poured into the drying box as a slurry, which allows sedimentation to take place. This leads to a non homogeneous material with most of the clay particles in the top portion of the layer.

The calculated shear strength versus suction at depths of 0cm and 8 cm for the first lifts are illustrated in Figure 4.20 and 4.21 respectively. For the 0cm depth the shear strength graphs for drying box test 2.1and 4.1 increases sharply to a shear strength of 30 – 35 kPa over the first 70kPa increase in suction pressures. The plots of drying box test 3.1 increase at a slower rate, but continue to increase until it reaches approximately 50 kPa shear strength, before the plot reaches its asymptote.

The maximum difference between the results can be observed for drying box test 2.1 and 3.1, at 130kPa suction pressure, where the difference in shear strengths are approximately 15kPa. With the shear strength being calculated from the volumetric water content, obtained from the samples, the errors encountered during the experimental measurements are propagated to the calculated shear strengths. This leads to the deviation in calculated shear strength between the three individual tests.

The calculated shear strength versus suction plots at 8cm for the first lift is illustrated in Figure 4.21. The plots in Figure 4.22 do not follow the same trend as observed in Figure 4.20. Deviations from the expected trend can be observed in the three plots, with large deviations between the results of the three tests.

Figure 5.11 compares the calculated shear strengths for the first lift at 0 and 8cm for drying box test 2.1, 3.1 and 4.1 respectively. It can be that at 0cm a maximum shear strength of 50 - 60kPa is obtained, with the average calculated shear strength being 10kPa less at a depth of 8cm.

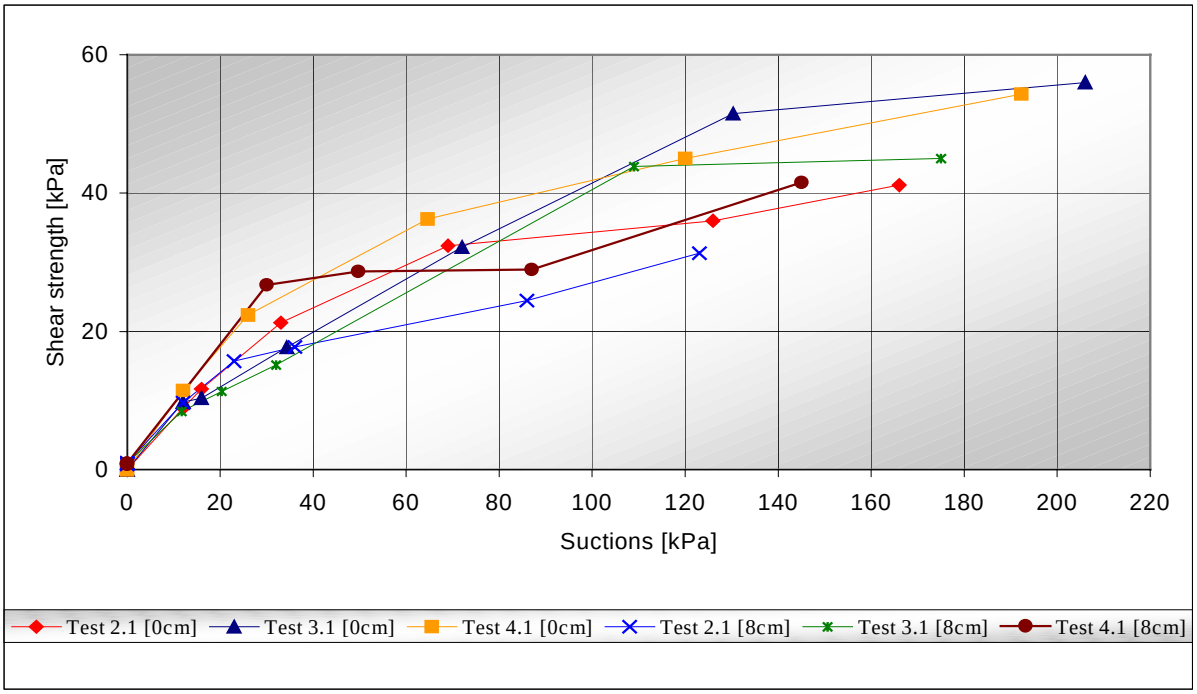

Figure 5.11: Calculated shear strength versus suction at 0 and 8cm – Lift 1

Figure 4.22, 4.23 and 4.24 illustrates the calculated shear strength versus suction pressure relationship at depths of 0cm, 10cm and 20cm for drying box test 2.2, 3.2 and 4.2 respectively. The trend of the plots in Figure 4.22 also indicate a large increase in shear strength over the first portion of the graph between 0kPa and 70kPa suction pressures. Above 70kPa the rate of shear strength increase starts to decrease until a constant value between 50kPa and 60kPa.

Figure 5.12 compares the plots obtained during the first and second lifts at a depth of 0cm. All the plots follow approximately the same trend, with an occasional deviation in the individual plots. These deviations are again the result of the errors propagated from the volumetric water content, obtained from the sampled material. This graph illustrates that the depth of material below the surface did not influence the shear strength versus suction pressure relationship.

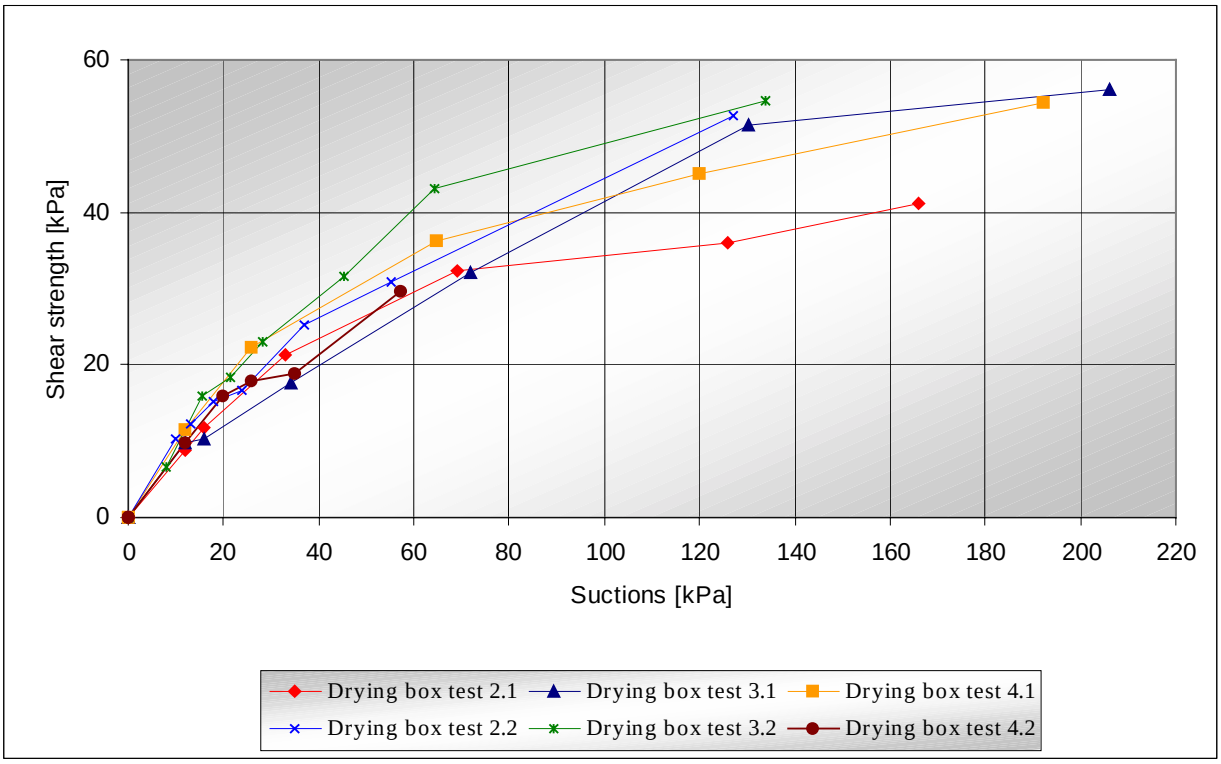

Figure 5.12: Calculated shear strength versus suction at 0cm – Lift 1 and Lift 2

From Figure 4.23 it can be seen that that there is a high rate of shear strength increase over the first 20kPa increase in suction pressures. Above 20kPa the plots start to flatten as the rate decreases. The scattering of the data points is noticeable. This is another result of the inaccurate determination of the volumetric water content from the sampled material. The same trend can be seen in Figure 4.24 with some scattering occurring.

Figure 5.13 illustrates the plots of shear strength versus suction at 0cm, 10cm and 20cm during the second lift. By comparing the plots it can be seen that the suction induced portion of the shear strength decreases, as the distance from the surface increases. Due to the sedimentation of the tailings, the grading of the material changes from very fine clay particles to rougher sandy-silt particles as the depth increases, thus making the sampling of the lower material increasingly difficult. This is due to the sampled material crumbling once it is removed from the sampler.

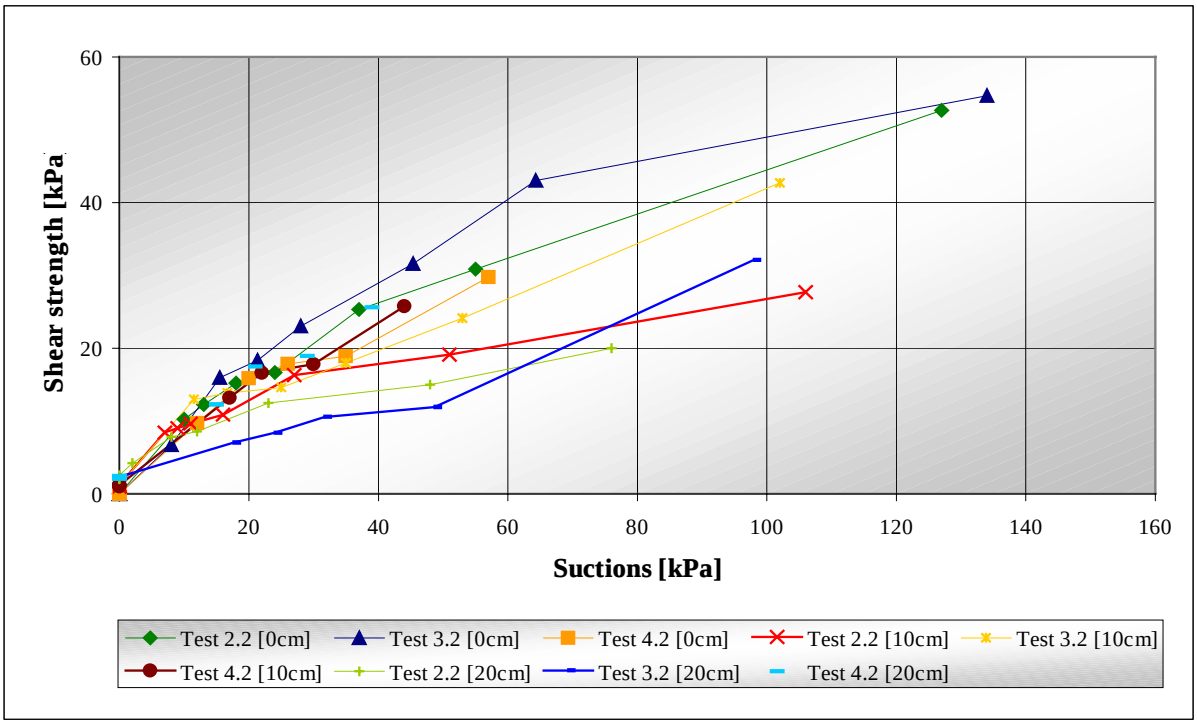

Figure 5.13: Calculated shear strength versus suction at 0cm, 10cm and 20 cm – Lift 2

Figure 4.25 and 4.26 compare the calculated shear strength values with the vane shear readings taken at the corresponding depths. From Figure 4.25 it can be seen that the vane shear and calculated shear strength values correlate very well at the lower range of suctions between 0kPa and 40kPa. Above 40kPa the calculated shear strength starts to deviate from the vane shear readings as the suction pressures increase. The same observation can be made at the lower suction range between 0kPa and 40kPa in Figure 4.26.

Figure 5.14 contains the plots of the calculated shear strength at 0cm and 8cm for the first lift, as well as the vane shear reading between the depth of 0cm and 10cm. The maximum difference in shear strength at 0cm and 8cm is approximately 10kPa. It can be seen from Figure 5.8 that the shear strength decreases as the depth of measurement increases, and since the contribution of the normal stress to the calculated shear strength is negligible it indicates that there is a difference in volumetric water contents for the same value of suction pressure.

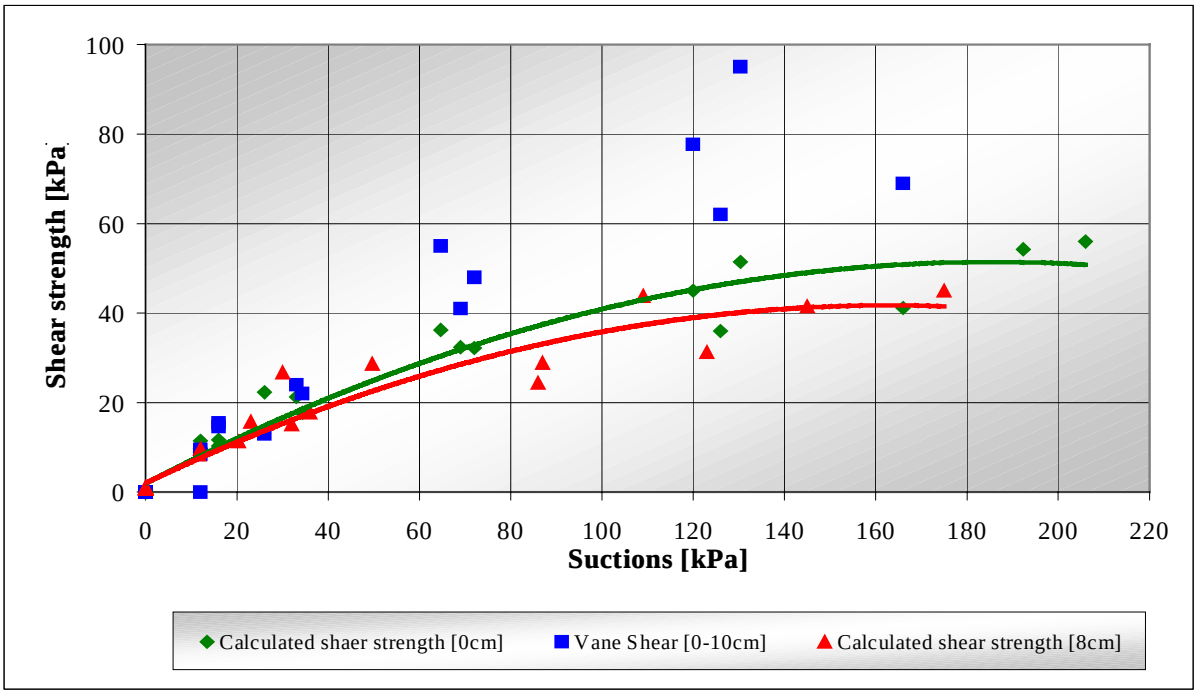

Figure 5.14: Comparison of calculated shear strength and vane shear readings at 0cm and 8cm – Lift 1

Figure 4.27, 4.28 and 4.29 compares the calculated shear strength at depths of 0cm, 10cm and 20cm with the vane shear readings taken at the corresponding depths in the drying box during the second lift. From the plots in Figure 4.27 the can be seen that the calculated shear strength and vane shear readings follow approximately the same trend, with a maximum difference of 10kPa between the two plots. The increase in shear strength for both plots is quite rapid, between 0kPa and 80kPa suction pressures. Above 80kPa the shear strength values starts to stabilise.

The difference between the calculated and the vane shear strength is considerably larger at a depth of 10cm, as shown in Figure 2.28. Both plots follow the same trend with a rapid rate of increase over the first 60kPa of suction pressures. Above 60kPa the plots start to flatten. At the 20cm depth, the difference between the vane shear and the calculated shear strength is on average 20kPa as illustrated in Figure 2.29.

The same decrease in the calculated shear strength (with increase in depth), can be seen in Figure 5.15, which is a graph of all the calculated shear strength versus suction plots at 0cm, 10cm and 20cm during the second lift. This indicates that there are different values of volumetric water content for the same value of suction pressure.

The reason for this variation can be due to the sedimentation that takes place after the pouring of the tailings. This leads to a variation of grading over the depth of the layer. This in turn also makes the sampling and measuring of the deeper coarser tailings more difficult, and causes a variation in the soil water characteristics of the material with depth, thus leading to a decrease in the suction induced shear strength. The effects of grading on the soil water characteristics of tailings, were illustrated well by the research done by Van Heerden 2000, where the air-entry value decreases as the grading of the tailings becomes more coarsely grained.

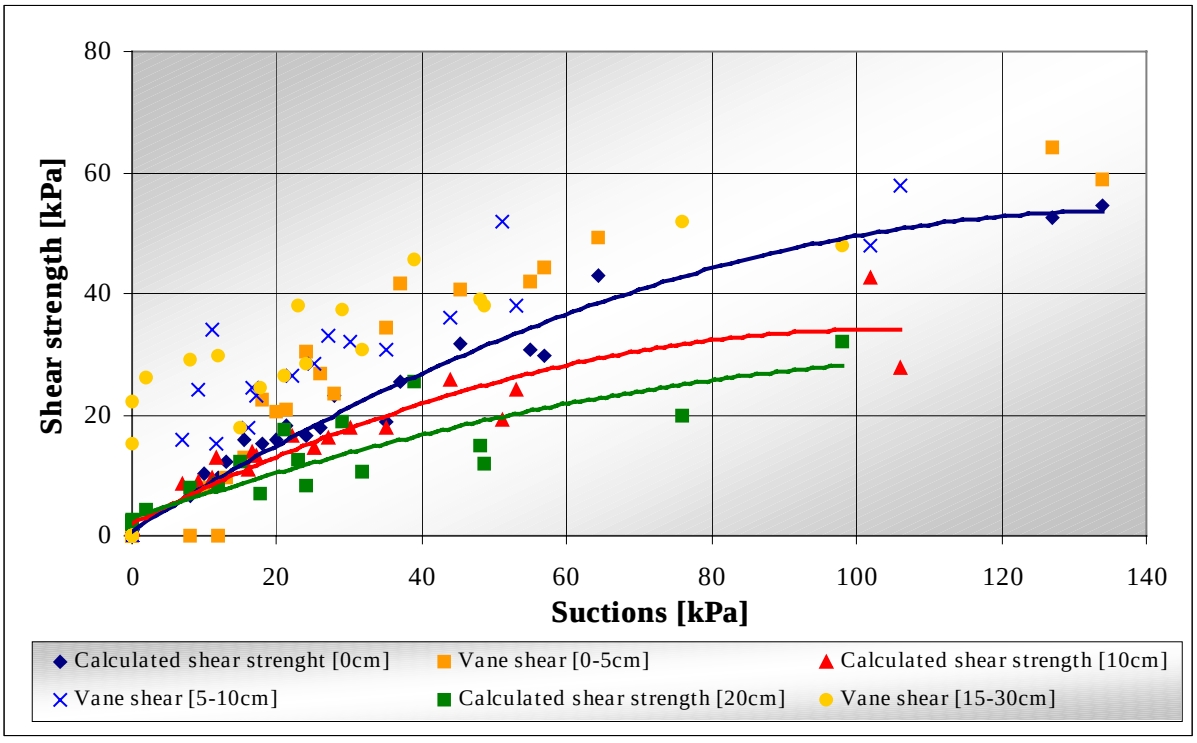

Figure 5.15: Comparison of calculated shear strength and vane shear readings at 0cm, 10cm and 20cm – Lift 2

Figure 4.30 and 4.31 illustrates the calculated shear strength, determined by using the volumetric water content from the SWCC, versus suction plots for the first lift at 0cm and 8cm. By using the volumetric water content values corresponding to the specific suction pressures, the sampling and measuring errors are avoided. By doing this, however, an assumption is made that the layers are homogeneous and that the SWCC determined for the mixture of the material applies to the whole layer.

It can be seen from Figure 4.30 that a near linear relationship exists between the calculated shear strength, and suction pressures up to 130kPa suction for all three test. Above 130kPa there is a decrease in the calculated shear strength as the suctions continue to increase. This behavior correlates well with the behavior observed for the suction induced shear strength graph, where there is an initial near linear increase in the calculated shear strength with suction pressures up to 130 - 150kPa (air-entry value). Above the air-entry value the calculated strength appears to decrease as the suctions continue to increase.

The same behavior can be seen in Figure 4.31 where the plots all exhibit initial near linear relationships between the calculated shear strength and suctions up to approximately 140kPa.

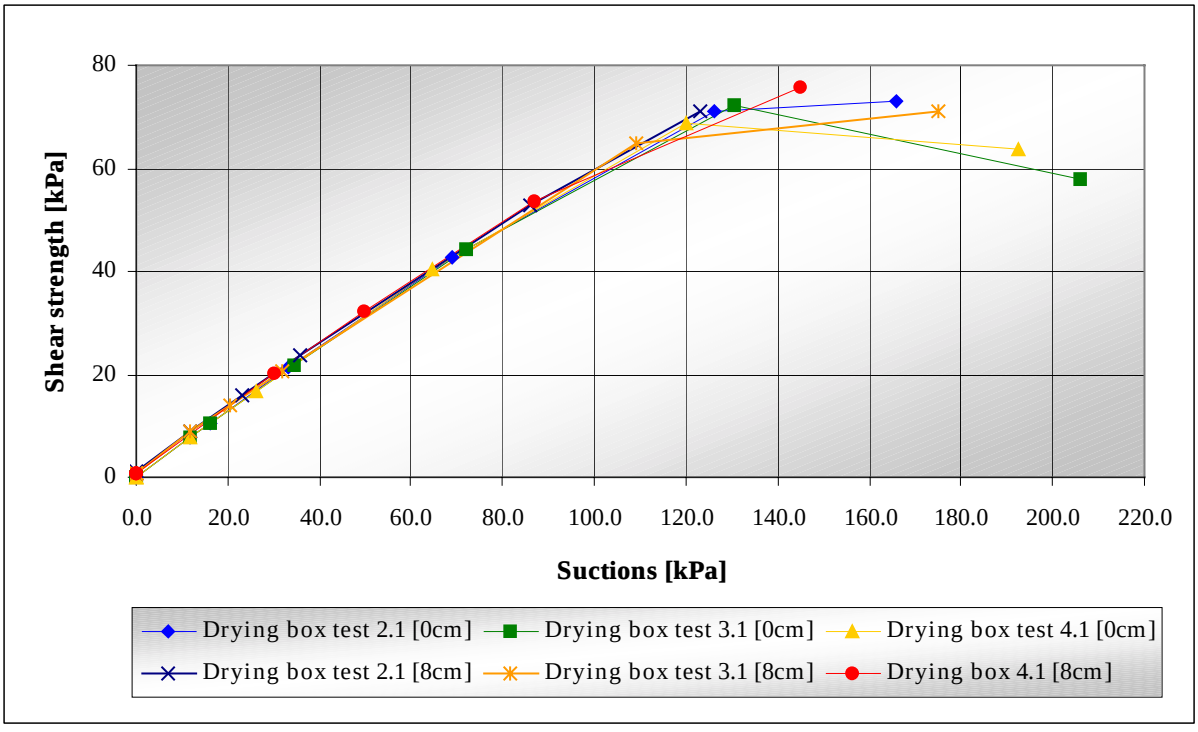

Figure 5.16: Theoretical shear strength versus suction at 0cm and 8 cm – Lift 1

From Figure 5.16, it can be seen that the plots of calculated shear strength at 0cm and 8cm coincide up to 130kPa suction pressures in a near linear manner. For suction pressures larger than 130kPa the calculated shear strength of the material at 8cm is slightly larger than the calculated shear strength of the material at 0cm. This is due to the small normal loads that contributes to the shear strength.

Figure 4.32, 433 and 4.34 illustrates the relationship between the shear strengths calculated using the SWCC and suction pressures at 0cm, 10cm and 20cm during the second lift respectively. These three graphs are compiled into Figure 5.11, which illustrates that all the plots exhibit the same near linear behavior up to 120kPa where after it starts to deviate.

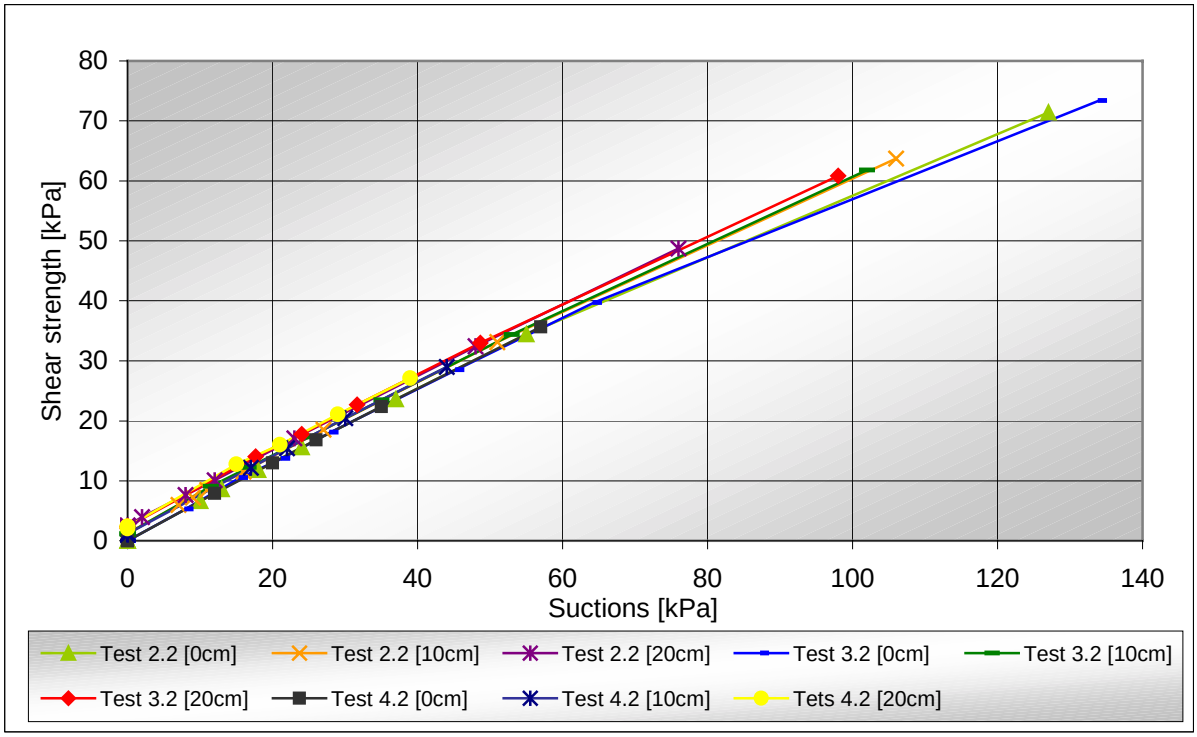

Figure 5.17: Theoretical shear strength versus suction at 0, 10 and 20 cm – Lift 2

Figure 4.35 and 4.36 compares the vane shear readings with the calculated shear strength readings. This is calculated using the SWCC, at 0cm and 8cm during the first lift. It can be seen that the theoretically calculated shear strength values correspond better with the vane shear readings than the normally calculated shear strength values, illustrated in Figure 4.25 and 4.26. For both depths, the vane shear values form an envelope around the calculated values, indicating a good fit.

Figure 5.18 compares the calculated shear strength plots and vane shear readings from Figure 4.35 and 4.36. Once again, it is noted that the shear strength of the material has increased over the 8cm depth, due to the contribution of the normal stress.

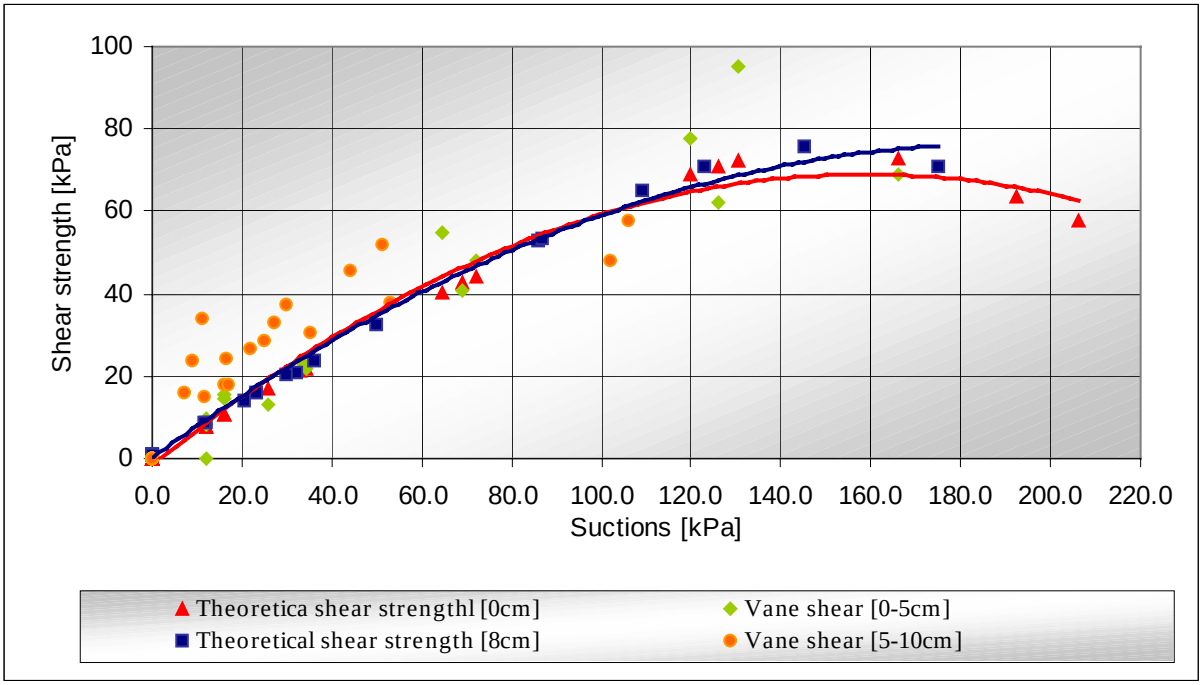

Figure 5.18: Comparison of theoretical shear strength and vane shear readings at 0cm and 8cm – Lift 1

Figure 4.37, 4.38 and 4.39 compare the theoretical shear strength with the vane shear readings at 0cm, 10cm and 20 cm during the second lift respectively. The good correlation between the vane shear and theoretical shear strength values are noticeable on all three graphs. From Figure 5.12 the same increase in shear strength can be seen as shown in Figure 5.11.

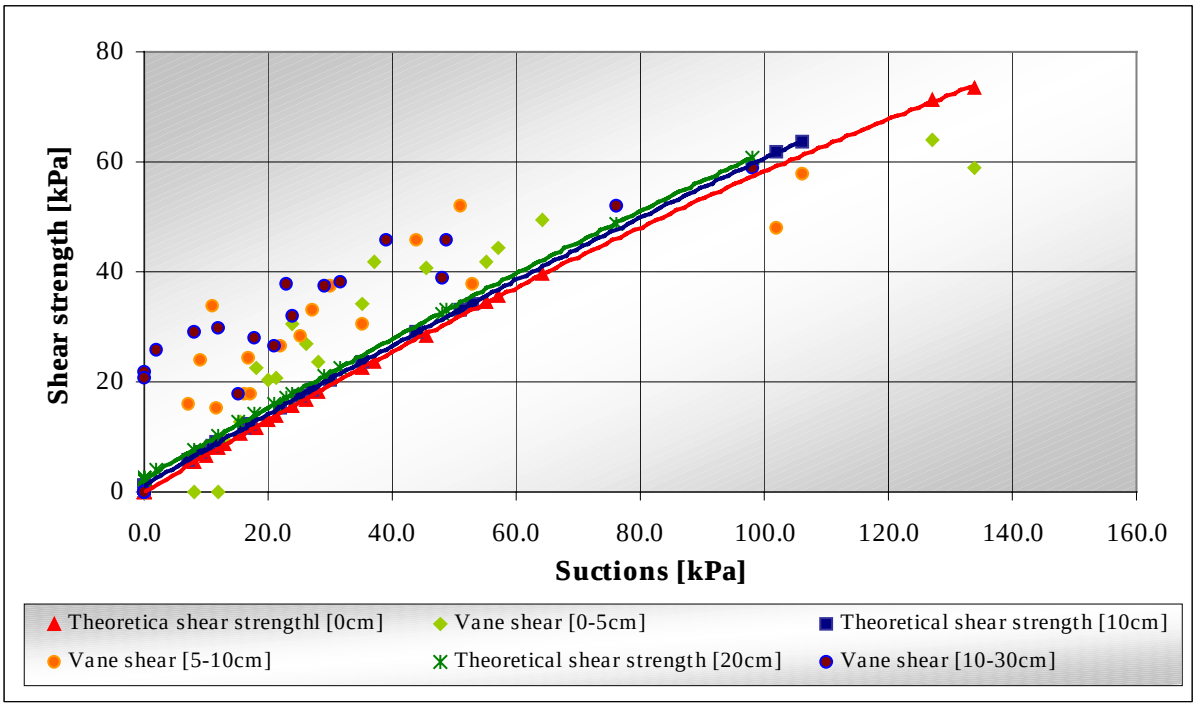

Figure 5.19: Comparison of theoretical shear strength and vane shear readings at 0cm, 10cm and 20cm – Lift 2

To illustrate the difference between using the volumetric water content from the sample measurements, and using the volumetric water content from the SWCC, Figure 5.20 and 5.21 compare the shear strength versus suction plots of both methods for the first and second lift respectively. From Figure 5.20 and 5.21 it can be seen that the set of plots for the first and second lift exhibits the same trend, with the theoretical shear strength plots having a higher and more linear rate of shear strength increase.

There is a remarkable difference in the maximum shear strength obtained by the theoretical and normally calculated plots. The suction pressure at the point of maximum curvature varies for each plot, indicating a variation in air-entry values.

From these plots it can be concluded that effects of sampling and measurement errors, on the calculated shear strength calculated, are minimal.

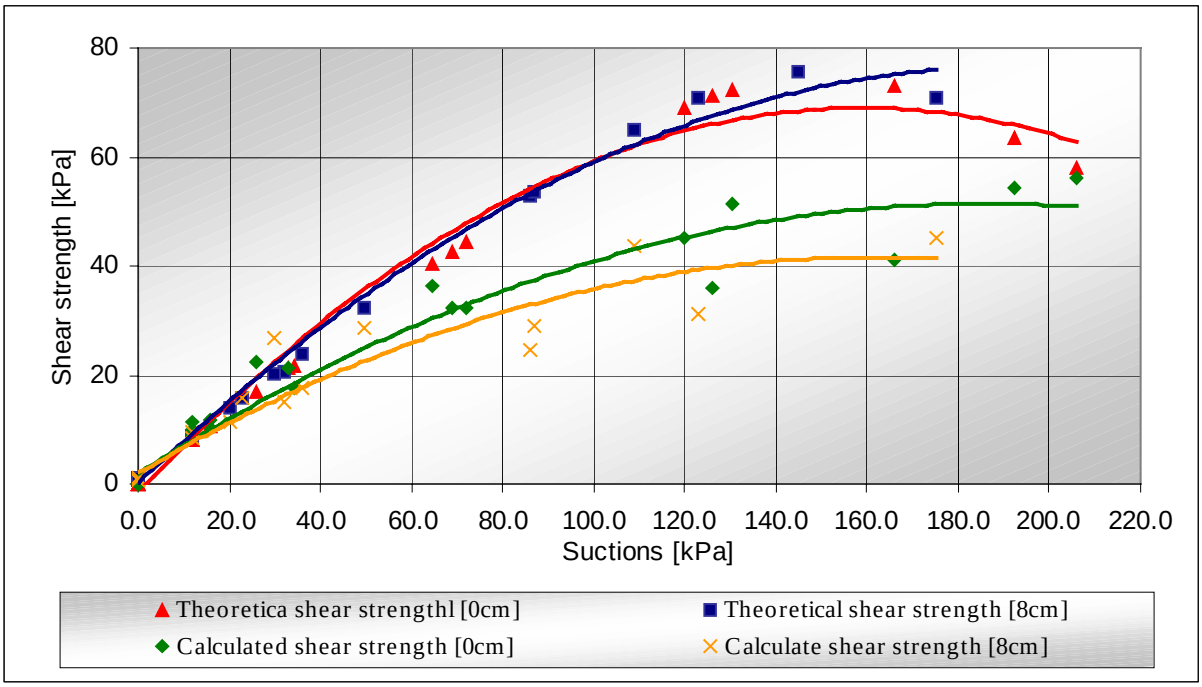

Figure 5.20: Comparison of theoretical and normally calculated shear strength at 0cm and 8cm – Lift 1

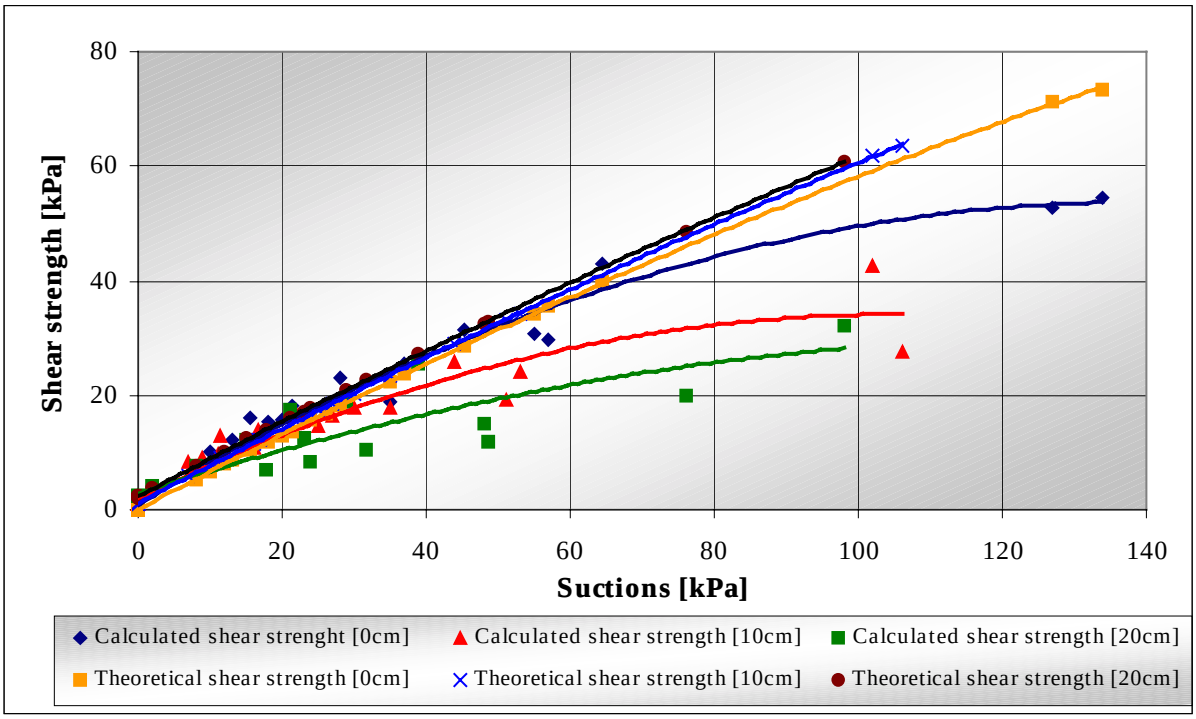

Figure 5.21: Comparison of theoretical and normally calculated shear strength at 0cm, 10cm and 20cm – Lift 1

5.5 Field Tests

The results given in Section 4.5 were obtained from the field tests that were carried out on the daywall of Mispah residue dam. Figure 4.40, 4.41 and 4.42 illustrates the depth versus suction relationship for site visit 1, 2 and 3. From Figure 4.40 it can be seen that there exists a large gradient in suction pressures over the first 15cm depth. The suction readings on the surface were in the range of 80-130kPa and dropped to between 10kPa and 30kPa at a depth of 15cm. Between the depth of 15cm and 30cm there was only a 10kPa drop in suction pressures.

The very large suction pressures of the surface material (crust), is due to the concentration of clay particles in the top regions of the poured layer, due to sedimentation, as well as due to the chemical reactions that have taken place on the exposed surface. After scraping off the crust, which is about 1cm thick, the suction pressures dropped with 30-40kPa. This is illustrated by the plots of block 2 and 3 on Figure 4.40, where suction readings were taken before and after the crust was scraped off.

For the plots shown in Figure 4.41 and 4.42 the 0cm depth represents the depth after the crust had been removed. The gradient of the plots shown in Figure 4.41 and 4.42 is much flatter with an average drop of only 30kPa over the depth range of 0-15cm.

Figure 4.43 and 4.44 compare the average volumetric water content calculated from the results of the drying box tests 1 and 2, with the volumetric water content obtained from the extracted samples during the field testing. The scatter plot of the field results correlate well with the three plots illustrated in Figure 4.43 and 4.44. The various volumetric water content data points shown for the same suction pressure is, again, the result of sampling and measurement inaccuracies, as well as the variation of grading with depth due to sedimentation.

Figure 4.45 and 4.46 compares the calculated shear strength, theoretical shear strength and vane shear readings from the drying box at 0-5cm and 5-10cm during the first lift with the vane shear readings from the field testing at 0-5cm and 5-10cm respectively.

For both plots the vane shear readings obtained from the day wall is higher than the rest of the shear strength data points. This can be due to a difference in the drainage conditions, and also a too high shear rate. This causes dilation to take place and thus increases the measured shear strength. Between the two calculated values of shear strength, the ones calculated with the use of the SWCC correlate the best with the vane shear readings obtained both in the drying box and on the daywall.

Figure 4.47, 4.48 and 4.49 compare the calculated shear strengths, theoretical shear strengths and vane shear readings from the drying box at 0-5cm, 5-10cm and 15-30cm (during the second lift), with the vane shear readings from the field testing at 0-5cm, 5-10cm and 15-30cm, respectively. The same trend is followed in all three graphs, with the vane shear readings from the daywall being greater than all the strength data values for the same suction pressure. The theoretical shear strength plot again correlates the best with the vane shear readings.

6. CONCLUSIONS

6.1 Summary of conclusions from experimental programme

- The model for the prediction of the soil water characteristic curve, derived by Fredlund and Xing (1992), was used successfully to predict the complete soil water characteristics curve for Mispah gold tailings. The fitting parameters for the model was derived from partial plots obtained from the trough test results. From the complete soil water characteristic curve it was possible to determine the residual volumetric water content, θ_r, and the air-entry value.

- The linear shrinkage behaviour of thickened tailings is different to the behaviour of slurry tailings. Sedimentation that occurs in slurry tailings causes a concentration of clay particles in the top region of the poured layer, resulting in an increased linear shrinkage.

- From the results it is evident that suction induced shear strength increases nearly linear until the air-entry suction is reached. Above the air-entry suction the suction induced shear strength decreases, as the continuity of the pore fluid is broken. As the volume of air increases within the pore fluid, the suction induced shear strength will decrease until it diminishes completely.

- In gold tailings deposits the material is non-homogeneous due to the sedimentation, which causes a variation of soil water characteristics with depth in each layer.

- By assuming that the tailings deposits are homogeneous and that the soil water characteristic curve of a representative sample applies over the whole depth, a better estimate of the suction induced shear strength can be obtained. Thus the suction induced shear strength of tailings can be determined, with depth, with the use of the suction probe and the soil water characteristic curve for the material

6.2 Conclusions in reference to research objectives

- The mid-plane suction was calibrated and successfully used to obtain accurate suction pressure measurements.

- The trough test method developed proofed to be successful in the construction of an accurate soil-water characteristic curve for Mispah gold tailings.

- The drying box method proposed provided an adequate testing procedure to simulate the actual processes, which occurs on the daywall of Mispah tailings dam. This method serves as bases for setting up a standard test method. Future research needs to be conducted to improve on some of the shortcomings of the method such as simulating changing environmental conditions.

- The equation derived by Vanapalli et al. (1996) was successfully used to calculate both the normal and suction induced shear strength of gold mine tailings using either the volumetric water content from the extracted samples or from the soil water characteristic curve. Investigate the increase in suction induced shear strength of drying tailings with depth.